STARS

Electronic Theses and Dissertations, 2004-2019

2019

Semi-Analytical Solutions of Non-linear Differential Equations Arising in Science and Engineering

Mangalagama Dewasurendra

University of Central Florida

Part of the Mathematics Commons

Find similar works at: https://stars.library.ucf.edu/etd

University of Central Florida Libraries http://library.ucf.edu

University of Central Florida

STARS
Showcase of Text, Archives, Research & Scholarship

SEMI-ANALYTICAL SOLUTIONS OF NON-LINEAR DIFFERENTIAL EQUATIONS
ARISING IN SCIENCE AND ENGINEERING

by

MANGALAGAMA DEWASURENDRA
B.S. University of Peradeniya, 2009
M.S. University of North Florida, 2013
M.S. University of Central Florida, 2015

A dissertation submitted in partial fulfilment of the requirements
for the degree of Doctor of Philosophy
in the Department of Mathematics
in the College of Sciences
at the University of Central Florida
Orlando, Florida

Summer Term
2019

Major Professor: Kuppalapalle Vajravelu

ABSTRACT

Systems of coupled non-linear differential equations arise in science and engineering are inherently nonlinear and difficult to find exact solutions. However, in the late nineties, Liao introduced Optimal Homotopy Analysis Method (OHAM), and it allows us to construct accurate approximations to the systems of coupled nonlinear differential equations.

The drawback of OHAM is, we must first choose the proper auxiliary linear operator and then solve the linear higher-order deformation equation by spending lots of CPU time. However, in the latest innovation of Liao's " Method of Directly Defining inverse Mapping (MDDiM)" which he introduced to solve a single nonlinear ordinary differential equation has great freedom to define the inverse linear map directly. In this way, one can solve higher order deformation equations quickly, and it is unnecessary to calculate an inverse linear operator.

Our primary goal is to extend MDDiM to solve systems of coupled nonlinear ordinary differential equations. In the first chapter, we will introduce MDDiM and briefly discuss the advantages of MDDiM Over OHAM. In the second chapter, we will study a nonlinear coupled system using OHAM. Next three chapters, we will apply MDDiM to coupled non-linear systems arise in mechanical engineering to study fluid flow and heat transfer. In chapter six we will apply this novel method to study coupled non-linear systems in epidemiology to investigate how diseases spread throughout time. In the last chapter, we will discuss our conclusions and will propose some future work. Another main focus is to compare MDDiM with OHAM.

To My Loving Wife Narmada and Parents

ACKNOWLEDGMENTS

TABLE OF CONTENTS

LIST OF FIGURES

LIST OF TABLES

CHAPTER 1: INTRODUCTION

Most of the real world problems are inherently non-linear and can be quantitatively model as systems of nonlinear differential equations. In the field of differential equations, solutions to most of the linear problems are well-known and have been existence for quite a while. However, in many cases, exact solutions to non-linear systems of differential equations not to be found, and used numerical schemes to understand the non-linear phenomena. When exact or analytical solutions were found, it is still difficult to generalize such results for other non-linear systems of differential equations. Due to such difficulties, we frequently seek mathematical techniques to obtain approximate solutions to non-linear systems of differential equations.

In early nineteenth-century perturbation technique has been widely used to obtain analytical approximation of a nonlinear differential equation

$$\mathcal{A}[u(x)] = f(x). \tag{1.1}$$

If this nonlinear differential equation has a small physical parameter ϵ, and nonlinear operator $\mathcal{A}$ contains a linear part $\mathcal{L}$, such that $\mathcal{A} = \mathcal{L} + \mathcal{N}$, then, assuming solution to the nonlinear differential equation as

$$\phi(x) = \phi_0(x) + \phi_1(x)\epsilon + \phi_2(x)\epsilon^2 + \dots \tag{1.2}$$

and substituting it in to the (1.1), can transfer the original nonlinear problem into an infinite number of linear sub problems

$$\mathcal{L}[\phi_0(x)] = f(x), \quad \mathcal{L}[\phi_k(x)] = \mathcal{Q}_k(\phi_0(x), \phi_1(x), ..., \phi_{k-1}(x)). \tag{1.3}$$

In the perturbation method, we have no freedom to chose the linear operator. Even, subproblems become singular if the order of the linear subproblems are less when compared to the original problem. Further, the perturbation technique fails if there is no small physical parameter ϵ. To overcome those issues, in 1992 Liao introduce Homotopy Analysis Method using a fundamental concept in algebraic topology ([1]-[2]).

In topology, homotopy between two continuous functions f and g from a topological space X to a topological space Y is defined to be a continuous function $H : X \times [0,1] \to Y$ from the product of the space X with the unit interval $[0,1]$ to Y such that, if $x \in X$ then $H(x,0) = f(x)$ and $H(x,1) = g(x)$.

Let us consider the nonlinear ordinary differential equation

$$\mathcal{N}[u(x)] = 0, \quad x \in \Omega \tag{1.4}$$

subjecto to μ boundary conditions

$$\mathcal{B}_i[u(x)] = \beta_i, \quad \text{at} \quad x = \alpha_i, \quad i = 1, 2, ..., \mu, \tag{1.5}$$

where $u(x)$ is an unknown function, x is an independent variable, Ω is an interval of x, $\mathcal{N}$ denote nonlinear operator, $\mathcal{B}_i$ denote linear operator, $1 \leq \mu \leq n$ are positive integers, $\alpha_i \in \Omega$, and β_i ($1 \leq \mu \leq n$) are constants, respectively. We construct one-parameter family of equations with the homotopy parameter $q \in [0,1]$ in order to obtain a continuous deformation, $\phi(x; q)$, using the idea

2

of homotopy as follows

$$(1-q)\mathcal{L}[\phi(x,q) - u_0(x)] = qc_0\mathcal{N}[\phi(x,q)], \quad q \in [0,1], \tag{1.6}$$

subject to conditions

$$(1-q)\mathcal{B}_i[\phi(x,q) - u_0(x)] = qc_i\{\mathcal{B}_i(\phi(x,q) - \beta_i\}, \text{at} \quad x = \alpha_i. \tag{1.7}$$

It is clear that $\phi(x,0) = u_0(x)$ when $q = 0$ and $\phi(x,1) = u(x)$ when $q = 1$. So, $\phi(x,q)$ equation continuously deform from $u_0(x)$ to $u(x)$ when embedded parameter q varing from 0 to 1.

Assuming $\phi(x,q)$ analytic at $q = 0$, define homotopy-maclauriin series for the zeroth-deformation as

$$\phi(x,q) = u_0(x) + \sum_{k=1}^{+\infty} u_k(x)q^k, \tag{1.8}$$

where

$$u_k(x) = \frac{1}{n!}\frac{\partial^k}{\partial q^k}\phi(x;q)\Big|_{q=0} = \mathcal{D}_k\phi(x,q), \tag{1.9}$$

Here $\mathcal{D}_k$ is known as kth-order homotopy derivative.

Then applying Homotopy derivative $\mathcal{D}_k$ in to zeroth-order deformation equations (1.6)-(1.7), we can obtain higher order deformation equation in the frame of OHAM

$$\mathcal{L}[u_k - \chi_k u_{k-1}] = c_0\delta_{k-1}(x), \quad \text{for} \quad k \geq 1, \tag{1.10}$$

3

subject to boundary conditions

$$\mathcal{B}_i[u_k - \chi_k u_{k-1}] = c_i \Delta_{i,k}(x), \quad \text{at} \quad x = \alpha_i, \quad \text{for} \quad k \geq 1, \quad i = 1, 2, ..., \mu. \tag{1.11}$$

where

$$\delta_k(x) = \mathcal{D}_k\{\mathcal{N}[\phi(x; q)]\} \tag{1.12}$$

$$\Delta_{i,k}(x) = \mathcal{D}_k\{\mathcal{B}_i[\phi(x; q)] - \beta_i\} = \mathcal{B}_i[u_k(x)] - (1 - \chi_{k+1})\beta_i. \tag{1.13}$$

Here

$$\chi_k = \begin{cases} 0, & k \leq 1, \\ 1, & k > 1. \end{cases} \tag{1.14}$$

Now solving linear subproblems (1.10)-(1.13), we obtain the approximate series solution to the original nonlinear problem (1.4) in the frame of OHAM. Due to the way we define the zeroth order deformation equation we have considerable freedom to choose a linear operator. However, still finding the inverse operator to solve linear sub-problems will take lots of CPU time. To overcome this obstacle, Liao introduced the Method of Directly Defining the inverse Mapping (see [3]). Here, the freedom of choosing the linear operator in OHAM leads Liao to define the inverse linear mapping $\mathcal{J}$ directly in MDDiM.

Let $S_\infty = \{\phi_1(x), \phi_2(x), ...\}$ be a set of infinite number of base functions that are linearly independent and define the space of functions that is their linear combinations to be $V = \sum_{k=0}^{+\infty} \phi_k(x)$. This is the space where approximate solution comes from. Next define the space for the initial guess $V^* = \sum_{k=0}^{\mu} \phi_k(x)$, taking linear combination of first μ functions of the set S_∞, and $\hat{V} = \sum_{k=\mu+1}^{+\infty} \phi_k(x)$ so that $V = V^* \cup \hat{V}$. Similarly, letting $S_R = \{\psi_1(x), \psi_2(x), ...\}$, define $U = \sum_{k=0}^{+\infty} \psi_k(x)$ so that $u(x) \in U$. Finaly, directly defining the inverse map $\mathcal{J} : U \to V$ we

4

obtain following higher order deformation equations for the Method of Directly defining inverse Mapping

$$u_k(x) = \chi_k u_{k-1}(x) + c_0 \mathscr{J}[\delta_{k-1}(x)] + \sum_{n=1}^{\mu} a_{k,n}\phi_n(x). \tag{1.15}$$

For the error analysis we first consider the n-term series solution

$$\hat{u}(x) = u_0(x) + \sum_{k=1}^{n-1} u_k(x) \tag{1.16}$$

by adding the first n terms of the series solution. If n-term solution is exact solution to the original nonlinear problem (1.4), then $\mathcal{N}[\hat{u}(x)]$ must be equal to zero. Otherwise $\mathcal{N}[\hat{u}(x)] \neq 0$ and it gives residual error. This leads to define total error function $E[h]$ by taking square of the L^2-norm of the residual error function

$$E[h] = \int_{\Omega} (N[\hat{u}])^2(x)dx. \tag{1.17}$$

Now total error function is only depend on converge control parameter h. Finally we can obtain n-term OHAM solution by substituting value of h which minimize the total error.

The goal of this dissertation is to extend MDDiM to solve systems of nonlinear ordinary differential equations, which has been previously used to solve a single nonlinear ordinary differential equation. Also, we demonstrate the advantage of directly defining the inverse map in MDDiM compare to the auxiliary linear operator in OHAM.

In Chapter 2, the influence of the magnetic field on flow and heat transfer of an electrically conducting fluid at an impermeable elastic sheet is analyzed. The governing nonlinear differential equations are solved analytically via OHAM.

In chapter 3, convective heat transfer at a porous flat plate is studied. Approximate series solutions were obtained for a second order non linear coupled system of two differential equations by extending Liao's Method of Directly Defining the inverse Mapping Method.

In chapter 4, approximate series solutions to a fourth order coupled nonlinear system of two non linear differential equations in combine free and forced convection flow of a second-grade fluid over a stretching sheet were obtained by using extended version of MDDiM.

In chapter 5, we further extended MDDiM to study a third order non linear system of three ordinary differential equations arise in a steady, incompressible laminar flow of a nanofluid at a vertical wall.

In chapter 6, MDDiM used to solve the SIR and SIS models in epidemiology and this is the first time some one used MDDiM to solve problems arise in epidemiology. This analytical approach is more general and can be used to analyze complicated models arise in mathematical biology, physics and engineering.

CHAPTER 2: MIXED CONVECTIVE BOUNDARY LAYER MHD FLOW ALONG A VERTICAL ELASTIC SHEET

In this chapter, the influence of magnetic field on flow and heat transfer of an electrically conducting fluid at an impermeable elastic sheet is analyzed. The governing nonlinear differential equations are solved analytically via homotopy analysis method. To validate the approximate-analytical method, comparisons are made with the available results in the literature for some special cases and the results are found to be in good agreement. These results were considered in Vajravelu et al. [4].

2.1   Background

In recent years, the study of flow and heat transfer characteristics of a Newtonian fluid past a stretching sheet has attracted the attention of numerous researchers due to its extensive industrial and technological applications. In order to describe the motion of a viscous fluid adjacent to the surface, boundary layer equations are used. Blasius [5] initiated the study of velocity boundary layer on a flat surface. Several researchers (Pohlhausen [6], Howarth [7], Abu-Sitta [8], Wang [9] and Cortell [10]) extended the Blasius flow problem by considering several geometrical and physical aspects. Sakiadis [11] considered different boundary conditions than those in Ref. [1] and obtained similar equations as derived by Blasius. Crane [12] introduced the concept of a stretching sheet and extended the work of Sakiadis [11]. Furthermore, many researchers worked on the stretching sheet concept by considering heat and mass transfer with various geometric shapes (Chen and Char [13], Ali [14], Aman et al. [15], Abbas et al. [16], Rashidi et al. [17], [18], Garoosi et al. [19], and Bég et al. [20]).

All the above researchers restricted their analyses to flowand heat transfer in the absence of a magnetic field. There are many industrial and technological applications of MHD flow and heat transfer, such as petroleum industries, plasma studies, and geothermal energy extractions. In view of these applications, Chakrabarti and Gupta [21] analyzed the flow and heat transfer over a stretching sheet in the presence of a magnetic field. Vajravelu et al. [22] obtained exact solutions for the hydrodynamic and hydromagnetic unsteady flow of a viscous fluid with free stream velocity $[u_\infty = f(t)]$. Furthermore, Andersson [23] extended the work in Ref. [21] to power law fluid. Seini and Makinde [24] used an exponentially stretching surface to analyze MHD boundary layer flow with radiation andchemical reaction. Recently, Rashidi et al. [25] employed an optimal homotopy analysis method (OHAM) and analyzed convective flow of a non-Newtonian fluid over a linearly stretching sheet in the presence of a magnetic field. However, all these studies are centered on a linearly or nonlinear stretching sheet. Fang et al. [26] examined the fluid flow using a special form of non-linear stretching, $u_w(x) = U_0(x + b)^m$ at $y = A(x + b)^{(1-m)/2}$, for different values of m (that is, a stretching sheet with variable thickness). Lee [27] studied the boundary layer flow over a slender body with variable thickness (the flow passing a needle with variable diameters). Ishak et al. [28] examined the boundary layer flow over a horizontal thin needle and Ahmed et al. [29] analyzed mixed convection flow over a vertically moving thin needle. Recently, Khader and Megahed [30], Vajravelu et al. [31] and Prasad et al. [32] explained the effects of various physical parameters on the flow and heat transfer by considering a special form of stretching sheet and examined the effects of velocity power index m and variable thickness α on the flow pattern.

Motivated by the above studies, the problem studied here is the mixed convective flow and heat transfer with variable thickness in the presence of a magnetic field. By using a suitable similarity transformation, the governing nonlinear system of coupled partial equations has been reduced to a system of coupled nonlinear ordinary differential equations. An efficient homotopy analysis

method (HAM) is employed to solve the system of equations. The obtained results are analyzed graphically. The analysis revels that the fluid flow is appreciably influenced by the physical parameters. It is expected that the results obtained will not only provide useful information for industrial applications but also complement the existing literature.

2.2   Mathematical Formulation

Consider a steady, mixed convection boundary layer flow of a viscous incompressible fluid over a continuously stretching sheet of variable thickness, subject to a transverse magnetic field B(x). The sheet is drawn through a slit located at the origin, where the x-axis runs along the stretching surface, in the direction of the sheet motion, and the y-axis is perpendicular to it. The flow configuration is illustrated in Fig.2.1.

(i). The wall is impermeable [see for details Liao [33],[34], $(v_w = 0)$].

(ii). The sheet is stretched with a velocity $U_w(x) = U_0(x + b)^m$ where U_0 is constant, b is a physical parameter related to stretching sheet and m is the velocity exponent parameter.

(iii). The sheet is not flat and its thickness is defined by $y = A(x+b)^{(1-m)/2}$, where the coefficient A is small so that the sheet is sufficiently thin, to avoid pressure gradient along the sheet $(\partial p/\partial x = 0)$.

(iv). The magnetic Reynolds number is assumed to be small so that the induced magnetic field is negligible.

(v). The viscous dissipation and Ohmic heating terms are not included in the energy equation since they are generally small.
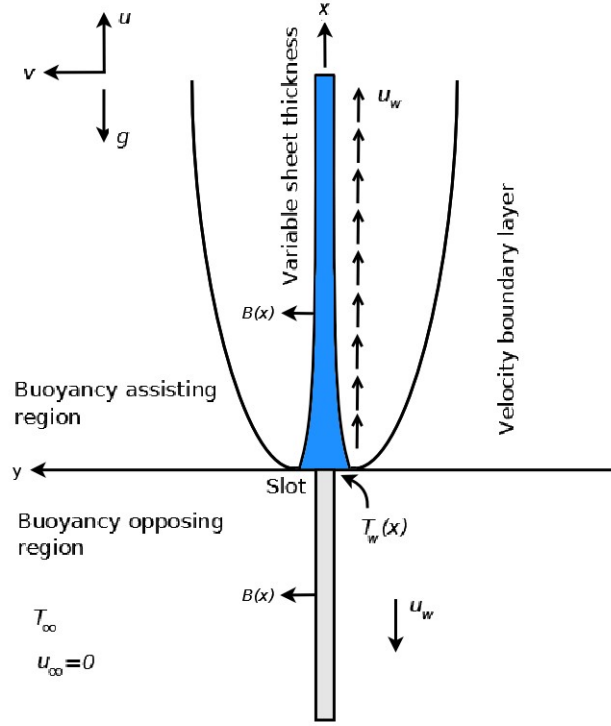
Figure 2.1: Schematic of the stretching sheet with variable thickness.

Under the usual boundary layer assumptions, the governing equations for mass, momentum and energy (see Fang et al. [26], and Ahmed et al. [29] for details) are

$$\frac{\partial u}{\partial x} + \frac{\partial v}{\partial y} = 0, \tag{2.1}$$

$$u\frac{\partial u}{\partial x} + v\frac{\partial v}{\partial y} = \nu\frac{\partial^2 u}{\partial y^2} - \frac{\sigma B_0^2}{\rho}u + g\beta(T - T_\infty), \tag{2.2}$$

$$u\frac{\partial T}{\partial x} + v\frac{\partial T}{\partial y} = \alpha_0\frac{\partial^2 T}{\partial y^2}, \tag{2.3}$$

10

where u, v are respectively the x, y-components of the fluid velocity; σ is the electrical conductivity; ρ is the density of the fluid and $B_0^2(x)$ is the strength of the magnetic field. The last term in right hand side of the Eq.(2.2) represents the influence of thermal buoyancy force on the flow field, with "+" and "−" signs refer to the buoyancy assisting and buoyancy opposing flows respectively. Figure 2.1 provides the necessary information of such a flow field for a stretching vertical heated sheet. For the assisting flow, the x-axis points upwards in the direction of the stretching hot surface such that the stretching induced flow and the thermal buoyant flow assist each other. For the opposing flow, the x-axis points vertically downwards in the direction of the stretching hot surface but in this case the stretching induced flow and the thermal buoyant flow oppose each other. The reverse trend occurs if the sheet is cooled below the ambient temperature. Here g is the acceleration due to gravity, β is the thermal expansion coefficient, T is the temperature of the fluid, and α_0 is the thermal diffusivity.We consider $B_0^2(x) = B_2^0(1 + x)^{1-m}$ (for details see Prasad et al. [32]). The corresponding boundary conditions are

$$u(x, y) = U_0(x + b)^m, \;\; v(x, y) = 0, \;\; T(x, y) = T_w = D\Big(\frac{x + b}{l}\Big)^{2m-1} \;\; at \;\; y = A(x + b)^{\frac{1-m}{2}},$$

$$u(x, y) \to 0, \;\; T \to T_\infty \;\; as \;\; y \to \infty,$$

$$\tag{2.4}$$

where T_w is the temperature at the surface, T_∞ is the free stream temperature, D is the thermal slip factor, and l is the characteristic length.We look for similarity solutions to Eqs. (2.1), (2.2) and (2.3), subject to the boundary conditions (2.4), of the form

$$\eta = y\sqrt{\frac{m + 1}{2} \frac{U_0(x + b)^{m-1}}{v}}, \tag{2.5}$$

$$\psi(x, y) = F(\eta)\sqrt{\frac{2}{m+1}vU_0(x+b)^{m+1}}, \tag{2.6}$$

$$\Theta(\eta) = \frac{T - T_\infty}{T_w - T_\infty}, \tag{2.7}$$

where η is the dimensionless similarity variable, $\psi(x, y)$ is the dimensionless stream function, and $\Theta(\eta)$ is the dimensionless temperature distribution. The stream function $\psi(x, y)$ identically satisfies the continuity Eq. (2.1), with $u = \frac{\partial \psi}{\partial y}$ and $v = -\frac{\partial \psi}{\partial x}$. From Eqs. (2.6) and (2.7), the velocity components can be written as

$$u = U_w f'(\eta) \quad \text{and} \quad v = -\sqrt{\nu\frac{m+1}{2}U_0(x+b)^{m-1}}\left[\eta f'(\eta)\left(\frac{m-1}{m+1}\right) + f(\eta)\right], \tag{2.8}$$

where $v = \frac{\mu}{\rho}$ is the kinematic viscosity and μ is the dynamic viscosity. In the present work, it is assumed $m > -1$ for the validity of the similarity transformations. Substituting Eqs. (2.5), (2.6) and (2.7) into Eqs. (2.1), (2.2) and (2.3), the non-dimensional governing equations become

$$F''' + FF'' - \left[\frac{2m}{m+1}\right](F')^2 - MnF' + \lambda\Theta = 0, \tag{2.9}$$

$$\Theta'' + Pr\left[F\Theta' - \frac{2(2m-1)}{m+1}F'\Theta\right] = 0, \tag{2.10}$$

subject to the boundary conditions

$$F(\alpha) = \alpha\left(\frac{1-m}{1+m}\right), \quad F'(\alpha) = 1, \quad F'(\infty) = 0, \quad \Theta(\alpha) = 1, \quad \text{and} \quad \Theta(\infty) = 0, \tag{2.11}$$

where $\lambda = \frac{Gr_x}{Re_x^2}$ is the mixed convection parameter, $Gr_x = \frac{g\beta(T_w - T_\infty)x^3}{\gamma^2}$ is the local Grashof number,

12

$Re_x = \frac{U_w x}{\gamma}$ is the local Reynolds number, and $Pr = \frac{\mu C_p}{k_\infty}$ is the Prandlt number. It should be mentioned that $\lambda > 0$ corresponds to the case of assisted flow, whereas $\lambda < 0$ corresponds to opposing flow, and $\lambda = 0$ corresponds to forced convection flow. Here, $\alpha = A\sqrt{\frac{m+1}{2}\frac{U_0}{\nu}}$ is a parameter related to the thickness of the wall (referred to as the wall thickness parameter) and $\eta = \alpha = A\sqrt{\frac{m+1}{2}\frac{U_0}{\nu}}$ indicates the plate surface.

In order to facilitate the computation, we define $F(\eta) = F(\eta - \alpha) = f(\xi)$ and $\Theta(\eta) = \Theta(\eta - \alpha) = \theta(\xi)$. The similarity Eqs. (2.9) - (2.10) and associated boundary conditions (2.11) become

$$f''' + ff'' - \left[\frac{2m}{m+1}\right](f')^2 - Mnf' + \lambda\theta = 0, \tag{2.12}$$

$$\theta'' + Pr\left[f\theta' - \frac{2(2m-1)}{m+1}f'\theta\right] = 0, \tag{2.13}$$

$$f(0) = \alpha\left(\frac{1-m}{1+m}\right), \quad f'(0) = 1, \quad f'(\infty) = 0, \quad \theta(0) = 1, \quad \text{and} \quad \theta(\infty) = 0, \tag{2.14}$$

where the prime denotes differentiation with respect to ξ. The non-dimensional magnetic parameter, Prandtl number, and mixed convection parameter are defined as follows:

$$Mn = \frac{\sigma B_0^2}{\rho U_0}, \quad Pr = \frac{\nu}{\alpha_0}, \quad \text{and} \quad \lambda = \frac{g\beta D}{l^{2m-1}U_0^2}. \tag{2.15}$$

The physical quantities of interest are the skin friction coefficient C_{f_x} and the local Nusselt number Nu_x, which are defined by

$$C_{f_x} = \frac{2\tau_{wx}}{\rho U_w^2} \quad \text{and} \quad Nu_x = \frac{(x+b)q_w}{k(T_w - T_\infty)}. \tag{2.16}$$

13

Here, τ_{wx} and q_w are the wall skin friction and heat flux, respectively

$$\tau_{wx} = \mu \left(\frac{\partial u}{\partial y} \right)_{y=A(x+b)^{\frac{1-m}{2}}} \quad \text{and} \quad q_w = -k \left(\frac{\partial T}{\partial y} \right)_{y=A(x+b)^{\frac{1-m}{2}}}, \tag{2.17}$$

where k is the thermal conductivity of the fluid. The non-dimensional local skin friction coefficient and non-dimensional local Nusselt number are

$$(Re)^{\frac{1}{2}} C_{f_x} \sqrt{\frac{2}{m+1}} = f''(0) \quad \text{and} \quad (Re)^{-\frac{1}{2}} Nu_x \sqrt{\frac{2}{m+1}} = -\theta'(0), \tag{2.18}$$

where $Re = \frac{U_w(x+b)}{\nu}$ is the local Reynolds number.

2.3   Homotopy Analysis Method

The governing equations are highly nonlinear, coupled ODEs with variable coefficients. We use the homotopy analysis method (HAM) to obtain appropriate analytic solutions to Eqs. (2.12)-(2.13) with associated boundary conditions (2.14). The HAM is based on the homotopy concept from topology. In this regard, a nonlinear problem is transformed into an infinite number of linear sub-problems. In the frame of the HAM, we have great freedom to choose the auxiliary linear operators and initial approximations. This is advantageous over other iterative techniques, where convergence is largely tied to good initial approximation of the solution. The HAM differs from other analytic approximation methods in that it does not depend on small or large physical parameters. This is achieved by inclusion of an artificial "convergence-control parameter," which conveniently guarantees convergence of the solution series. The HAM has been successfully applied to a wide variety of nonlinear problems(see for details Van Gorder and Vajravelu [35], Mallory and Van Gorder [36], Mallory and Van Gorder [37], Li et al. [38], Van Gorder et al. [39]).

For the considered problem, we choose the auxiliary linear operators $\mathcal{L}_f$ and $\mathcal{L}_\theta$ as

$$\mathcal{L}_f = \frac{\partial^3}{\partial \xi^3} - Mn\frac{\partial}{\partial \xi}, \tag{2.19}$$

$$\mathcal{L}_\theta = \frac{\partial^2}{\partial \xi^2} - 1, \tag{2.20}$$

and assume the following initial approximations

$$f_0(\xi) = \frac{1}{\sqrt{Mn}}\Big[1 + \alpha\Big(\frac{1-m}{1+m}\Big)\sqrt{Mn} - e^{-\sqrt{Mn}\xi}\Big], \tag{2.21}$$

$$\theta_0(\xi) = e^{-\xi}, \tag{2.22}$$

which satisfy the boundary conditions (2.14). The so-called zeroth-order deformation equations are given by

$$(1-q)\mathcal{L}_f[\hat{f}(\xi;q) - f_0(\xi)] + q\hbar_f \mathcal{N}_f[\hat{f}(\xi;q), \hat{\theta}(\xi;q)] = 0, \tag{2.23}$$

$$(1-q)\mathcal{L}_\theta[\hat{\theta}(\xi;q) - \theta_0(\xi)] + q\hbar_\theta \mathcal{N}_\theta[\hat{f}(\xi;q), \hat{\theta}(\xi;q)] = 0. \tag{2.24}$$

Here, $q \in [0,1]$ is an embedding parameter, $\hbar_f \neq 0$ and $\hbar_\theta \neq 0$ are the convergence-control parameters, and the nonlinear differential operators $\mathcal{N}_f$ and $\mathcal{N}_\theta$ are defined from Eqs. (2.12)-(2.13) as

$$\mathcal{N}_f[\hat{f}, \hat{\theta}] = \frac{\partial^3 \hat{f}}{\partial \xi^3} + \hat{f}\frac{\partial^2 \hat{f}}{\partial \xi^2} - \Big[\frac{2m}{m+1}\Big]\Big(\frac{\partial \hat{f}}{\partial \xi}\Big)^2 - Mn\frac{\partial \hat{f}}{\partial \xi} + \lambda\hat{\theta}, \tag{2.25}$$

$$\mathcal{N}_\theta[\hat{f}, \hat{\theta}] = \frac{\partial^2 \hat{\theta}}{\partial \xi^2} + Pr\Big[\hat{f}\frac{\partial \hat{\theta}}{\partial \xi} - \frac{2(2m-1)}{m+1}\frac{\partial \hat{f}}{\partial \xi}\hat{\theta}\Big]. \tag{2.26}$$

It can be seen that when $q = 0$, we have $\hat{f}(\xi;0) = f_0(\xi)$ and $\hat{\theta}(\xi;0) = \theta_0(\xi)$, while when $q = 1$

15

we have $\hat{f}(\xi; 1) = f(\xi)$ and $\hat{\theta}(\xi; 1) = \theta(\xi)$. By defining

$$f_n(\xi) = \frac{1}{n!} \frac{d^n f(\xi; q)}{d\xi^n}\bigg|_{q=0} \quad \text{and} \quad \theta_n(\xi) = \frac{1}{n!} \frac{d^n f(\xi; q)}{d\xi^n}\bigg|_{q=0}, \tag{2.27}$$

we may expand $\hat{f}(\xi; q)$ and $\hat{\theta}(\xi; q)$ about q, by means of Taylor series expansion to obtain

$$\hat{f}(\xi; q) = f_0(\xi) + \sum_{n=1}^{\infty} f_n(\xi) q^n, \quad \text{and} \quad \hat{\theta}(\xi; q) = \theta_0(\xi) + \sum_{n=1}^{\infty} \theta_n(\xi) q^n. \tag{2.28}$$

According to the method, if the series 2.28 converges at $q = 1$, then the HAM solution is given by

$$f(\xi) = f_0(\xi) + \sum_{n=1}^{\infty} f_n(\xi) \quad \text{and} \quad \theta(\xi) = \theta_0(\xi) + \sum_{n=1}^{\infty} \theta_n(\xi). \tag{2.29}$$

Thus, as q varies from 0 to 1, $\hat{f}(\xi; q)$ and $\hat{\theta}(\xi; q)$ vary continuously from the initial approximations, $f_0(\xi)$ and $\theta_0(\xi)$, to the solution of interest, $f(\xi)$ and $\theta(\xi)$.

To obtain $f_n(\xi)$ and $\theta_n(\xi)$, we recursively solve the so-called n^{th}-order deformation equations

$$\mathcal{L}_f[f_n(\xi) - \chi_n f_{n-1}(\xi)] = \hbar_f \mathcal{R}_n^f, \tag{2.30}$$

$$\mathcal{L}_\theta[\theta_n(\xi) - \chi_n \theta_{n-1}(\xi)] = \hbar_\theta \mathcal{R}_n^\theta, \tag{2.31}$$

with boundary conditions

$$f_n(0) = 0, \ f_n'(0) = 0, \ f_n'(\infty) = 0, \ \theta_n(0) = 0, \ \theta_n(\infty) = 0, \tag{2.32}$$

where

$$\mathcal{R}_n^f = \frac{1}{(n-1)!} \frac{\partial^{n-1} \mathcal{N}_f[\hat{f}(\xi;q), \hat{\theta}(\xi;q)]}{\partial q^{n-1}}\bigg|_{q=0}, \tag{2.33}$$

$$\mathcal{R}_n^\theta = \frac{1}{(n-1)!} \frac{\partial^{n-1} \mathcal{N}_\theta[\hat{f}(\xi;q), \hat{\theta}(\xi;q)]}{\partial q^{n-1}}\bigg|_{q=0}, \tag{2.34}$$

and

$$\chi_n = \begin{cases} 0, & n \le 1, \\ 1, & n > 1. \end{cases} \tag{2.35}$$

Finally, k^{th}-order approximate solution can be obtained by the partial sum

$$f_k(\xi) = f_0(\xi) + \sum_{n=1}^{k} f_n(\xi) \quad \text{and} \quad \theta_k(\xi) = \theta_0(\xi) + \sum_{n=1}^{k} \theta_n(\xi). \tag{2.36}$$

To compute the optimal value of the convergence-control parameters $\hbar_f$ and $\hbar_\theta$, we evaluate the error and minimize over $\hbar_f$ and $\hbar_\theta$. For the kth-order approximation, the exact squared residual error is given by

$$\hat{\mathcal{E}}_k^f(\hbar_f, \hbar_\theta) = \int_0^\infty \left(\mathcal{N}_f[f_k(\xi), \theta_k(\xi)] \right)^2 d\xi, \tag{2.37}$$

$$\hat{\mathcal{E}}_k^\theta(\hbar_f, \hbar_\theta) = \int_0^\infty \left(\mathcal{N}_\theta[f_k(\xi), \theta_k(\xi)] \right)^2 d\xi. \tag{2.38}$$

In practice, it is often too CPU intensive to evaluate $\hat{\mathcal{E}}_k^f$ and $\hat{\mathcal{E}}_k^\theta$, even for relatively low orders of approximation. To greatly decrease the computation time, we instead calculate the average squared
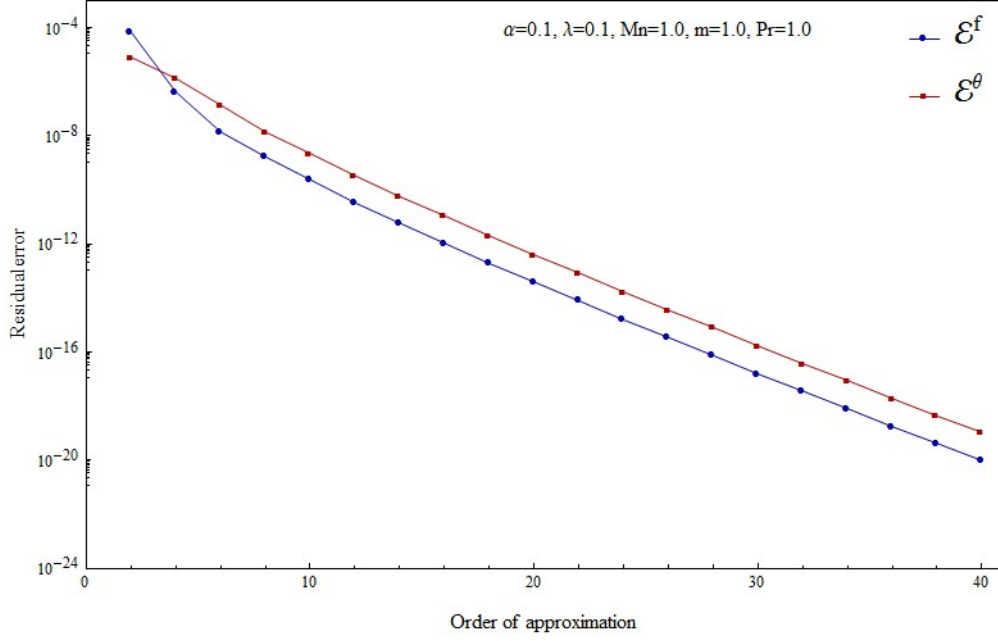
Figure 2.2: Residual error vs. order of approximation.

residual error,

$$\mathcal{E}_k^f(\hbar_f, \hbar_\theta) = \frac{1}{N+1} \sum_{i=0}^{N} \left(\mathcal{N}_f \left[\sum_{j=0}^{k} f_j(\xi_i), \sum_{j=0}^{k} \theta_j(\xi_i) \right] \right)^2, \qquad (2.39)$$

$$\mathcal{E}_k^\theta(\hbar_f, \hbar_\theta) = \frac{1}{N+1} \sum_{i=0}^{N} \left(\mathcal{N}_\theta \left[\sum_{j=0}^{k} f_j(\xi_i), \sum_{j=0}^{k} \theta_j(\xi_i) \right] \right)^2, \qquad (2.40)$$

where $\xi_i = i\delta\xi$, and N is an integer. For the kth-order approximation, the optimal values of $\hbar_f$ and $\hbar_\theta$ are determined by the minimizing the total error, defined by $\mathcal{E}_k^t(\hbar_f, \hbar_\theta) = \mathcal{E}_k^f(\hbar_f, \hbar_\theta) + \mathcal{E}_k^\theta(\hbar_f, \hbar_\theta)$. For computational purposes, we utilized the Mathematica package BVPH 2.0, developed by Liao. For more details, please refer to (http://numericaltank.sjtu.edu.cn/BVPH.htm).

2.4 Error Analysis

Here, we illustrate the accuracy of the method used in the present study. Without loss of generality, consider the case where $\alpha = 0.1$, $\lambda = 0.1$, $Mn = 1.0$, $m = 1.0$, and $Pr = 1.0$. Using the afore-mentioned technique, we obtain the 40th-order approximate solution. The corresponding optimal convergence-control parameters are found to be $\hbar_f = -0.6139$ and $\hbar_\theta = -1.2963$ with a total error of $\mathcal{E}_{40}^t = 9.9 \times 10^{-21}$. It is found that the residual error of each governing equation decreases as a function of order of approximation, as shown in Fig. 2.2. Moreover, errors of $\mathcal{E}_2^f = 1.3 \times 10^{-4}$ and $\mathcal{E}_2^\theta = 8.0 \times 10^{-4}$ can be obtained at only the 2nd-order approximation.

To validate the results obtained in the present work, we compare $-f''(0)$ with the numerical so-lution reported by Fang et al. [26], Khader and Megahed [30] for a special case where the mixed convection parameter and magnetic parameters have been neglected. The results, shown in Table 2.1, are in very good agreement. The effects of various pertinent parameters on the horizontal velocity field and temperature field are illustrated graphically in Figs. 2.3-2.13. It can be seen that both $f'(\xi)$ and $\theta(\xi)$ decrease monotonically and tend to zero asymptotically as the distance from the boundary increases. The effects of several parameters on the velocity and temperature gradients at the surface are shown in Table 2.2.

2.5 Results and Error Analysis

Figures 2.3-2.7 elucidate the effects of various pertinent parameters on the horizontal velocity. As m increases, $f'(\xi)$ increases and in turn velocity boundary layer thickness increases. This phenomenon is true even in the case of α and λ. Physically $\lambda > 0$ means heating of the fluid
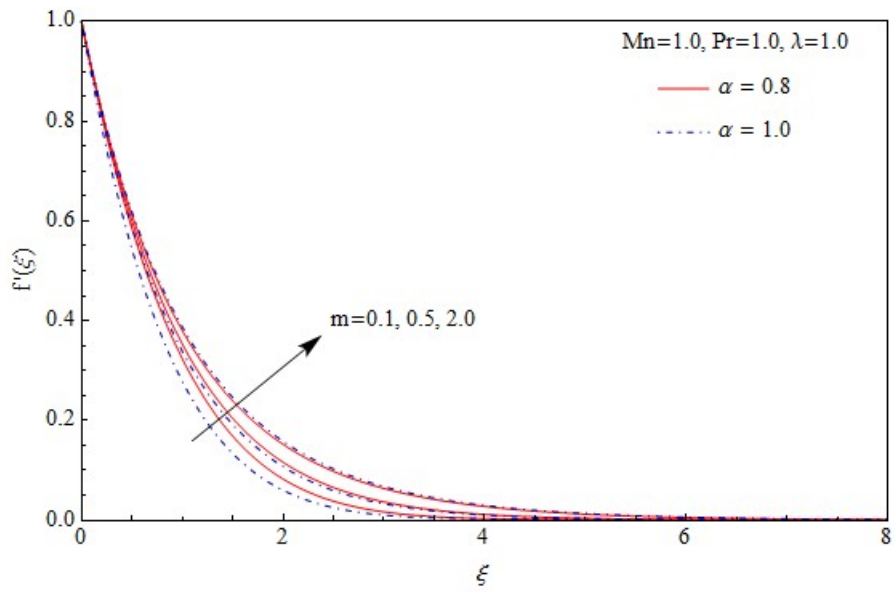
Figure 2.3: Horizontal velocity profiles for different values of α and m.
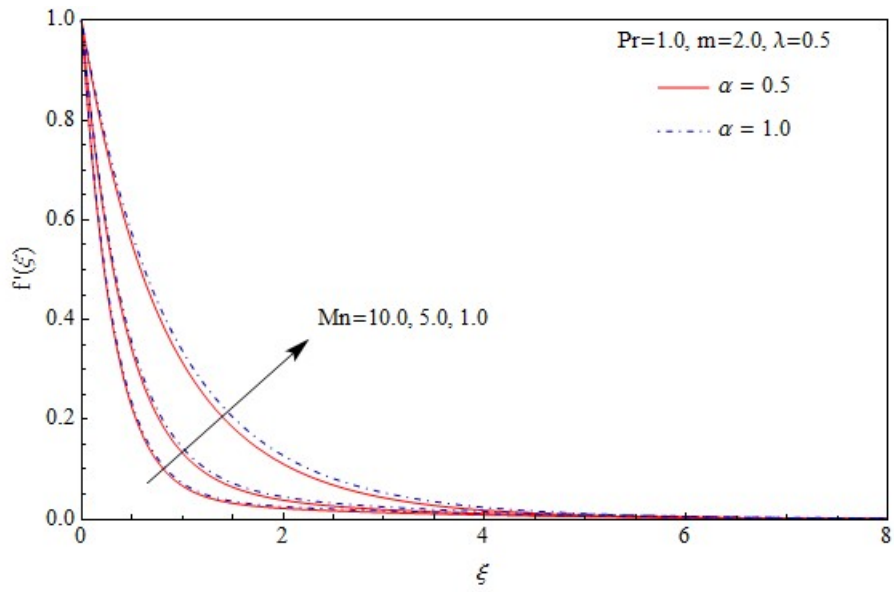
Figure 2.4: Horizontal velocity profiles for different values of α and Mn.
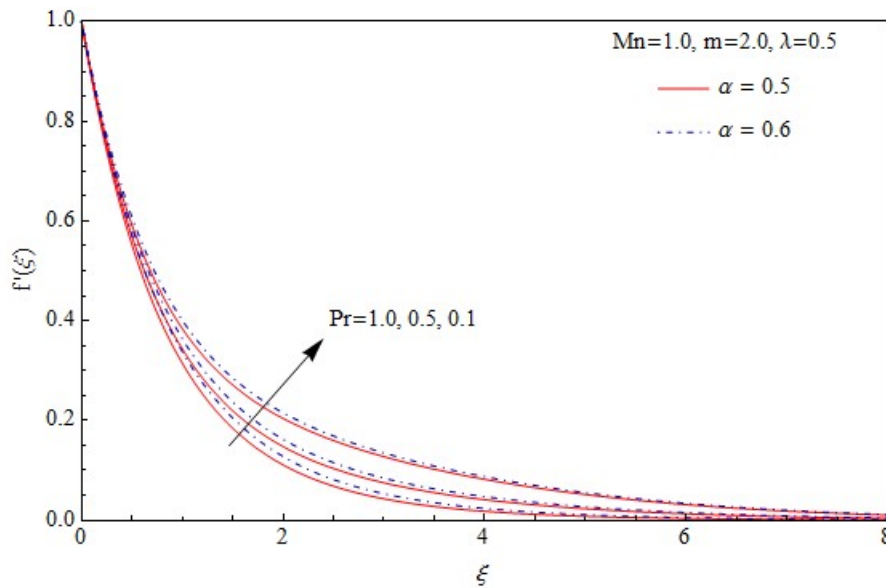
Figure 2.5: Horizontal velocity profiles for different values of α and Pr.

or cooling of the surface, $\lambda < 0$ means cooling of the fluid or heating of the surface, and $\lambda = 0$ corresponds to the absence of the mixed convection parameter. However, in the case of Mn and Pr the effect is completely reversed. Increase in Mn and Pr reduces the velocity and squeezes the thickness of the boundary layer (see Figs. 2.4-2.7). A change in the Lorentz force may be attributed to a change in Mn. Lorentz force produces resistance to the transport phenomena.

Figures 2.8- 2.13 demonstrate the nature of the temperature profiles with changes in the various physical parameters. Increasing values of m, α and λ reduce the profiles and decrease the thermal boundary layer thickness. Moreover, the effect of Mn and Pr is quite opposite to that of m and this is due to the Lorentz force phenomenon. However, the fluid with higher value of Pr possesses a large heat capacity, and hence intensifies the heat transfer.

Table 2.1: Comparison of results for $-f''(0)$ when $\lambda = 0$ and $Mn = 0$.

α	m	Khader and Megahed [30]	Fang et al. [26]	Present work		
				$-f''(0)$	$-\hbar_f$	$\mathcal{E}_{10}^f$
$^1/_2$	10	1.0603	1.0603	1.0603	1.0050	1.8×10^{-10}
	5	1.0486	1.0486	1.0486	1.0145	5.5×10^{-11}
	3	$* * *$	1.0359	1.0359	1.0299	9.2×10^{-12}
	2	$* * *$	1.0234	1.0234	1.0493	6.8×10^{-13}
	$^1/_2$	$* * *$	0.9799	0.9799	1.1012	1.9×10^{-14}
	0	0.9577	0.9576	0.9578	1.1438	6.2×10^{-8}
$^1/_4$	10	1.1433	1.1433	1.1433	0.8750	1.6×10^{-10}
	5	1.1186	1.1186	1.1186	0.9068	4.6×10^{-11}
	3	$* * *$	1.0905	1.0905	0.9463	7.6×10^{-12}
	$^1/_2$	$* * *$	0.9338	0.9338	1.1334	7.3×10^{-15}
	0	0.7843	0.7843	0.7845	1.2391	1.2×10^{-8}

Table 2.2: HAM results for $-f''(0)$ and $-\theta'(0)$ for different values of α, λ, Mn, m, and Pr.

α	λ	Mn	m	Pr	$-f''(0)$	$-\theta'(0)$	$-\hbar_f$	$-\hbar_\theta$	$\mathcal{E}_{10}^f$	$\mathcal{E}_{10}^\theta$
.5	.5	1	2	.71	1.2024	0.9763	0.7532	1.2563	1.9×10^{-9}	1.3×10^{-9}
1					1.1322	0.9304	0.7645	1.2952	3.7×10^{-9}	2.4×10^{-9}
		1			0.9481	0.9762	1.0978	1.1446	5.4×10^{-10}	5.2×10^{-10}
			2		1.2738	0.9064	1.1057	1.2091	1.3×10^{-8}	5.4×10^{-9}
			5		1.2398	1.0402	1.0090	0.9538	2.0×10^{-7}	1.1×10^{-7}
				7	1.3567	2.7146	0.1500	0.4551	2.3×10^{-5}	1.1×10^{-7}

The skin friction at the surface as a function of m is shown in Fig. 2.14 for various values of Pr. It is found that the skin friction decreases with an increase in m and Pr. Figure 2.15 depicts the local Nusselt number as a function of α for various values of Mn. It can be seen that the Nusselt number increases with increasing Mn and α.
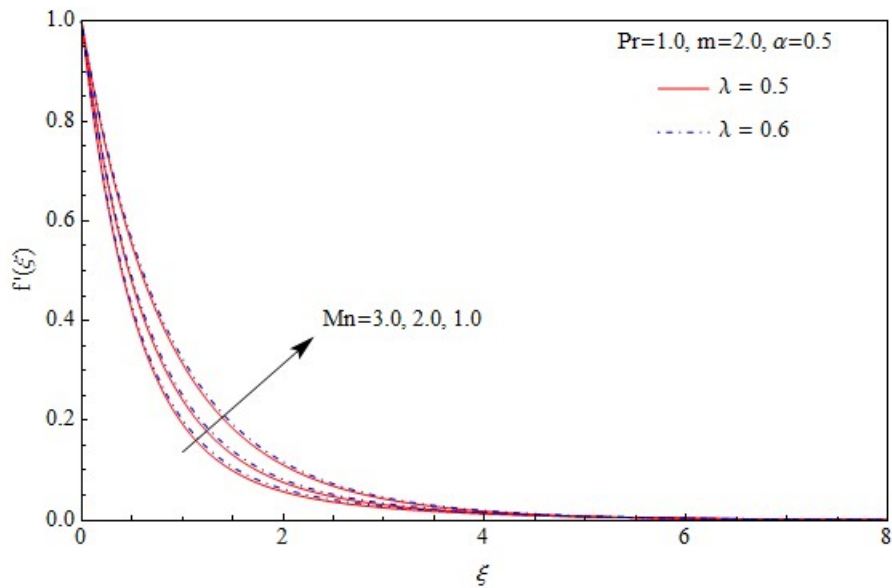
Figure 2.6: Horizontal velocity profiles for different values of λ and Mn.

2.6   Discussion

Heat transfer characteristics for mixed convection boundary layer flow of a viscous incompressible fluid over a continuously stretching sheet of variable thickness subject to a transverse magnetic field are analyzed. A transformed set of self-similar equations is obtained. The reduced equations are then solved via HAM. Fluid velocity is found to decrease with increasing magnetic parameter whereas quite the opposite is true with the temperature. The non-dimensional temperature decreases with increasing Prandtl number. It is observed that an increasein the wall thickness parameter significantly affect the velocity and the temperature gradients.
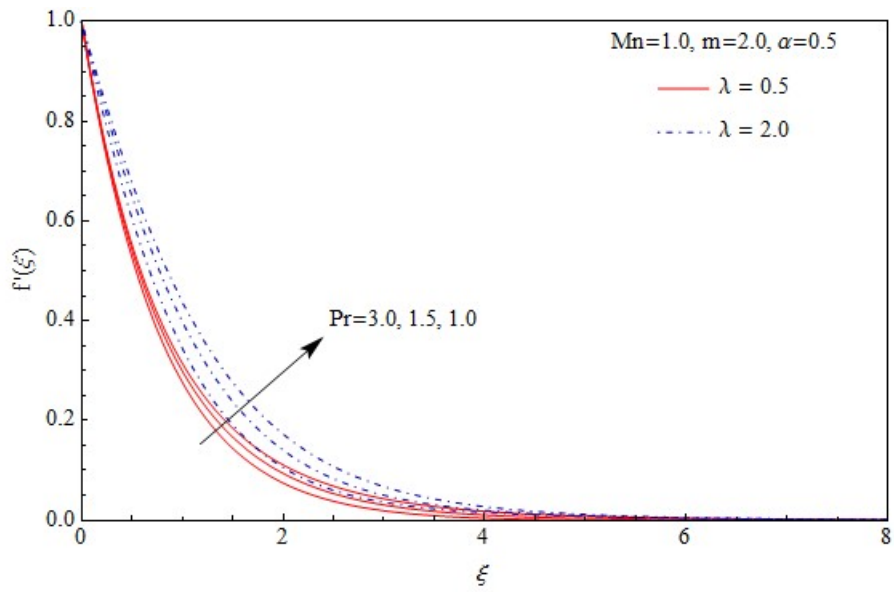
Figure 2.7: Horizontal velocity profiles for different values of λ and Pr.
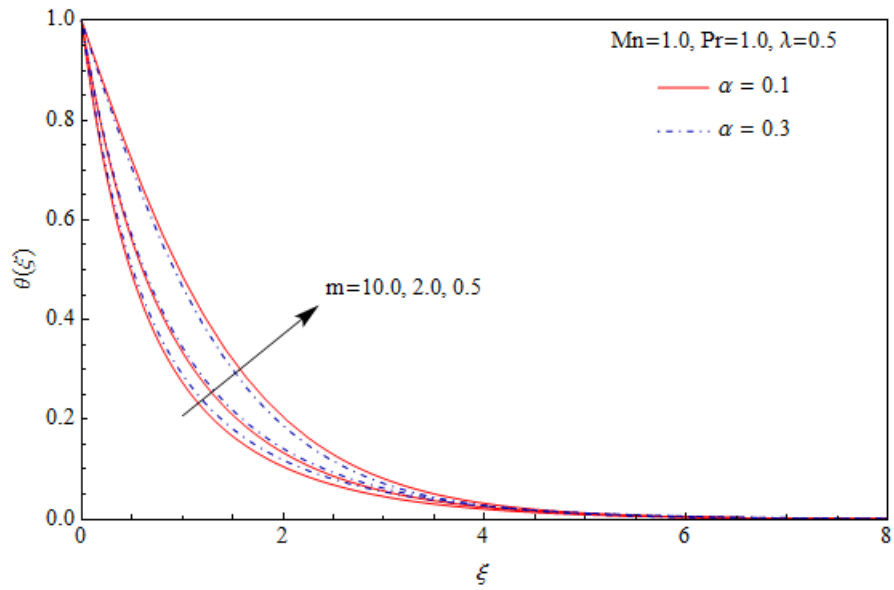
Figure 2.8: Temperature profiles for different values of α and m.
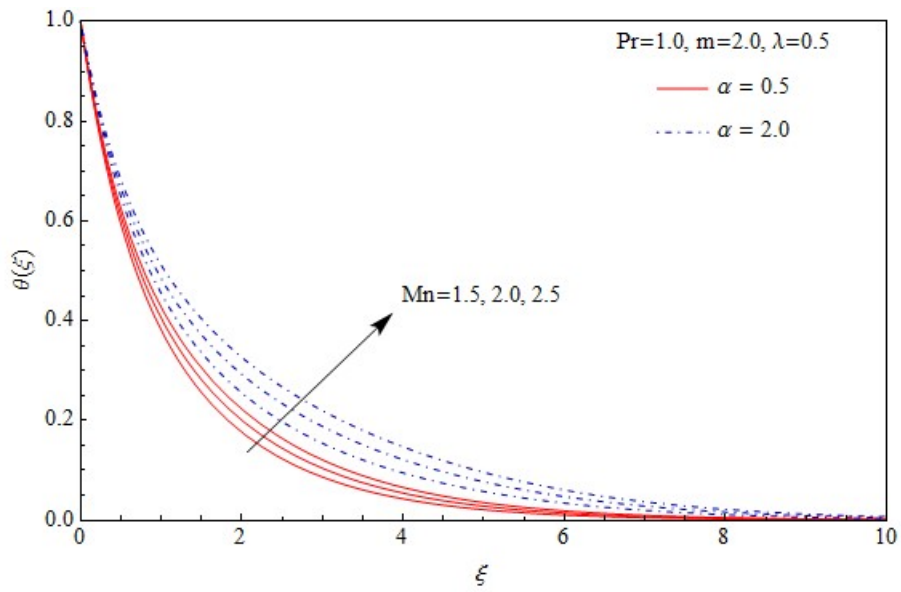
Figure 2.9: Temperature profiles for different values of α and Mm.
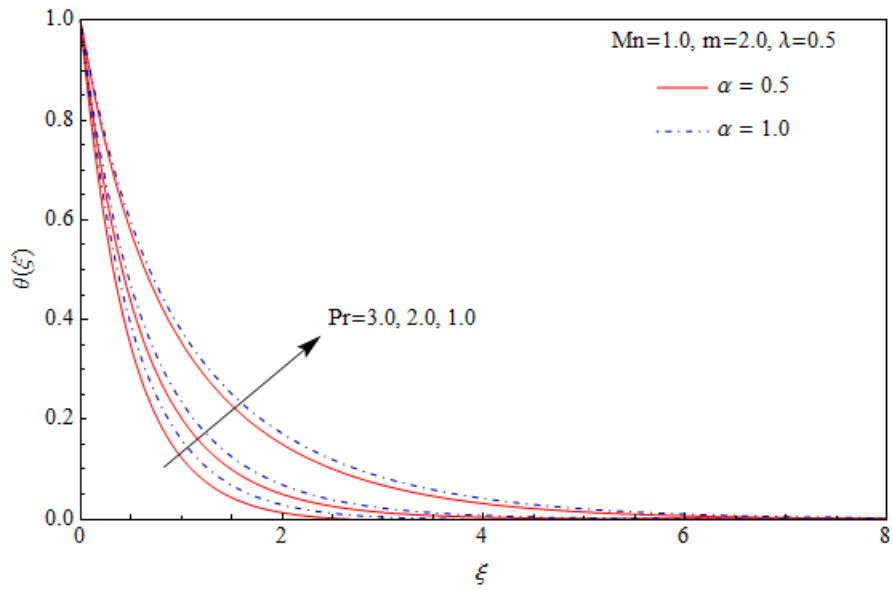
Figure 2.10: Temperature profiles for different values of α and Pr.
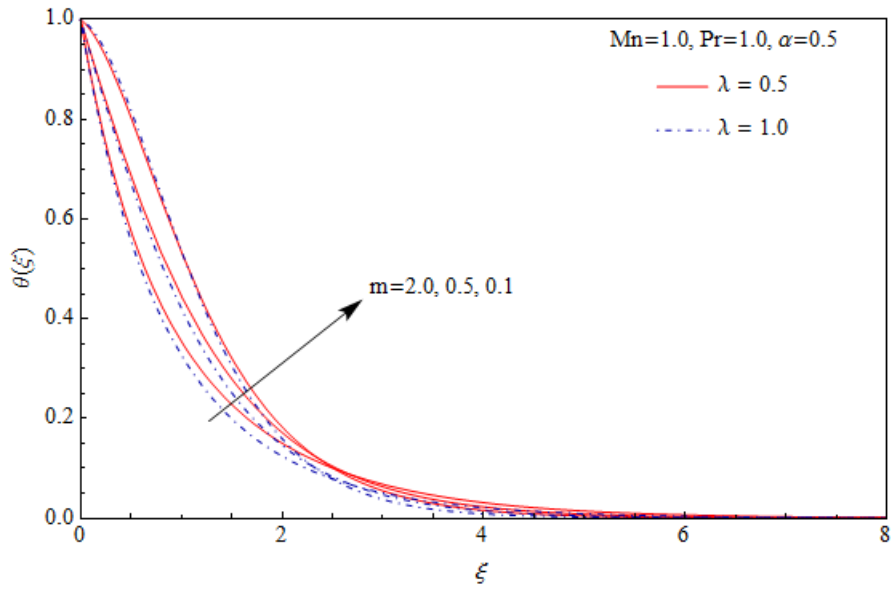
Figure 2.11: Temperature profiles for different values of λ and m.
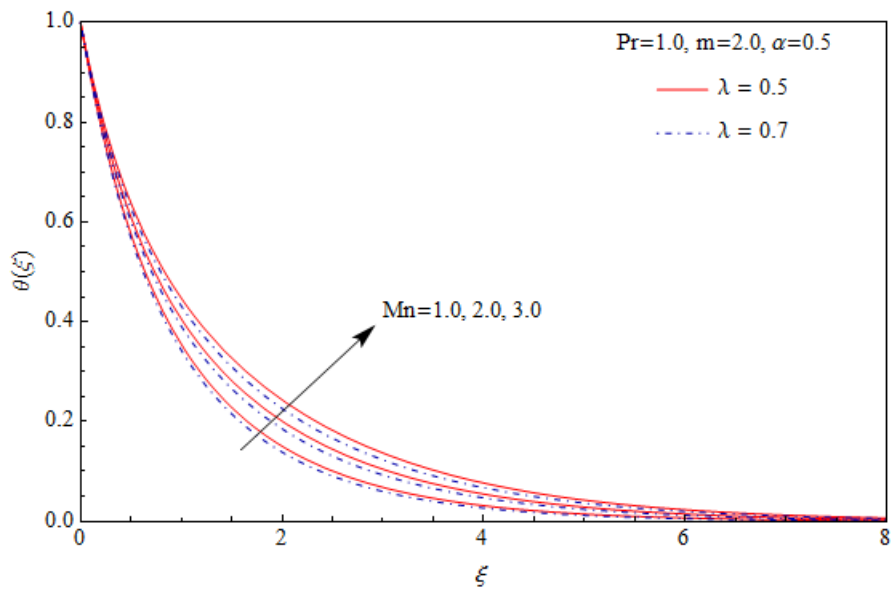
Figure 2.12: Temperature profiles for different values of λ and Mn.

26
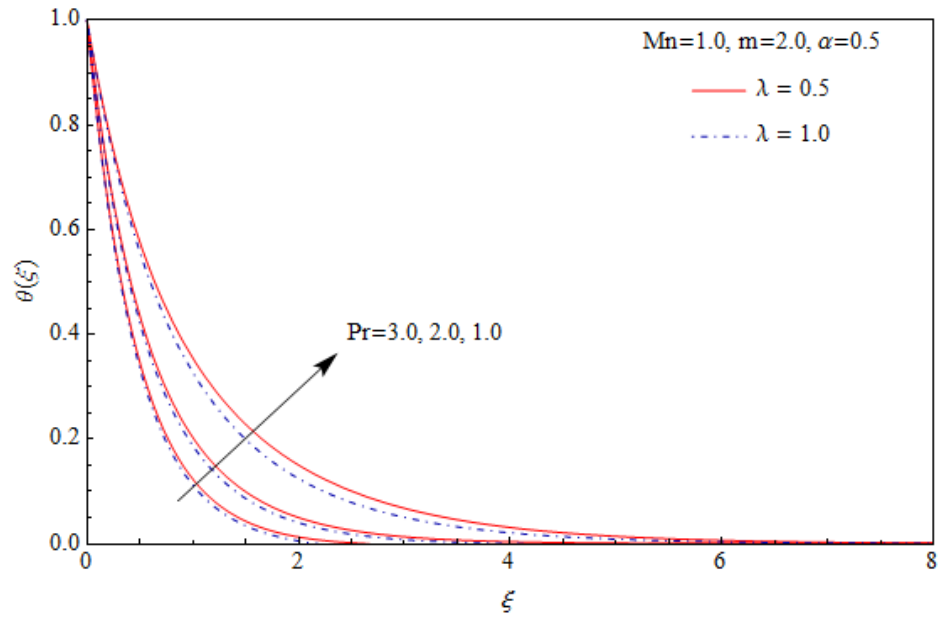
Figure 2.13: Temperature profiles for different values of λ and Pr.
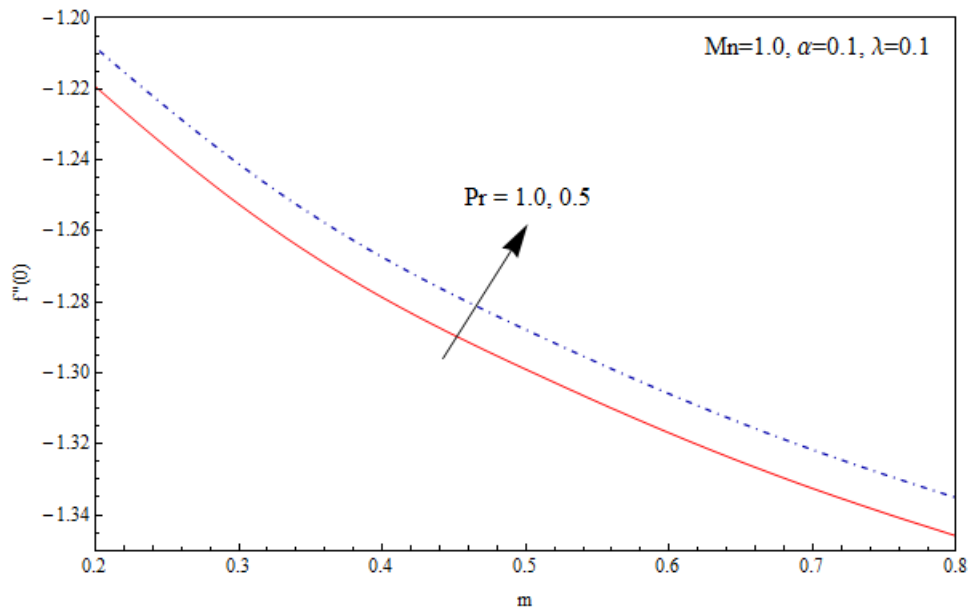
Figure 2.14: Skin friction coefficient versus m for different values of Pr.
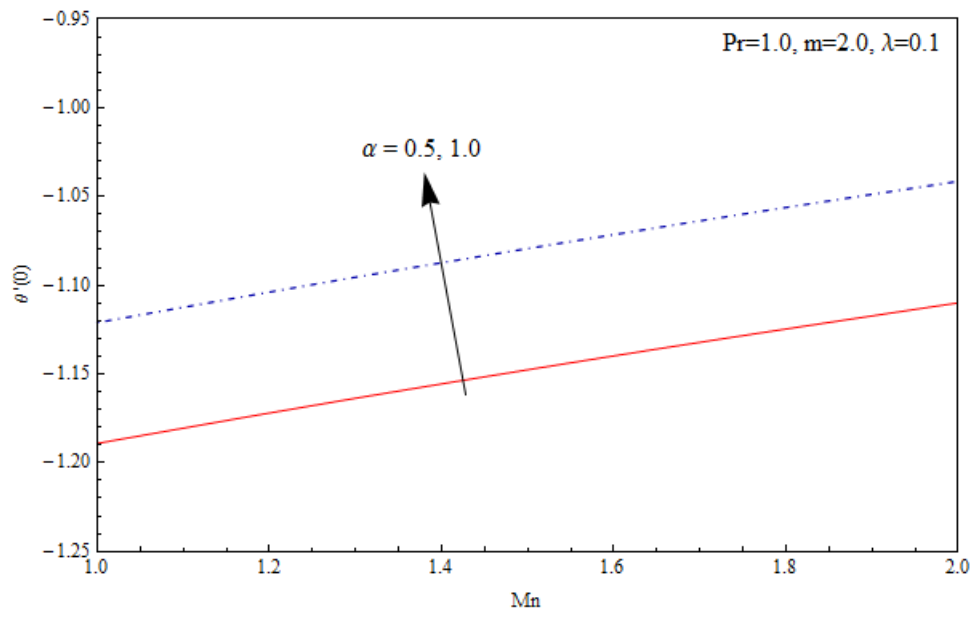
Figure 2.15: Nusselt number versus Mn for different values of α.

CHAPTER 3: A METHOD OF DIRECTLY DEFINING THE INVERSE MAPPING FOR SOLUTIONS OF COUPLED SYSTEMS OF NONLINEAR DIFFERENTIAL EQUATIONS

Recently, Liao introduced a new method for finding analytical solutions to nonlinear differential equations. In this chapter, we extend this idea to nonlinear systems. We study the system of nonlinear differential equations that governs nonlinear convective heat transfer at a porous flat plate, and find functions that approximate the solutions by extending Liao's Method of Directly Defining the Inverse Mapping (MDDiM). These results were considered in Baxter et al. [40].

3.1   Background

Consider the free convection flow at a vertical flat plate embedded in a saturated porous medium, where the temperature of the plate is described by a power function of distance given by $T_w = T_\infty \pm Ax^\lambda$ (with T_∞ denoting temperature far away from the plate, $A > 0$ and λ represents the exponent of the power function) and the discharge or withdrawal rate is given by $V_w = ax^n$, where $n = \frac{\lambda-1}{2}$, and where $a > 0$ for the discharge of fluid and $a < 0$ for withdrawal of the fluid. The

equations governing the fluid flow and heat transfer are (for details see Vajravelu et al. [41])

$$\frac{\partial u}{\partial x} + \frac{\partial v}{\partial y} = 0, \tag{3.1}$$

$$u = -\frac{K}{\mu}\left[\frac{\partial p}{\partial x} \pm pg\right], \tag{3.2}$$

$$v = -\left(\frac{K}{\mu}\right)\frac{\partial p}{\partial y}, \tag{3.3}$$

$$u\frac{\partial T}{\partial x} + v\frac{\partial T}{\partial y} = \alpha_0\left(\frac{\partial^2 T}{\partial x^2} + \frac{\partial^2 T}{\partial y^2}\right) + \frac{Q}{(\rho_\infty C_\rho)_f}(T - T_\infty), \tag{3.4}$$

$$\rho = \rho_\infty\left[1 - \beta_0(T - T_\infty) - \beta_1(T - T_\infty)^2\right]. \tag{3.5}$$

The boundary conditions for the problem are

$$v = ax^n, \quad T = T_\infty \pm Ax^n \text{ at } y = 0, \tag{3.6}$$

$$u \to 0, \quad T \to \text{ as } y \to \infty, \tag{3.7}$$

where u, v are the Darcy velocities in the x and y directions, ρ, μ, and β are, respectively, the density, viscosity, and thermal expansion coefficient of the fluid, K is the permeability of the saturated porous medium, and $\alpha_0 = \frac{K_m}{(\rho_\infty C_p)_f}$ is the equivalent thermal diffusivity, where K_m denotes the thermal conductivity of the saturated porous medium and $(\rho_\infty C_p)_f$ is the density and specific heat of the fluid. T, p, and g are temperature, pressure, and gravitational acceleration, respectively. It can be shown that similarity transformation and solutions to equations (2.1) - (2.7) exist if $n = \frac{\lambda-1}{2}$. Under this assumption and using the stream function ψ defined by $u = \frac{\partial \psi}{\partial y}$ and $v = -\frac{\partial \psi}{\partial x}$, the governing equation and the conditions can be written as (see [42] for details)

$$f'' - (1 + \gamma\theta)\theta' = 0, \tag{3.8}$$

$$\theta'' + \left(\frac{1+\lambda}{2}\right) f\theta' - (\lambda f' - \alpha)\theta = 0, \tag{3.9}$$

$$f(0) = f_w, \quad f' \to 0 \text{ as } \eta \to \infty, \tag{3.10}$$

$$\theta(0) = 1, \quad \theta \to 0, \text{ as } \eta \to \infty, \tag{3.11}$$

where

$$\eta = \left[\frac{\rho_\infty g \beta_0 K}{\mu \alpha_0 x}|T_w - T_\infty|\right]^{\frac{1}{2}} \cdot y, \tag{3.12}$$

$$\psi = \left[\frac{\alpha_0 \rho_\infty g \beta_0 K |T_w - T_\infty| x}{\mu}\right]^{\frac{1}{2}} f(\eta), \tag{3.13}$$

$$\theta(\eta) = \frac{T - T_\infty}{T_w - T_\infty}, \tag{3.14}$$

$$\gamma = 2\beta_1 |T_w - T_\infty|/\beta_0, \tag{3.15}$$

$$\alpha = Qx^2/\alpha Ra_x(\rho_\infty C_\rho)_f, \tag{3.16}$$

$$Ra_x = \rho_\infty g \beta_0 K |T_w - T_\infty| x/\mu \alpha_0. \tag{3.17}$$

and

$$f_w = -2a/(1+\lambda)[\alpha_0 \rho_\infty g \beta K A/\mu]^{\frac{1}{2}}. \tag{3.18}$$

Existence and uniqueness as well as numerical results are established for this system in [41].

The Homotopy Analysis Method (HAM) has been used to find analytical solutions to nonlinear differential equations where only numerical results exist in the literature (see [1], [2], [37], [43]-[52]). The method uses a homotopy of differential operators, where the homotopy parameter is
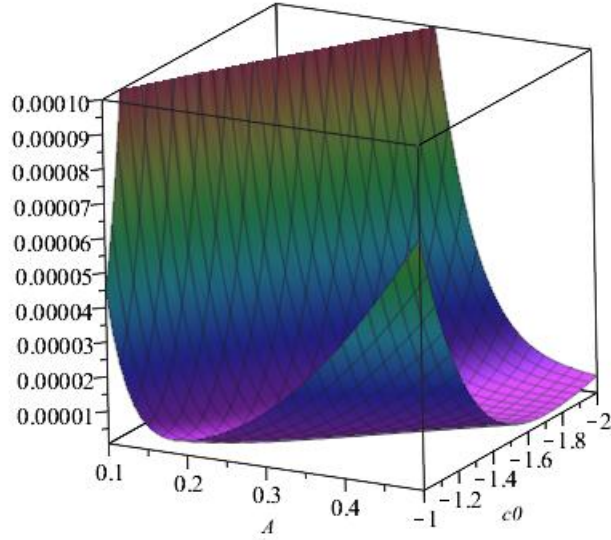
Figure 3.1: Plot of $E(c_0, A)$, the squared residual error over $\eta \in [0, 499]$ as a function of c_0 and A using parameter values $f_w = -1$, $\alpha = -1$, $\gamma = -0.5$, $\lambda = -0.2$. The error function has minimum $E(c_0, A) = 6.6049 \times 10^{-7}$ where $c_0 = -1.3279$ and $A = 0.2869$.

perturbed. This changes the nonlinear problem into infinitely many linear problems that can be solved one at a time, where each successive equation depends on the previous iterates.

In this paper we study the coupled system through the Homotopy Analysis Method using the Directly Defined Inverse Method (MDDiM). This method was outlined by Liao for single equations (see [3]). Here we extend this method to a coupled system of nonlinear differential equations.

3.2 HAM and MDDIM

In this section, we discuss the setup of the problem using the details of the HAM (see [1] and [2] for details) and MDDiM for the nonlinear system. First, we discuss the spaces that the solutions and
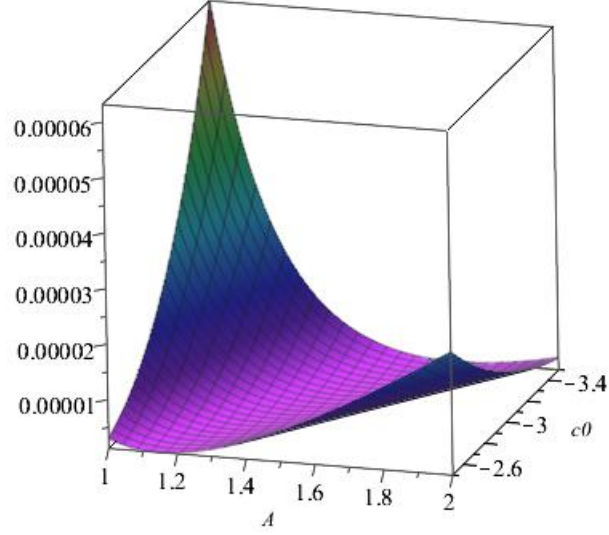
Figure 3.2: Plot of $E(c_0, A)$, the squared residual error over $\eta \in [0, 499]$ as a function of c_0 and A using parameter values $f_w = -1$, $\alpha = -1$, $\gamma = 0$, $\lambda = 0.2$. The error function has minimum $E(c_0, A) = 1.2539 \times 10^{-6}$ where $c_0 = -3$ and $A = 1.4257$.

base functions are coming from. Then we derive the deformation equations we are trying to solve. Finally, we use the Method of directly defining the inverse mapping to solve these deformation equations, and discuss the solutions. Define two nonlinear operators

$$N_1[f(\eta), \theta(\eta)] = f'' - (1 + \gamma\theta)\theta', \tag{3.19}$$

$$N_2[f(\eta), \theta(\eta)] = \theta'' + \left(\frac{1+\lambda}{2}\right) f\theta' - (\lambda f' - \alpha)\,\theta, \tag{3.20}$$

so that $N_1[f(\eta), \theta(\eta)] = 0$ and $N_2[f(\eta), \theta(\eta)] = 0$ give the original coupled equations (3.8) and

33

(3.9), respectively. Take the linearly independent set of functions

$$S_\infty = \left\{ 1, e^{-\eta}, e^{-2\eta}, \ldots \right\},$$ (3.21)

and define the space of functions that is their linear combinations to be

$$V = \left\{ \sum_{k=0}^{\infty} a_k e^{-k\eta} \middle| a_k \in \mathbb{R} \right\}.$$ (3.22)

This is the space of functions that the approximate solutions $f(\eta)$ and $\theta(\eta)$ will come from. Take the first two members of S_∞ and define

$$S^* = \left\{ 1, e^{-\eta} \right\}.$$ (3.23)

Two members are chosen because there are two boundary conditions on each of the equations. The functions from the space

$$V^* = \left\{ a_0 + a_1 e^{-\eta} \middle| a_0, a_1 \in \mathbb{R} \right\}$$ (3.24)

have their coefficients determined in order to satisfy the boundary conditions. Then the primary solution, $\mu(\eta) \in V^*$, which is the initial guess, has the form

$$\mu(\eta) = \sum_{j=0}^{1} a_j e^{-\eta}.$$ (3.25)

Next, define $\widehat{S}$ to be the remaining base functions

$$\widehat{S} = \left\{ e^{-2\eta}, e^{-3\eta}, \ldots \right\},$$ (3.26)
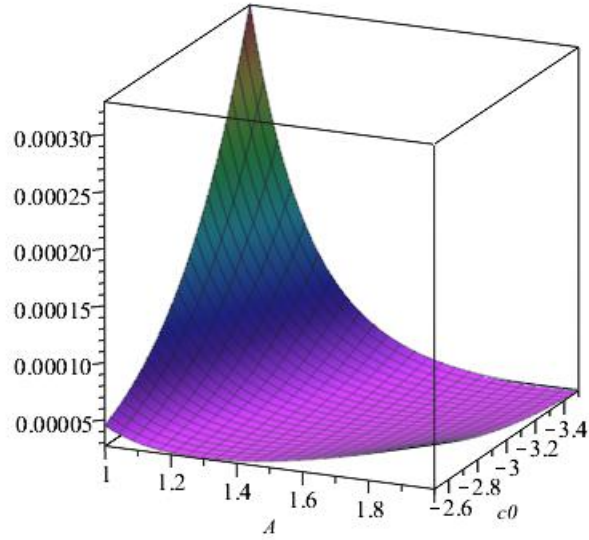
Figure 3.3: Plot of $E(c_0, A)$, the squared residual error over $\eta \in [0, 499]$ as a function of c_0 and A using parameter values $f_w = -1$, $\alpha = -1$, $\gamma = 0.5$, $\lambda = 0$. The error function has minimum $E(c_0, A) = 2.7322 \times 10^{-5}$ where $c_0 = -3$ and $A = 1.5851$.

and define $\widehat{V}$ so that $V = \widehat{V} \cup V^*$. That is,

$$\widehat{V} = \left\{ \sum_{k=2}^{\infty} b_k e^{-k\eta} \Big| b_k \in \mathbb{R} \right\}. \tag{3.27}$$

Define a linearly independent set of functions

$$S_R = \{\psi_1(\eta), \psi_2(\eta), \ldots\}, \tag{3.28}$$

so that S_R is a basis for expressions in the codomain of the operators N_1 and N_2. Then let U be

35
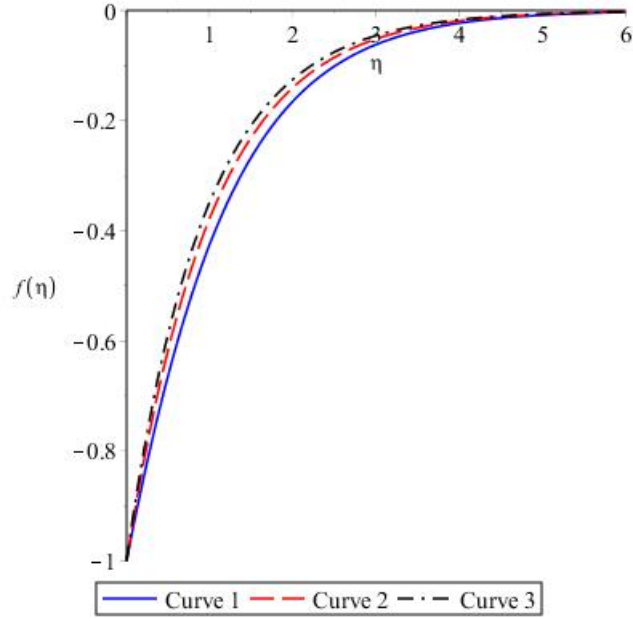
Figure 3.4: Plot of $\widehat{f}(\eta)$, where Curve 1 has $f_w = -1$, $\alpha = -1$, $\gamma = -0.5$, $\lambda = -0.2$, Curve 2 has $f_w = -1$, $\alpha = -1$, $\gamma = 0$, $\lambda = 0.2$, and Curve 3 has $f_w = -1$, $\alpha = -1$, $\gamma = 0.5$, $\lambda = 0$ using their respective error-minimizing convergence control parameter.

the set of all linear combinations of functions from S_R:

$$U = \left\{ \sum_{k=1}^{\infty} c_k \psi_k(\eta) \big| c_k \in \mathbb{R} \right\}. \tag{3.29}$$

Assuming that $N_1[f(\eta), \theta(\eta)], N_2[f(\eta), \theta(\eta)] \in U$, then $N_1 : V \to U$ and $N_2 : V \to U$. Now let us look into the implementation of the Homotopy Analysis Method. Define two homotopies of operators

$$0 \equiv \mathcal{H}_1(f, \theta, q) = (1 - q)L_1[f] - c_0 q N_1[f, \theta], \tag{3.30}$$

$$0 \equiv \mathcal{H}_2(f, \theta, q) = (1 - q)L_2[\theta] - c_1 q N_2[f, \theta]. \tag{3.31}$$
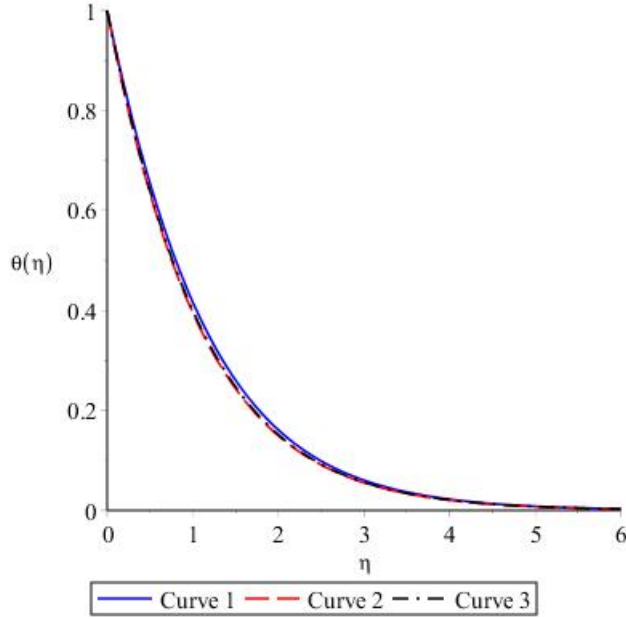
Figure 3.5: Plot of $\widehat{\theta}(\eta)$, where Curve 1 has $f_w = -1$, $\alpha = -1$, $\gamma = -0.5$, $\lambda = -0.2$, Curve 2 has $f_w = -1$, $\alpha = -1$, $\gamma = 0$, $\lambda = 0.2$, and Curve 3 has $f_w = -1$, $\alpha = -1$, $\gamma = 0.5$, $\lambda = 0$ using their respective error-minimizing convergence control parameter.

Here $\mathcal{H}_1$ and $\mathcal{H}_2$ are the homotopies of operators between linear operators L_1, L_2 and nonlinear operators N_1, N_2. The homotopy parameter $q \in [0, 1]$ and the convergence control parameters are c_0 and c_1. The convergence control parameters will be used to optimize the function approxima-tions in the next section. Now assume expansions of f and θ in terms of the homotopy parameter:

$$f(\eta) = f_0(\eta) + \sum_{k=1}^{\infty} f_k(\eta)q^k, \tag{3.32}$$

$$\theta(\eta) = \theta_0(\eta) + \sum_{k=1}^{\infty} \theta_k(\eta)q^k. \tag{3.33}$$

Here $f_0(\eta) \in V^*$ and $\theta_0(\eta) \in V^*$ are initial guesses that satisfy the boundary conditions.

37
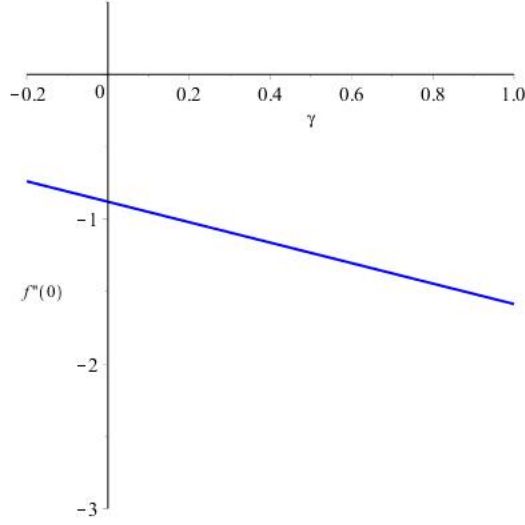
Figure 3.6: Plot of $\widehat{f}''(0)$ versus γ, using $f_w = -1$, $\alpha = -1$, $\lambda = 0.2$, $A = 1.4257$ and $c_0 = -3$.

Note that when $q = 0$ in the homotopies (3.30) and (3.31), they become $L_1[f] = 0$ and $L_2[\theta] = 0$; but when $q = 1$, the original nonlinear differential equations $N_1[f, \theta] = 0$ and $N_2[f, \theta] = 0$ are recovered. Likewise, when $q = 1$ in the expansions (3.32) and (3.33), the solutions f and θ are a sum of the components $f_1, f_2, \ldots$ and $\theta_1, \theta_2, \ldots$. We get these expansions (3.32) and (3.33) into the first homotopy (3.30), and the deformation equations are

$$L_1[f_0(\eta)] = 0, \quad f_0(0) = f_w, \quad f_0' \to 0 \text{ as } \eta \to \infty, \tag{3.34}$$

and for $k \geq 1$ we have

$$L_1[f_k(\eta)] = \chi_k L_1[f_{k-1}(\eta)] + c_0 \delta_{k-1}^1(\eta), \quad f_k(0) = 0, \quad f_k' \to 0 \text{ as } \eta \to \infty, \tag{3.35}$$

38
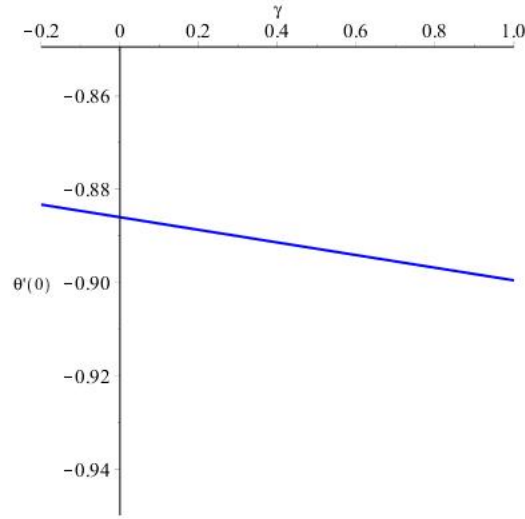
Figure 3.7: Plot of $\widehat{\theta'}(0)$ versus γ, using $f_w = -1$, $\alpha = -1$, $\lambda = 0.2$, $A = 1.4257$ and $c_0 = -3$.

where

$$
\chi_k = \begin{cases} 0, & k \leq 1, \\ 1, & k \geq 1. \end{cases} \tag{3.36}
$$

Here δ_k^ξ, for $\xi = 1, 2$, is the homotopy derivative defined to be

$$
\delta_{k-1}^\xi(\eta) = \frac{1}{(k-1)!} \left(\frac{\partial^{k-1}}{\partial q^{k-1}} N_\xi \left[\sum_{j=0}^{\infty} f_j(\eta) q^j, \sum_{j=0}^{\infty} \theta_j(\eta) q^j \right] \right) \Big|_{q=0}. \tag{3.37}
$$

On the other hand, if the expansions (3.32) and (3.33) are plugged into the second homotopy (5.29), then the other set of deformation equations is obtained:

$$
L_2[\theta_0(\eta)] = 0, \quad \theta_0(0) = 1, \quad \theta_0 \to 0 \text{ as } \eta \to \infty, \tag{3.38}
$$

and for $k \geq 1$

$$L_2[\theta_k(\eta)] = \chi_k L_2[\theta_{k-1}(\eta)] + c_1 \delta_{k-1}^2(\eta), \quad \theta_k(0) = 0, \quad \theta_k \to 0 \text{ as } \eta \to \infty. \tag{3.39}$$

The benefit of the Homotopy Analysis Method is that the linear operators L_1 and L_2 can be chosen so that the corresponding type of equations (3.35) and (3.39) are determined. Then, the number of terms desired of $f_k \in V$ and $\theta_k \in V$ can be computed iteratively. That is, f_0 and θ_0 are used to find f_1 and θ_1, and so on.

There has been great success in refining the method. The choice of auxiliary linear operator and convergence control parameters has been studied in [43] - [45]. Progress is made in the search for a linear operator that works well with partial differential equations in [46], [47], [50]. Control of residual error and stability of the choice of linear operator that leads to the so-called optimal HAM is studied in [37], [48], [49], [51]. The latest innovation by Liao [3] is to directly define the inverse mapping in the linear deformation equations. This is done because even with a few terms the HAM can lead to overwhelming computations, even with the simplest linear operator.

Using Liao's Method of Directly Defined Inverses, the deformation equations (3.35) and (3.39) are

$$f_k(\eta) = \chi_k f_{k-1}(\eta) + c_0 \mathscr{J}\left[\delta_{k-1}^1(\eta)\right] + a_{k,1}e^{-\eta} + a_{k,0}, \tag{3.40}$$

$$\theta_k(\eta) = \chi_k \theta_{k-1}(\eta) + c_1 \mathscr{J}\left[\delta_{k-1}^2(\eta)\right] + b_{k,1}e^{-\eta} + b_{k,0}. \tag{3.41}$$

In our work the inversely defined mapping, $\mathscr{J}$, is the same for both equations. But different directly defined inverses could be chosen if a different structure for the solutions f and θ is required.

Define $\mathscr{J}: U \to V$ by

$$\mathscr{J}\left[e^{-k\eta}\right] = \frac{e^{-k\eta}}{Ak^3 + k},$$ (3.42)

where the $Ak^3 + k$ is used to weight terms with larger values of k less than terms with smaller values of k, and A is a parameter.

It is possible to associate this inverse linear operator with the linear operator $L[u] = -(u''' + u')$. However, note that $L[c_1 + c_2 \sin \eta + c_3 \cos \eta] = 0$. Since $\sin \eta$ and $\cos \eta$ are periodic functions, they do not tend to zero as $\eta \to \infty$ and therefore do not satisfy the boundary conditions. So in the normal HAM, this linear operator does not work. However, it will work in the frame of MDDiM. This is an advantage of the MDDiM.

The choice of exponential base functions is due to the fact that the boundary value problem (3.8)-(3.11) admits an exact solution when $\alpha = \lambda = 0$ and $\lambda = 1$. From [41] the exact solution is

$$f(\eta) = \zeta - (\zeta - f_w)e^{-\zeta\eta},$$ (3.43)

$$\theta(\eta) = \zeta(\zeta - f_w)e^{-\zeta\eta},$$ (3.44)

where

$$\zeta = \frac{f_w + \sqrt{(f_w)^2 + 4}}{2}.$$ (3.45)

Note that each function f_k can be split into

$$f_k(\eta) = \widehat{f_k}(\eta) + f_k^*(\eta),$$ (3.46)

where each $\widehat{f_k} \in \widehat{V}$ and each $f_k^* \in V^*$, so that $f_k \in V$. The $\widehat{f_k}$ comes from the inverse linear operator, and the f_k^* has coefficients used to satisfy the boundary conditions of the kth deformation

41

equation. Similarly for θ_k.

3.3   Results and Error Analysis

In this section the functions found as approximation to the solutions of the differential equations are discussed. Moreover, error analysis is used to develop a notion of how good the approximations are.

To get an idea of error in the approximations, define $\widehat{f}$ and $\widehat{\theta}$ to be the sum of the first three solutions to the deformation equations. If the approximations $\widehat{f}$ and $\widehat{\theta}$ are plugged into the coupled system (3.8)-(3.9) and 0 is obtained, the solutions are exact. If they are not exact, then $N_1 \left[\widehat{f}(\eta), \widehat{\theta}(\eta) \right]$ and $N_2 \left[\widehat{f}(\eta), \widehat{\theta}(\eta) \right]$ become residual error functions that can be evaluated at any point η in the domain of the problem. To get a sense of how good these residual errors are, we find the square of their L^2-norm. Taking the convergence control parameters to be $c_0 = c_1$, these squared residual error functions are

$$E_\xi(f_w, \alpha, \lambda, \gamma, c_0, A) = \int_0^\infty \left(N_\xi \left[\widehat{f}(\eta), \widehat{\theta}(\eta) \right] \right)^2 d\eta, \tag{3.47}$$

for $\xi = 1, 2$.

Since we have two error functions, we will take an affine combination of them (see [52] for details):

$$E(c_0, A) = E_1(f_w, \alpha, \lambda, \gamma, c_0, A) + E_2(f_w, \alpha, \lambda, \gamma, c_0, A). \tag{3.48}$$

With the parameters $f_w, \alpha, \lambda, \gamma$, and A, we can check the residual error is small by choosing a suitable c_0. Then the approximate solutions are $\widehat{f}(\eta)$ and $\widehat{\theta}(\eta)$ using the parameter values chosen.

Sometimes, integration over an infinite domain can be difficult, and leads to aggregate error for a domain that is not always useful. In this case, we can evaluate the squared residual error at several

points. This is a weighted sum that has the form

$$\widehat{E}_\xi(f_w, \alpha, \lambda, \gamma, c_0, c_1) = \frac{1}{M} \sum_{j=0}^{M} \left(N_\xi \left[\widehat{f}(j), \widehat{\theta}(j) \right] \right)^2. \tag{3.49}$$

If the squaring is too complex for a computer algebra system like Maple to handle, sometimes an absolute value of the residual error will also work.

With this in mind, we start with initial guesses $f_0(\eta)$ and $\theta_0(\eta)$ that satisfy the boundary conditions (3.10) and (3.11), respectively. We choose

$$f_0(\eta) = f_w e^{-\eta}, \tag{3.50}$$

and

$$\theta_0(\eta) = e^{-\eta}. \tag{3.51}$$

Now, using the equations (3.40) and (3.41) to find $f_1(\eta)$ and $\theta_1(\eta)$, they are

$$f_1(\eta) = \frac{c_0 \gamma}{8A + 2} \left(e^{-2\eta} - e^{-\eta} \right), \tag{3.52}$$

and

$$\theta_1(\eta) = e^{-2\eta} \left(\frac{\frac{1}{2} c_0 \lambda f_w - \frac{1}{2} c_0 f_w}{8A + 2} \right) + e^{-\eta} \left(\frac{\frac{1}{2} c_0 f_w - \frac{1}{2} c_0 \lambda f_w}{8A + 2} \right). \tag{3.53}$$

The third term in each approximation $f_2(\eta)$ and $\theta_2(\eta)$ can be computed similarly. Using only three terms, let $\widehat{f}(\eta) = f_0(\eta) + f_1(\eta) + f_2(\eta)$ and $\widehat{\theta}(\eta) = \theta_0(\eta) + \theta_1(\eta) + \theta_2(\eta)$. The sum of squared residual error functions is given by

$$E(c_0, A) = \frac{1}{500} \sum_{j=0}^{499} \left\{ \left(N_1 \left[\widehat{f}(j), \widehat{\theta}(j) \right] \right)^2 + \left(N_2 \left[\widehat{f}(j), \widehat{\theta}(j) \right] \right)^2 \right\} \tag{3.54}$$

43

Note that $E(c_0, A)$ is a function of c_0 and A with parameters f_w (from the initial condition), γ, λ, and α in it.

Using three different sets of values for the parameters f_w, γ, α, λ, we have found the sum of squared residual error $E(c_0, A)$ in the given table.

Table 3.1: Minimum of the squared residual error $E(c_0, A)$ for four different sets of parameters.

f_w	γ	α	λ	A	c_0	$E(c_0, A)$
-1	-0.5	-1	-0.2	0.2869	-1.3279	6.6049×10^{-7}
-1	0	-1	0.2	1.4257	-3	1.2539×10^{-6}
-1	-0.5	-1	0	1.5851	-3	2.7322×10^{-5}

The plot of the error functions $E(c_0, A)$ for their respective parameter values is given in Figures 3.1-3.3.

The plot of the approximate solution $\widehat{f}(\eta)$ using these parameter values and their corresponding convergence control parameters is given in Figure 3.4, and similarly for $\widehat{\theta}(\eta)$ in Figure 3.5.

The skin friction as a function of γ is graphed in Figure 3.6. This is the plot of $\widehat{f}''(0)$ versus γ using $f_w = -1$, $\alpha = -1$, $\lambda = 0.2$, $A = 1.4257$ and $c_0 = -3$. Note that $\alpha < 0$ signifying a heat sink, so the skin friction decreases as the nonlinear density temperature γ increases.

Consider the Nusselt number, as presented in Figure 3.7. This is the plot of $\widehat{\theta}'(0)$ versus γ using $f_w = -1$, $\alpha = -1$, $\lambda = 0.2$, $A = 1.4257$ and $c_0 = -3$. Note that the wall temperature slightly decreases as γ increases. The effect of skin friction is significantly higher compared to

wall temperature, due to the steeper slope of the skin friction graph.

Both of the graphs of skin friction and Nusselt number compare very well with the graphs given in the literature (see [41]).

3.4   Discussion

In this paper, we extended the Method of Directly Defining the inverse mapping from a single equation to a system of two equations governing the free convection flow and heat transfer at a vertical flat plate embedded in a saturated porous medium. This is novel in the sense that it has not been done before, but also shows that the method can be applied to a system of two or more nonlinear differential equations.

Since the inverse linear operator is directly defined, calculating terms in the approximation can be done quickly. It is also interesting to note that using only three terms (which was an initial guess and two iterates) of the approximate solution, we get the sum of squared residual error on the order of 10^{-7} and 10^{-6} (see Figures 3.1 and 3.2). This shows that Liao's Method of Directly Defining the Inverse Mapping is not only easy to use, but accurate. Also, for better accuracy one can use as many terms as needed, still keeping the calculations simple.

Extension of this idea can still be applied to other nonlinear systems. This idea is still relatively new, and for the first time (as far as the authors are aware) applied to a system of nonlinear differential equations. In [3], Liao mentions that several inverse linear operators could work for a single problem. This means many other classes of inverse linear operators can be defined and different parameter values used to find differing results. The search for a general inverse linear operator (or operators) for a specific type of problem would be worth investigating.

CHAPTER 4: A METHOD OF DIRECTLY DEFINING THE INVERSE MAPPING FOR SOLUTIONS OF NON-LINEAR COUPLED SYSTEMS ARISING IN CONVECTION HEAT TRANSFER IN A SECOND GRADE FLUID

In this chapter, we extend Liao's newly invented Directly Defining Inverse Mapping Method (MD-DiM) to obtain solutions to fourth order nonlinear systems arising in combined free and forced convection flow of a second-grade fluid, over a stretching sheet. These results were considered in Dewasurendra et al. [53].

4.1 Background

Consider the flow of a second-grade fluid obeying the gradually fading memory(i.e., the notion that deformations which occurred in the distant past should have less effect on the present value of the stress than deformation occurred in the resent past, see [54]-[55]) adjacent to a vertical sheet coinciding with the plane $y = 0$, the flow being confined to $y > 0$. Here the gradually fading memory equation is given by

$$T = -PI + \mu A_1 + \alpha_1 A_2 + \alpha_2 A_1^2 \tag{4.1}$$

where T is the stress tensor, P is the pressure, μ is the dynamic viscosity, α_1, α_2 are first and second normal stress coefficients to the material modulus and for the present second grade fluid

with $\alpha_1 < 0$. The kinematics tensors A_1 and A_2 are defined as

$$A_1 = \nabla\mathbf{v} + (\nabla\mathbf{v})^T, \tag{4.2}$$

$$A_2 = \frac{\mathbf{d}}{\mathbf{dt}}A_1 + A_1 \cdot \nabla\mathbf{v} + (\nabla\mathbf{v})^T \cdot A_1, \tag{4.3}$$

where $\mathbf{v}$ is the velocity vector and $\frac{\mathbf{d}}{\mathbf{dt}}$ is the material time derivative. To keep the wall stretched and the origin fixed, two equal and opposite forces were applied along the positive x-axis. The basic boundary layer equations for the steady flow and heat transfer with internal heat generation or absorption in usual notation for the title problem are (for details see [56]-[59])

$$u\frac{\partial u}{\partial x} + v\frac{\partial u}{\partial y} = \nu\frac{\partial^2 u}{\partial y^2} - \lambda_1 \left[\frac{\partial}{\partial x}\left(u\frac{\partial^2 u}{\partial y^2} \right) + \frac{\partial u}{\partial y}\frac{\partial^2 v}{\partial y^2} + v\frac{\partial^3 u}{\partial y^3} \right] + g\beta(T - T_\infty), \tag{4.4}$$

$$\frac{\partial u}{\partial v} + \frac{\partial v}{\partial y} = 0, \tag{4.5}$$

$$\rho C_p \left(u\frac{\partial T}{\partial x} + v\frac{\partial T}{\partial y} \right) = k\frac{\partial^2 T}{\partial y^2} + Q(T - T_\infty), \tag{4.6}$$

where $\nu = \frac{\mu}{\rho} = -\frac{\alpha_1}{\rho}$, is the buoyancy force-term [with the well-known Boussinesq approximation $\rho - \rho_\infty = -\rho\beta(T - T_\infty)$].

The boundary conditions for the problem are

$$u = Bx, \quad v = 0, \quad T = T_w(= T_\infty + A(x/l)) \text{ at } y = 0, \tag{4.7}$$

$$u \to 0, \quad \frac{\partial u}{\partial y} \to 0, \quad T \to T_\infty \text{ as } y \to \infty, \tag{4.8}$$

where A is defined in such a way that $A(x/l)$ has the dimension of temperaturer, l is the characteristic length and $B > 0$ is the linear stretching rate constant.

Defining the similarity variables

$$u = Bxf'(\eta), \quad v = -(B\nu)^{\frac{1}{2}}f(\eta), \quad \eta = (B/\nu)^{\frac{1}{2}}y, \qquad (4.9)$$

$$\theta = (T - T_\infty)/(T_w - T_\infty), \qquad (4.10)$$

and substituting in (3.4)-(3.8), we obtain

$$(f')^2 - ff'' = f''' - \lambda[2f'f''' - (f'')^2 - ff^{iv}] + G\theta, \qquad (4.11)$$

$$\theta'' + \sigma f\theta' - \sigma(f' - \alpha)\theta = 0, \qquad (4.12)$$

$$f(0) = 0, \quad f'(0) = 1, \quad f' \to 0 \text{ as } \eta \to \infty, \quad f'' \to 0 \text{ as } \eta \to \infty, \qquad (4.13)$$

$$\theta(0) = 1, \quad \theta \to 0 \text{ as } \eta \to \infty, \qquad (4.14)$$

where $\lambda = \frac{\lambda_1 B}{\nu}$ is the viscoelastic parameter, $G = \frac{gA}{B^2 l}$ the free convection parameter, $\sigma = \frac{\mu C_p}{k}$ the Prandtl number and $\alpha = \frac{Q}{B\rho C_p}$ the heat source/sink parameter, and a prime denotes differentiation with respect to η.

Vajravelu and Soewono[56] showed that the system (4.11)-(4.14) has unique solution of the form

$$f(\eta) = a_0 + a_1 e^{-\delta\eta} \qquad (4.15)$$

and

$$\theta(\eta) = b_1 e^{-\delta\eta} \qquad (4.16)$$

for

(i) $G = 0, \delta = \frac{1}{\sqrt{1-\lambda}}, \lambda < 1$ and $\sigma(1 - \alpha)(1 - \lambda) = 1$

(ii) $G \neq 0, \delta = \sqrt{\sigma - \sigma\alpha}$, $\alpha = \frac{2}{3}$, $4\sigma\lambda(1 - \alpha) - 2\sigma(1 - \alpha) - 2\sigma(1 - \alpha) + 1 \neq 0$

and $\sigma(1 - \alpha)(\lambda - 1) - 1 \neq 0$.

Also, Vajravelu and Soewono [56] proved existence of convergent series solution of the form

$$f(\eta) = \sum_{n=0}^{\infty} a_n e^{-n\delta\eta} \tag{4.17}$$

$$\theta(\eta) = \sum_{n=2}^{\infty} b_n e^{-n\delta\eta} \tag{4.18}$$

when $\lambda a_0 \delta^2 - \delta + a_0 = 0, 4\delta^2 - 2\sigma a_0 \delta + \sigma\alpha = 0$ have common positive solution to $\delta, |a_1| = B, |b_2| \leq \frac{CB^2}{2^2}, CB < 1$ and

$$C_1 = \sup \left\{ \frac{|\sigma\delta|}{|\delta^2 - \frac{\sigma_0\delta}{n} + \frac{\sigma\alpha}{n^2}|}, n > 2 \right\} \tag{4.19}$$

$$C_2 = \sup \left\{ \frac{1}{|\lambda a_0 \delta^2 - \frac{\delta}{n} + \frac{a_0}{n^2}|}, n \geq 2 \right\} \tag{4.20}$$

$$C = \sup\{C_1, C_2\}. \tag{4.21}$$

In the present paper, we study the coupled system through the Homotopy Analysis Method by directly defining an inverse mapping $\mathscr{I}$, i.e without calculating any inverse operator. This method was introduced by Liao in [3] for a single differential equation and named as the method of directly defining inverse mapping (MDDiM). Here we extend MDDiM to a coupled system using a common inverse linear mapping and approximating $f(\eta)$ and $\theta(\eta)$ by two different sets of base functions.

49

4.2 HAM and MDDIM

The Directly Defining Inverse Mapping Method is based on the Homotopy analysis method (HAM) [[1],[2], [43]-[44]] which is an analytical approximation method for highly nonlinear differential equations. The results are functions, rather than numerical data. In this section, first we discuss the space that the solution and base functions come from and then we derive the deformation equations for the nonlinear system. Finally, we apply the Method of Directly Defined inverse to solve these deformation equation by introducing an appropriate inverse linear mapping $\mathscr{J}$.

Define two nonlinear operators

$$N_1[f(\eta), \theta(\eta)] = f''' + ff'' - (f')^2 - \lambda[2f'f''' - (f'')^2 - ff^{iv}] + G\theta, \qquad (4.22)$$

$$N_2[f(\eta), \theta(\eta)] = \theta'' + \sigma f\theta' - \sigma(f' - \alpha)\theta, \qquad (4.23)$$

so that $N_1[f(\eta), \theta(\eta)] = 0$ and $N_2[f(\eta), \theta(\eta)] = 0$ give the original coupled equations (4.11) and (4.12), respectively. After complete study of the convergent series solution (4.17)-(4.21) and the nonlinear system (4.11)-(4.14), take the linearly independent set of functions

$$S_\infty = \left\{1, e^{-\delta\eta}, e^{-2\delta\eta}, \dots\right\}, \qquad (4.24)$$

and define

$$V^1 = \left\{\sum_{k=0}^{\infty} a_k e^{-k\delta\eta} \big| a_k \in \mathbb{R}\right\}, V^2 = \left\{\sum_{k=2}^{\infty} a_k e^{-k\delta\eta} \big| a_k \in \mathbb{R}\right\}. \qquad (4.25)$$

Here V^1 and V^2 are solution and base spaces for $f(\eta)$ and $\theta(\eta)$ respectively. Next, introduce a base set for an initial guess as $S^{1*} = \left\{1, e^{-\delta\eta}\right\}$ by considering the first two members of S_∞, and

50

define the space for the initial guess for $f(\eta)$ as

$$V^{1*} = \left\{ a_0 + a_1 e^{-\delta\eta} | a_0, a_1 \in \mathbb{R} \right\}. \tag{4.26}$$

We took two members for the set S^{1*} because there are two boundary conditions at zero. This leads to the initial guess, and boundary conditions at infinity are automatically satisfied if we consider the initial guess as a linear combination of elements of the set S^{1*}. Also, introduce the base set for initial guess as $S^{2*} = \left\{ e^{-2\delta\eta} \right\}$ by considering only the third member of S_∞ and define space for the initial guess for $\theta(\eta)$ as

$$V^{2*} = \left\{ b_2 e^{-2\delta\eta} | b_2 \in \mathbb{R} \right\}. \tag{4.27}$$

We take only one member for the set S^{2*} because, only one boundary condition at zero leads to the initial guess for $\theta(\eta)$, and boundary conditions at infinity are automatically satisfied if we consider the initial guess as a linear combination of the set S^{2*}.

Then the primary solutions, or our initial guesses, $\mu_1(\eta) \in V^{1*}$, and $\mu_2(\eta) \in V^{2*}$, have the form

$$\mu_1(\eta) = \sum_{j=0}^{1} a_j e^{-\delta\eta}, \quad \mu_2(\eta) = b_2 e^{-2\delta\eta}. \tag{4.28}$$

Next, define $\widehat{S^1}$ and $\widehat{S^2}$ as follows:

$$\widehat{S^1} = \left\{ e^{-2\delta\eta}, e^{-3\delta\eta}, \ldots \right\}, \widehat{S^2} = \left\{ e^{-3\delta\eta}, e^{-4\delta\eta}, \ldots \right\} \tag{4.29}$$

and define $\widehat{V^1}$, $\widehat{V^2}$ so that $V^1 = \widehat{V^1} \cup V^{1*}$, $V^2 = \widehat{V^2} \cup V^{2*}$. Hence,

$$\widehat{V^1} = \left\{ \sum_{k=2}^{\infty} b_k e^{-k\delta\eta} | b_k \in \mathbb{R} \right\}, \widehat{V^2} = \left\{ \sum_{k=3}^{\infty} b_k e^{-k\delta\eta} | b_k \in \mathbb{R} \right\}. \tag{4.30}$$

Define a linearly independent set of functions

$$S_R = \{\psi_1(\eta), \psi_2(\eta), \ldots\}, \tag{4.31}$$

so that S_R is a basis for expressions in the codomain of the operators N_1 and N_2. Then let U be the set of all linear combinations of functions from S_R:

$$U = \left\{ \sum_{k=1}^{\infty} c_k \psi_k(\eta) \big| c_k \in \mathbb{R} \right\}. \tag{4.32}$$

Assuming that $N_1[f(\eta), \theta(\eta)], N_2[f(\eta), \theta(\eta)] \in U$, then $N_1 : V^1 \to U$ and $N_2 : V^2 \to U$.

Now let us look into the implementation of the Homotopy Analysis Method. Define two homotopies of operators

$$0 \equiv \mathcal{H}_1(f, \theta, q) = (1 - q)L_1[f] - c_0 q N_1[f, \theta], \tag{4.33}$$

$$0 \equiv \mathcal{H}_2(f, \theta, q) = (1 - q)L_2[\theta] - c_1 q N_2[f, \theta]. \tag{4.34}$$

Here $\mathcal{H}_1$ and $\mathcal{H}_2$ are the homotopies of operators between linear operators L_1, L_2 and nonlinear operators N_1, N_2. The homotopy parameter $q \in [0, 1]$ and the convergence control parameters are c_0 and c_1. The convergence control parameters will be used to optimize the function approximations in the next section. Now assume expansions of f and θ in terms of the homotopy parameter:

$$f(\eta) = f_0(\eta) + \sum_{k=1}^{\infty} f_k(\eta) q^k, \tag{4.35}$$

$$\theta(\eta) = \theta_0(\eta) + \sum_{k=1}^{\infty} \theta_k(\eta) q^k. \tag{4.36}$$

Here $f_0(\eta) \in V^{1*}$ and $\theta_0(\eta) \in V^{2*}$ are initial guesses that satisfy the boundary conditions.

Note that when $q = 0$ in the homotopies (4.33) and (4.34), they become $L_1[f] = 0$ and $L_2[\theta] = 0$; but when $q = 1$, the original nonlinear differential equations $N_1[f, \theta] = 0$ and $N_2[f, \theta] = 0$ are recovered. Likewise, when $q = 1$ in the expansions (4.35) and (4.36), the solutions f and θ are a sum of the components $f_1, f_2, \ldots$ and $\theta_1, \theta_2, \ldots$. Substituting these expansions (4.35) and (4.36) into the first homotopy (4.33), we get the deformation equations

$$L_1[f_0(\eta)] = 0, \tag{4.37}$$

$$f_0(0) = 0, f_0'(0) = 1, \quad f_0' \to 0 \text{ as } \eta \to \infty, f_0'' \to 0 \text{ as } \eta \to \infty \tag{4.38}$$

and for $k \geq 1$ we have

$$L_1[f_k(\eta)] = \chi_k L_1[f_{k-1}(\eta)] + c_0 \delta_{k-1}^1(\eta), \tag{4.39}$$

$$f_k(0) = 0, f_k'(0) = 0, f_k' \to 0 \text{ as } \eta \to \infty, f_k'' \to 0 \text{ as } \eta \to \infty \tag{4.40}$$

where

$$\chi_k = \begin{cases} 0, & k \leq 1, \\ 1, & k > 1. \end{cases} \tag{4.41}$$

Here δ_k^ξ, for $\xi = 1, 2$, is the homotopy derivative defined to be

$$\delta_{k-1}^\xi(\eta) = \frac{1}{(k-1)!} \left(\frac{\partial^{k-1}}{\partial q^{k-1}} N_\xi \left[\sum_{j=0}^{\infty} f_j(\eta) q^j, \sum_{j=0}^{\infty} \theta_j(\eta) q^j \right] \right) \bigg|_{q=0}. \tag{4.42}$$

On the other hand, if the expansions (4.35) and (4.36) are plugged into the second homotopy (4.34),

then the other set of deformation equations is obtained:

$$L_2[\theta_0(\eta)] = 0, \tag{4.43}$$

$$\theta_0(0) = 1, \quad \theta_0 \to 0 \text{ as } \eta \to \infty, \tag{4.44}$$

and for $k \geq 1$

$$L_2[\theta_k(\eta)] = \chi_k L_2[\theta_{k-1}(\eta)] + c_1 \delta_{k-1}^2(\eta), \tag{4.45}$$

$$\theta_k(0) = 0, \quad \theta_k \to 0 \text{ as } \eta \to \infty. \tag{4.46}$$

Using Liao's Method of Directly Defined Inverses, the deformation equations (4.39) and (4.45) are

$$f_k(\eta) = \chi_k f_{k-1}(\eta) + c_0 \mathscr{J}\left[\delta_{k-1}^1(\eta)\right] + a_{k,1} e^{-\delta\eta} + a_{k,0}, \tag{4.47}$$

$$\theta_k(\eta) = \chi_k \theta_{k-1}(\eta) + c_1 \mathscr{J}\left[\delta_{k-1}^2(\eta)\right] + b_{k,1} e^{-2\delta\eta}. \tag{4.48}$$

The benefit of the Homotopy Analysis Method is that one has great freedom to choose the auxillary linear operators L_1, L_2 and initial guesses $f_0(\eta), \theta_0(\eta)$. After auxillary linear operators and initial guesses are properly choosen we are free to determine how many terms $f_k \in V^1$ and $\theta_k \in V^2$ we want and can do it iteratively. There has been great success in solving systems of nonlinear differential equations using HAM(see [2], [4], [37], [43]-[52]).

The only drawback of this homotopy analysis method is spending a lot of CPU time. First we choose auxiliary linear operators, and then solving the linear higher deformation equation only to

find out the inverse operators and applying them to quickly-growing expressions. However, in the latest innovation of Liao we have the freedom to directly define the inverse operator by completely neglecting the linear operator (for details see [3], [40]). In this way, one can solve higher order deformation equations quickly and it is unnecessary to calculate inverse linear operators.

In our work the inversely defined mapping, $\mathscr{J}$, is the same for both equations. Define $\mathscr{J} : U^{1,2} \to V^{1,2}$ by

$$\mathscr{J}\left[e^{-k\delta\eta}\right] = \frac{e^{-k\delta\eta}}{k^3 + k}, \tag{4.49}$$

where the $k^3 + k$ is used to weight terms with lager values of k less than terms with smaller values of k.

Note that each function f_k can be split into

$$f_k(\eta) = \widehat{f}_k(\eta) + f_k^*(\eta), \tag{4.50}$$

where each $\widehat{f}_k \in \widehat{V^1}$ and each $f_k^* \in V^{1*}$, so that $f_k \in V^1$. The $\widehat{f}_k$ comes from the inverse linear operator, and the f_k^* has coefficients used to satisfy the boundary conditions of the kth deformation equation.

Similarly, θ_k can be split into

$$\theta_k(\eta) = \widehat{f}_k(\eta) + \theta_k^*(\eta), \tag{4.51}$$

where each $\widehat{\theta}_k \in \widehat{V^2}$ and each $\widehat{\theta}_k^* \in V^{2*}$, so that $\theta_k \in V^2$. Further, $\widehat{\theta}_k$ comes from the inverse linear operator, and the θ_k^* has coefficients used to satisfy the boundary conditions of the kth deformation equation.

4.3 Results and Error Analysis

In this section the functions found as approximations to the solutions of the differential equations are discussed. Moreover, error analysis is used to develop a notion of how good the approximations are.

To get an idea of error in the approximations, define $\widehat{f}$ and $\widehat{\theta}$ to be the sum of the first few solutions to the deformation equations. If the approximations $\widehat{f}$ and $\widehat{\theta}$ are plugged into the coupled system (4.11)-(4.12) and 0 is obtained, the solutions are exact. If they are not exact, then $N_1 \left[\widehat{f}(\eta), \widehat{\theta}(\eta) \right]$ and $N_2 \left[\widehat{f}(\eta), \widehat{\theta}(\eta) \right]$ become residual error functions that can be evaluated at any point η in the domain of the problem. To get a sense of how good these residual errors are, we find the square of their L^2-norm. Taking the convergence control parameters to be $c_0 = c_1$, these squared residual error functions are

$$E_\xi(G, \lambda, \sigma, \alpha, c_0, \delta) = \int_0^\infty \left(N_\xi \left[\widehat{f}(\eta), \widehat{\theta}(\eta) \right] \right)^2 d\eta, \tag{4.52}$$

for $\xi = 1, 2$.

Since we have two error functions, we will take an affine combination of them:

$$E(c_0, \delta) = E_1(G, \lambda, \sigma, \alpha, c_0, \delta) + E_2(G, \lambda, \sigma, \alpha, c_0, \delta). \tag{4.53}$$

Varying the parameters $G, \lambda, \sigma,$ and α, we can make sure the residual errors are small by choosing a suitable δ and c_0. Then the approximate solutions are $\widehat{f}(\eta)$ and $\widehat{\theta}(\eta)$.

Sometimes, integration over an infinite domain can be difficult, and leads to aggregate error for a domain that is not always useful. In this case, we can evaluate the squared residual error at several
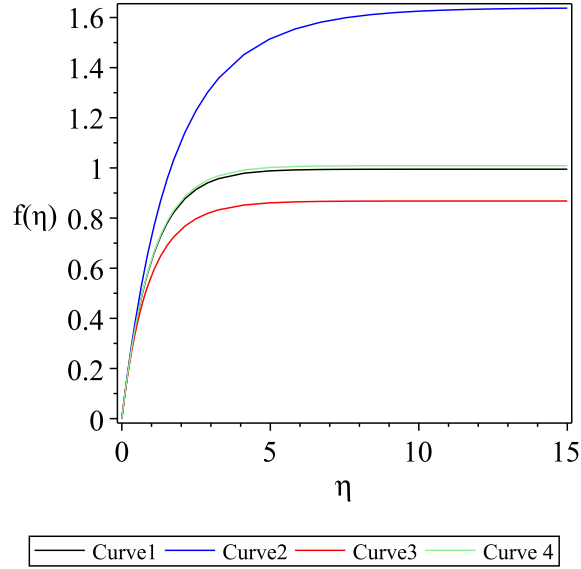
Figure 4.1: Plot of $\widehat{f}(\eta)$, where Curve 1 has $\sigma = 0.71$, $\lambda = 0.01$, $\alpha = -3.75$, $G = 0$, Curve 2 has $\sigma = 0.71$, $\lambda = 0.01$, $\alpha = 0.4$, $G = 0.5$, Curve 3 has $\sigma = 7$, $\lambda = 0.9$, $\alpha = 0.9$, $G = 1.1$ and Curve 4 has $\sigma = 3.855$, $\lambda = 0.01$, $\alpha = 0.83$, $G = 0.0001$ using their respective error-minimizing convergence control parameter.

points. This is a weighted sum that has the form

$$\widehat{E}_\xi(G, \lambda, \sigma, \alpha, c_0, \delta) = \frac{1}{M} \sum_{j=0}^{M} \left(N_\xi \left[\widehat{f}(j), \widehat{\theta}(j) \right] \right)^2. \tag{4.54}$$

If the squaring is too complex for a computer algebra system like Maple to handle, sometimes an absolute value of the residual error will also work.

With this in mind, we start with initial guesses $f_0(\eta)$ and $\theta_0(\eta)$ that satisfy the boundary conditions (4.13) and (4.14), respectively. We choose

$$f_0(\eta) = \frac{1}{\delta}(1 - e^{-\delta\eta}), \tag{4.55}$$

57
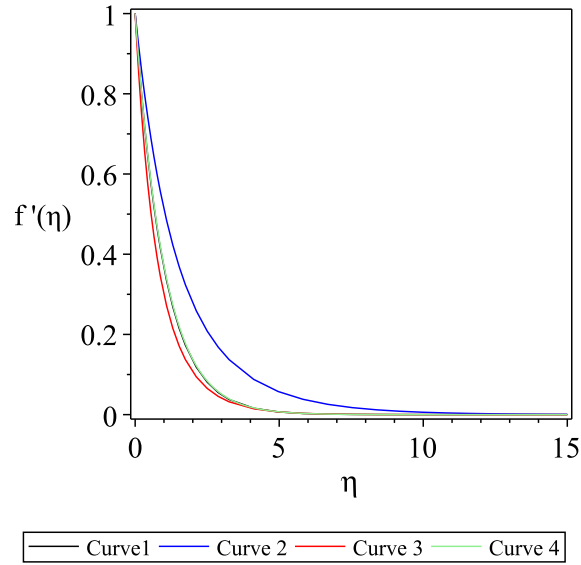
Figure 4.2: Plot of $\widehat{f}'(\eta)$, where Curve 1 has $\sigma = 0.71$, $\lambda = 0.01$, $\alpha = -3.75$, $G = 0$, Curve 2 has $\sigma = 0.71$, $\lambda = 0.01$, $\alpha = 0.4$, $G = 0.5$, Curve 3 has $\sigma = 7$, $\lambda = 0.9$, $\alpha = 0.9$, $G = 1.1$ and Curve 4 has $\sigma = 3.855$, $\lambda = 0.01$, $\alpha = 0.83$, $G = 0.0001$ using their respective error-minimizing convergence control parameter.

and

$$\theta_0(\eta) = e^{-2\delta\eta}. \tag{4.56}$$

Now, using the equations (4.47) and (4.48) to find $f_1(\eta)$ and $\theta_1(\eta)$; they are

$$f_1(\eta) = \frac{c_0 G}{10} \left(e^{-2\delta\eta} + 1 - 2e^{-\delta\eta} \right), \tag{4.57}$$

and

$$\theta_1(\eta) = -\frac{1}{30} c_0 \sigma (-e^{-3\delta\eta} + e^{-2\delta\eta}). \tag{4.58}$$

The third term in each approximation $f_2(\eta)$ and $\theta_2(\eta)$ can be computed similarly.
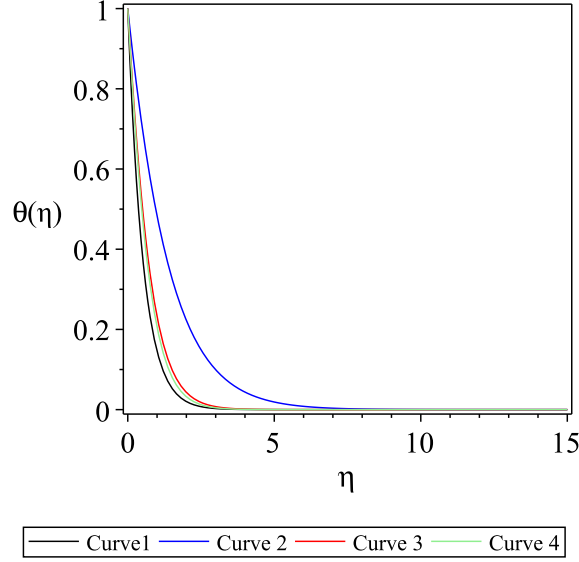
Figure 4.3: Plot of $\widehat{\theta}(\eta)$, where Curve 1 has $\sigma = 0.71$, $\lambda = 0.01$, $\alpha = -3.75$, $G = 0$, Curve 2 has $\sigma = 0.71$, $\lambda = 0.01$, $\alpha = 0.4$, $G = 0.5$, Curve 3 has $\sigma = 7$, $\lambda = 0.9$, $\alpha = 0.9$, $G = 1.1$ and Curve 4 has $\sigma = 3.855$, $\lambda = 0.01$, $\alpha = 0.83$, $G = 0.0001$ using their respective error-minimizing convergence control parameter.

$$
\begin{aligned}
f_2(\eta) = {}& -\frac{2}{25}c0^2G\delta^3 + \frac{1}{10}c0G - \frac{1}{900}c0^2G\sigma + \frac{1}{30}c0^2G\delta + \frac{19}{150}c0^2G\lambda\delta^3 \\
& + (-\frac{7}{100}c0^2G\delta - \frac{27}{100}c0^2G\lambda\delta^3 - \frac{1}{5}c0G + \frac{4}{25}c0^2G\delta^3 + \frac{1}{300}c0^2G\sigma)e^{-\delta\eta} \\
& + (\frac{1}{25}c0^2G\delta + \frac{1}{10}c0G + \frac{4}{25}c0^2G\lambda\delta^3 - \frac{2}{25}c0^2G\delta^3 - \frac{1}{300}c0^2G\sigma)e^{-2\delta\eta} \\
& + (-\frac{1}{60}c0^2G\lambda\delta^3 - \frac{1}{300}c0^2G\delta + \frac{1}{900}c0^2G\sigma)e^{-3\delta\eta}.
\end{aligned}
\tag{4.59}
$$

$$
\begin{aligned}
\theta_2(\eta) = {}& (-\frac{1}{30}c0\sigma + \frac{1}{30}c0^2\sigma(-\frac{3}{5}G\delta - \frac{1}{10}\sigma\alpha - \frac{2}{5}\delta^2 + \frac{1}{5}\sigma) + \frac{1}{15300}c0^2\sigma(-49\sigma + 34\sigma\alpha \\
& + 204G\delta + 51\delta^2))e^{-2\delta\eta} + (\frac{1}{30}c0\sigma + \frac{1}{30}c0^2\sigma(-\frac{2}{15}\sigma + \frac{3}{10}\delta^2 + \frac{1}{30}\sigma\alpha + \frac{1}{5}G\delta))e^{-3\delta\eta} \\
& + \frac{1}{1020}c0^2\sigma^2 e^{-4\delta\eta}
\end{aligned}
\tag{4.60}
$$

59
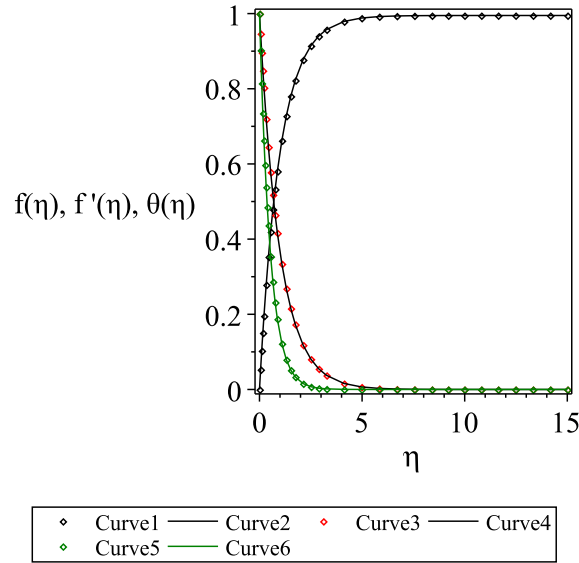
Figure 4.4: Comparison of $f(\eta)$, $f'(\eta)$ and $\theta(\eta)$ obtained by the MDDiM and HAM with $\sigma = 0.71$, $\lambda = 0.01$, $\alpha = -3.75$ and $G = 0$, where Curve1 is HAM results of $f(\eta)$, Curve 2 is MDDiM results of $f(\eta)$, Curve 3 is HAM results of $f'(\eta)$, Curve 4 is MDDiM results of $f'(\eta)$, Curve 5 is HAM results of $\theta(\eta)$, Curve 6 is MDDiM results $\theta(\eta)$.

Using only four terms, let $\widehat{f}(\eta) = f_0(\eta) + f_1(\eta) + f_2(\eta) + f_3(\eta)$ and $\widehat{\theta}(\eta) = \theta_0(\eta) + \theta_1(\eta) + \theta_2(\eta) + \theta_3(\eta)$, the sum of squared residual error functions is given by

$$E(c_0, \delta) = \frac{1}{100} \sum_{j=0}^{99} \left\{ \left(N_1 \left[\widehat{f}(j), \widehat{\theta}(j) \right] \right)^2 + \left(N_2 \left[\widehat{f}(j), \widehat{\theta}(j) \right] \right)^2 \right\}. \tag{4.61}$$

Note that $E(c_0, \delta)$ is a function of c_0 and δ with parameters G, λ, σ, and α in it.

Using different sets of values for the parameters G, λ, σ, α, we have found the sum of squared residual error $E(c_0, \delta)$ and are presented in the table below.

The plot of the approximate solution $\widehat{f}(\eta)$ using these parameter values and their corresponding

60

convergence control parameters is presented in Figure 4.1, and similarly for $\widehat{f}'(\eta), \widehat{\theta}(\eta)$ in Figures 4.2-4.3. HAM has been used (for details see [2], [4], [37], [43]-[52]) and a very good validation of the present analytical results has been achieved as shown in Figures 4.4-4.5.

Table 4.1: Minimum of the squared residual error $E(c_0, \delta)$ for four different sets of parameters.

σ	λ	α	G	c_0	δ	$E(c_0, \delta)$
0.71	0.01	-3.75	0	-2.4764	1.0051	2.33×10^{-9}
0.71	0.01	0.4	0.5	-7.0304	0.4280	7.84×10^{-5}
7	0.9	0.9	1.1	-0.9912	0.9004	9.27×10^{-5}
3.855	0.01	0.83	0.0001	-2.139	0.9911	5.83×10^{-5}

The skin friction at the surface as a function of the free convection parameter G is presented in Figure 4.6 for heat source/sink parameter values $\alpha = -3.75$ and $\alpha = 0.4$. Note that $\alpha = -3.75 < 0$ signifying a heat sink and $\alpha = 0.4 > 0$ signifying heat source. It is found that the skin friction decreases with an increase in G but increases for increasing α. Figure 4.7 illustrated Nusselt number as a function of G for a heat sink and a source. It can be seen that the Nusselt number decreases with increasing G but increases with increasing α. Also, it is noticeable that the skin friction is significantly affected compared to the Nusselt number because of the steeper slope of the skin friction graph.

4.4   Discussion

Liao's Directly Defining inverse Mapping method has been extended to a fourth-order nonlinear coupled system arising in combined free and forced convection flow of a second-grade fluid over
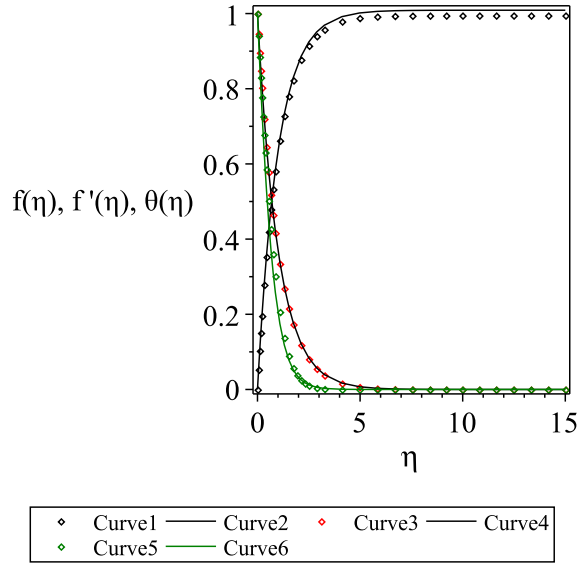
Figure 4.5: Comparison of $f(\eta)$, $f'(\eta)$ and $\theta(\eta)$ obtained by the MDDiM and HAM with $\sigma = 3.855$, $\lambda = 0.01$, $\alpha = 0.83$ and $G = 0.0001$, where Curve1 is HAM results of $f(\eta)$, Curve 2 is MDDiM results of $f(\eta)$, Curve 3 is HAM results of $f'(\eta)$, Curve 4 is MDDiM results of $f'(\eta)$, Curve 5 is HAM results of $\theta(\eta)$, Curve 6 is MDDiM results $\theta(\eta)$.

a stretching sheet. Approximate series solutions for velocity and temperature profiles were found. Also, illustrated velocity and temperature profiles for four sets of parameters (see Figures 4.2 and 4.3). Further, present results are compared with the HAM results (see Figures 4.4-4.5). This is useful because only the existence of solutions has been studied previously.

Since the inverse operator is directly defined, the series solutions were obtained with less CPU time. The freedom of picking the inverse linear operator leads to obtaining less complicated terms for the approximate solution. Further, the selected inverse operator leads to series solutions with square residual error between 10^{-5} and 10^{-9} (see Table 4.1). Hence we can conclude that MDDiM is not only easy to use, but accurate. Theoretically, even if smaller error was desired, it would just amount to computing more terms in the series by solving higher-order deformation equations.
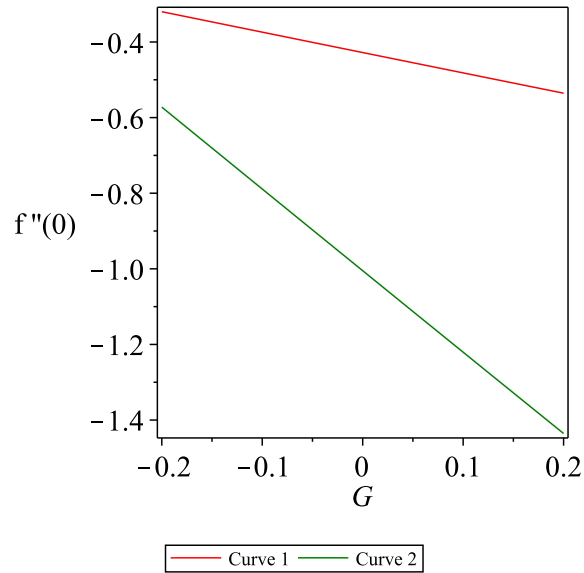
Figure 4.6: Plot of $\widehat{f''}(0)$ versus G, where Curve 1 has $\sigma = 0.71$, $\lambda = 0.01$, $\alpha = 0.4$, $\delta = 0.4280$ and $c_0 = -7.0304$ and curve 2 has $\sigma = 0.71$, $\lambda = 0.01$, $\alpha = -3.75$, $\delta = 1.5500$ and $c_0 = -2.4735$.

The idea is novel and this is the first time MDDiM has been used for a fourth-order coupled system. So, this idea is not limited to a single equation, but can also be used for coupled equations. The same idea could be applied to systems of several equations, etc. Also, it is important to note that finding an inverse linear operator that works well (gives low error, or leads to easily generated solution terms, or both) for a specific type of problem would be worth investigating.
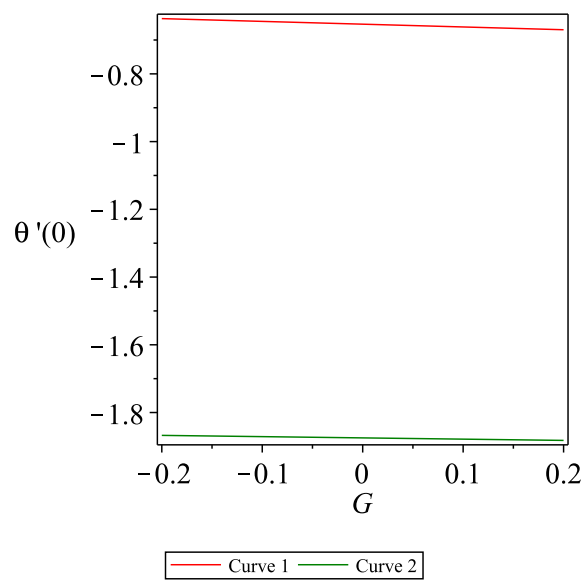
Figure 4.7: Plot of $\widehat{\theta'}(0)$ versus G, where Curve 1 has $\sigma = 0.71$, $\lambda = 0.01$, $\alpha = 0.4$, $\delta = 0.4280$ and $c_0 = -7.0304$ and curve 2 has $\sigma = 0.71$, $\lambda = 0.01$, $\alpha = -3.75$, $\delta = 1.5500$ and $c_0 = -2.4735$.

CHAPTER 5: ON THE METHOD OF INVERSE MAPPING FOR SOLUTIONS OF COUPLED SYSTEMS OF NONLINEAR DIFFERENTIAL EQUATIONS ARISING IN NANOFLUID FLOW, HEAT AND MASS TRANSFER

In this chapter, we extend the Directly Defining Inverse Mapping Method (MDDiM) to obtain solutions to nonlinear-coupled systems of three differential equations arising in steady, incompressible, laminar, two-dimensional boundary layer flow of a nanofluid at a vertical wall. These results were considered in Dewasurendra et al. [60].

5.1 Background

Consider a steady, incompressible, laminar, two-dimensional boundary layer flow of a nanofluid at a vertical wall coincide with the plane $y = 0$, the flow being confined to $y > 0$ (see Figure 5.1). Two equal and opposite forces are introduced along the x-axis so that the wall is stretched while keeping the origin fixed. The sheet is then stretched with a velocity $u_w = ax^n$ where a is a constant, n is a nonlinear stretching parameter and x is the coordinate measured along the stretching surface. We make following assumptions:

  (i) the pressure gradient and external forces are neglected

 (ii) the stretching surface is maintained at a constant temperature and concentration, T_w and C_w, respectively,

(iii) T_w and C_w values are greater than the ambient temperature and concentration, T_∞ and C_∞ respectively.

65
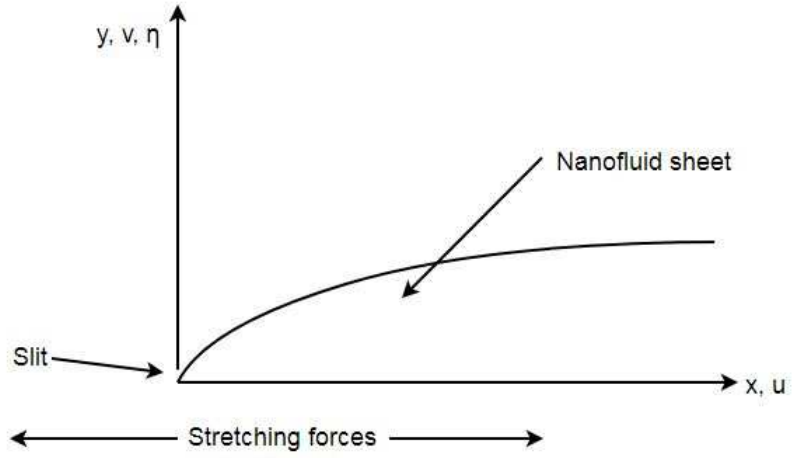
Figure 5.1: Flow configuration.

Under these assumptions, the basic equations for the conservation of mass, momentum, thermal energy and nanoparticles of the nanofluid can be written in Cartesian coordinates x and y as (for details see Rana and Bhargava [61])

$$\frac{\partial u}{\partial x} + \frac{\partial v}{\partial y} = 0, \tag{5.1}$$

$$u\frac{\partial u}{\partial x} + v\frac{\partial u}{\partial y} = v\frac{\partial^2 u}{\partial y^2}, \tag{5.2}$$

$$u\frac{\partial T}{\partial x} + v\frac{\partial T}{\partial y} = \alpha_m \nabla^2 T + \tau \left[D_B \frac{\partial C}{\partial y}\frac{\partial T}{\partial y} + \frac{D_T}{T_\infty}(\frac{\partial T}{\partial y})^2 \right], \tag{5.3}$$

$$u\frac{\partial C}{\partial x} + v\frac{\partial C}{\partial y} = D_B\frac{\partial^2 C}{\partial y^2} + (\frac{D_T}{T_\infty})\frac{\partial^2 T}{\partial y^2}, \tag{5.4}$$

66

where

$$\alpha_m = \frac{k_m}{(\rho c)_f}, \quad \tau = \frac{(\rho c)_p}{(\rho c)_f}. \tag{5.5}$$

The boundary conditions for the problem are

$$v = 0, \quad u_w = ax^n, \quad T = T_w, \quad C = C_w \quad \text{at} \quad y = 0, \tag{5.6}$$

$$u = v = 0, \quad T = T_\infty, \quad C = C_\infty \quad \text{as} \quad y \to \infty. \tag{5.7}$$

Here u and v are the velocity in the x and y directions, ρ_f is the density of the base fluid, α_m is the thermal diffusivity, ν is the kinematic viscosity, a is a positive constant, D_B is the Brownian coefficient, D_T is the thermophoretic diffusion coefficient, τ is the ratio between the effective heat capacity of the nanoparticle material and heat capacity of the fluid, c is the volumetric volume expansion coefficient and ρ_p is the density of the nanoparticles.

Defining the new variables

$$\eta = y\sqrt{\frac{a(n+1)}{2v}}x^{\frac{n-1}{2}}, \quad u = ax^n f'(\eta), \quad v = -\sqrt{\frac{av(n+1)}{2}}x^{\frac{n-1}{2}}(f + (\frac{n-1}{n+1})\eta f'), \tag{5.8}$$

$$\theta(\eta) = \frac{T - T_\infty}{T_w - T_\infty}, \quad \phi(\eta) = \frac{C - C_\infty}{C_w - C_\infty}, \tag{5.9}$$

and substituting in (5.1)-(5.4), we obtained

$$f''' + ff'' - \left(\frac{2n}{n+1}\right)f'^2 = 0, \tag{5.10}$$

$$\frac{1}{Pr}\theta'' + f\theta' + Nb\theta'\phi' + Nt(\theta')^2 = 0, \tag{5.11}$$

$$\phi'' + \frac{1}{2}Lef\phi' + \frac{Nt}{Nb}\theta'' = 0, \tag{5.12}$$

with boundary conditions,

$$\text{at} \quad \eta = 0, \quad f = 0, \quad f' = 1, \quad \theta = 1, \quad \phi = 1, \tag{5.13}$$

$$\text{as} \quad \eta \to \infty, \quad f' = 0, \quad \theta = 0, \quad \phi = 0. \tag{5.14}$$

The key thermophysical parameters are defined by:

$$Pr = \frac{v}{\alpha}, \quad Le = \frac{v}{D_B}, \quad Nb = \frac{(\rho c)_p D_B (C_w - C_\infty)}{(\rho c)_f v}, \quad Nt = \frac{(\rho c)_p D_T (T_w - T_\infty)}{(\rho c)_f v T_\infty}. \tag{5.15}$$

Here $Pr, Le, Nb,$ and Nt denote the Prandtl number, the lewis number, the Brownian motion parameter and the thermophoresis parameter respectively.

In the present paper, we study the nonliner system analyticaly through the Optimam Homotopy Analysis Method by directly defining an inverse mapping $\mathscr{I}$, i.e. without calculating any inverse operator. This method was intoduced by Liao [3] for a single differentiall equation. Vajravelu et al. [40] extended it to solve coupled systems. Here, we extend the method to a system of three nonlinear diferential equations using a common inverse linear mapping and approximated $f(\eta)$, $\theta(\eta)$ and $\phi(\eta)$.

5.2   HAM and MDDIM

In this section, we discuss the set up of the problem using the details of OHAM (see [1]-[2] for more details) and MDDiM for the nonlinear system. First, we discuss the space that solution and base functions come from and then we derive deformation equations that we are trying to solve (nonlinear system). Finally, we use MDDiM to solve these deformation equations by introducing an appropriate inverse linear map $\mathscr{J}$.

Define three nonlinear operators

$$N_1[f(\eta), \theta(\eta), \phi(\eta)] = f''' + ff'' - \left(\frac{2n}{n+1}\right) f'^2, \tag{5.16}$$

$$N_2[f(\eta), \theta(\eta), \phi(\eta)] = \frac{1}{Pr}\theta'' + f\theta' + Nb\theta'\phi' + Nt(\theta')^2, \tag{5.17}$$

$$N_3[f(\eta), \theta(\eta), \phi(\eta)] = \phi'' + \frac{1}{2}Lef\phi' + \frac{Nt}{Nb}\theta'' = 0, \tag{5.18}$$

so that $N_1[f(\eta), \theta(\eta), \phi(\eta)] = 0$, $N_2[f(\eta), \theta(\eta), \phi(\eta)] = 0$ and $N_3[f(\eta), \theta(\eta), \phi(\eta)] = 0$ give the original system (5.10)-(5.12). Take complete set of an infinite number of base functions that are linearly independent

$$S_\infty = \left\{1, e^{-\delta\eta}, e^{-2\delta\eta}, \ldots\right\}, \tag{5.19}$$

and define the space of functions that is their linear combinations to be

$$V = \left\{\sum_{k=0}^{\infty} a_k e^{-k\delta\eta} \,\middle|\, a_k \in \mathbb{R}\right\}. \tag{5.20}$$

That is, V is the solution and base space for $f(\eta)$, $\theta(\eta)$ and $\phi(\eta)$.

Let

$$S^* = \left\{ 1, e^{-\delta\eta} \right\}. \tag{5.21}$$

denote a set, consists of first 2 members of S_∞. Next, form the space of functions taking their linear combinations

$$V^* = \left\{ a_0 + a_1 e^{-\delta\eta} \middle| a_0, a_1 \in \mathbb{R} \right\}. \tag{5.22}$$

Then the primary solutions, or our initial guesses, $\mu(\eta) \in V^*$ have the form

$$\mu(\eta) = \sum_{j=0}^{1} a_j e^{-\delta\eta}. \tag{5.23}$$

Write

$$\widehat{S} = \left\{ e^{-2\delta\eta}, e^{-3\delta\eta}, \ldots \right\}, \tag{5.24}$$

and define

$$\widehat{V} = \left\{ \sum_{k=2}^{\infty} a_k e^{-k\delta\eta} \middle| a_k \in \mathbb{R} \right\}. \tag{5.25}$$

Obviously, $V = \widehat{V} \cup V^*$.

Next, define

$$S_R = \left\{ \psi_1(\eta), \psi_2(\eta), \ldots \right\}, \tag{5.26}$$

which is an infinite set of base functions that are linearly independent, and set of linear combinations of functions from S_R

$$U = \left\{ \sum_{k=1}^{\infty} c_k \psi_k(\eta) \middle| c_k \in \mathbb{R} \right\}. \tag{5.27}$$

Assuming that $N_1[f(\eta), \theta(\eta), \phi(\eta)], N_2[f(\eta), \theta(\eta), \phi(\eta)], N_3[f(\eta), \theta(\eta), \phi(\eta)] \in U$, then $N_1, N_2, N_3 :$ $V \to U$.

Optimal Homotopy Analysis Method allows us to obtain approximate series solutions to wide variety of nonlinear systems. Define three homotopies of operators $\mathcal{H}_1, \mathcal{H}_2$ and $\mathcal{H}_3$

$$0 \equiv \mathcal{H}_1(f, \theta, \phi, q) = (1-q)L_1[f] - c_0 q N_1[f, \theta, \phi], \qquad (5.28)$$

$$0 \equiv \mathcal{H}_2(f, \theta, \phi, q) = (1-q)L_2[\theta] - c_1 q N_2[f, \theta, \phi], \qquad (5.29)$$

$$0 \equiv \mathcal{H}_3(f, \theta, \phi, q) = (1-q)L_3[\phi] - c_2 q N_3[f, \theta, \phi], \qquad (5.30)$$

through the homotopy embedding parameter $q \in [0, 1]$, between nonlinear operators N_1, N_2, N_3 and an auxiliary linear operators L_1, L_2, L_3. Here, $c_0, c_1, c_2 \neq 0$ are the converge control parameters which will be used to optimize the function approximations in the next section. In the frame of OHAM, the series solution of f, θ and ϕ is given by

$$f(\eta) = f_0(\eta) + \sum_{k=1}^{\infty} f_k(\eta) q^k, \qquad (5.31)$$

$$\theta(\eta) = \theta_0(\eta) + \sum_{k=1}^{\infty} \theta_k(\eta) q^k, \qquad (5.32)$$

$$\phi(\eta) = \phi_0(\eta) + \sum_{k=1}^{\infty} \phi_k(\eta) q^k, \qquad (5.33)$$

where $f_0(\eta), \theta_0(\eta)$ and $\phi_0(\eta)$ are initial guesses that satisfy boundary conditions (5.13)-(5.14) and belong to the set V.

It is clear that when $q = 0$ in the homotopies (5.28)-(5.30), they become $L_1[f] = 0$, $L_2[\theta] = 0$ and $L_3[\phi] = 0$; but for $q = 1$, the original nonlinear differential equations $N_1[f, \theta, \phi] = 0$, $N_2[f, \theta, \phi] =$

0 and $N_3[f, \theta, \phi] = 0$ are recovered. In addition, when $q = 1$ in the expansions (5.31)-(5.33), the solutions f, θ and ϕ are a sum of the components $f_0, f_1, f_2, \ldots, \theta_0, \theta_1, \theta_2, \ldots$ and $\phi_0, \phi_1, \phi_2, \ldots$. Substituting (5.31)-(5.33) in to the first homotopy (5.28), we get the deformation equations

$$L_1[f_0(\eta)] = 0, \quad f_0(0) = 0, \quad f_0'(0) = 1 \quad f_0' \to 0 \text{ as } \eta \to \infty, \tag{5.34}$$

and for $k \geq 1$ we have

$$L_1[f_k(\eta)] = \chi_k L_1[f_{k-1}(\eta)] + c_0 \mathscr{D}_{k-1}^1(\eta), \quad f_k(0) = 0, \quad f_k'(0) = 0, \quad f_k' \to 0 \text{ as } \eta \to \infty, \tag{5.35}$$

where

$$\chi_k = \begin{cases} 0, & k \leq 1, \\ 1, & k \geq 1. \end{cases} \tag{5.36}$$

Here $\mathscr{D}_k^\xi$, for $\xi = 1, 2, 3$, is the homotopy derivative defined to be

$$\mathscr{D}_{k-1}^\xi(\eta) = \frac{1}{(k-1)!} \left(\frac{\partial^{k-1}}{\partial q^{k-1}} N_\xi \left[\sum_{j=0}^{\infty} f_j(\eta) q^j, \sum_{j=0}^{\infty} \theta_j(\eta) q^j \right] \right) \Big|_{q=0}. \tag{5.37}$$

Similarly, substituting (5.31)-(5.33) into (5.29) and (5.30) obtained:

$$L_2[\theta_0(\eta)] = 0, \quad \theta_0(0) = 1, \quad \theta_0 \to 0 \text{ as } \eta \to \infty, \tag{5.38}$$

$$L_3[\phi_0(\eta)] = 0, \quad \phi_0(0) = 1, \quad \phi_0 \to 0 \text{ as } \eta \to \infty, \tag{5.39}$$

and for $k \geq 1$

$$L_2[\theta_k(\eta)] = \chi_k L_2[\theta_{k-1}(\eta)] + c_1 \mathscr{D}_{k-1}^2(\eta), \quad \theta_k(0) = 0, \quad \theta_k \to 0 \text{ as } \eta \to \infty. \tag{5.40}$$

72

$$L_3[\phi_k(\eta)] = \chi_k L_3[\phi_{k-1}(\eta)] + c_1 \mathscr{D}_{k-1}^3(\eta), \quad \phi_k(0) = 0, \quad \phi_k \to 0 \text{ as } \eta \to \infty. \tag{5.41}$$

Using Liao's Method of Directly Defined Inverses, the deformation equations (5.35) and (5.40)-(5.41) are

$$f_k(\eta) = \chi_k f_{k-1}(\eta) + c_0 \mathscr{J} \left[\mathscr{D}_{k-1}^1(\eta) \right] + a_{k,1} e^{-\delta\eta} + a_{k,0}, \tag{5.42}$$

$$\theta_k(\eta) = \chi_k \theta_{k-1}(\eta) + c_1 \mathscr{J} \left[\mathscr{D}_{k-1}^2(\eta) \right] + b_{k,1} e^{-\delta\eta} + b_{k,0}, \tag{5.43}$$

$$\phi_k(\eta) = \chi_k \phi_{k-1}(\eta) + c_1 \mathscr{J} \left[\mathscr{D}_{k-1}^3(\eta) \right] + c_{k,1} e^{-\delta\eta} + c_{k,0}. \tag{5.44}$$

The benifit of the Optimal Homotopy Analysis Mehod is that it has a great freedom to choose the auxillary linear operators L_1, L_2 and L_3 and initial guesses $f_0(\eta), \theta_0(\eta), \phi_0(\eta)$. After auxillary linear operator and initial guesses are properly choosen we are free to determine how many terms $f_k, \theta_k, \phi_k \in V$ we want and can do iteratively. There has been great success in solving systems of nonlinear differential equations using OHAM (see [1], [2], [37], [43]-[52]).

The only drawback of this homotopy analysis method is spending a lot of CPU time. First we choose auxiliary linear operators, and then solving the linear higher order deformation equation only to find out the inverse operators and applying them to quickly-growing expressions. However, in the latest innovation of Liao we have the freedom to directly define inverse operator by completely neglecting the linear operator. So, using this novel method can solve higher order deformation equations quickly and it's unnecessary to calculate inverse linear operators.

In our work the inversely defined mapping, $\mathscr{I}$, is the same for all three equations. But different directly defined inverses could be chosen if a different structure for the solutions f, θ and ϕ is required.

Define $\mathscr{I} : U \to V$ by

$$\mathscr{I}\left[e^{-k\delta\eta}\right] = \frac{e^{-k\delta\eta}}{Ak^3 + k}, \tag{5.45}$$

where A, δ are parameters which will be used to optimize the square residual error functions.

5.3   Results and Error Analysis

The appropriate solutions for the system (5.10)-(5.12) with boundary conditions (5.13)-(5.14) are obtained using MDDiM. Further used error analysis to get a general idea of how good the approximations are.

Define three term approximation $\widehat{f}, \widehat{\theta}$ and $\widehat{\phi}$ which is sum of the first three solutions to the deformation equations. If they are exact, then they solve system (5.10)-(5.12), i.e., if $N_1\left[\widehat{f}, \widehat{\theta}, \widehat{\phi}\right] = 0$, $N_2\left[\widehat{f}, \widehat{\theta}, \widehat{\phi}\right] = 0$ and $N_3\left[\widehat{f}, \widehat{\theta}, \widehat{\phi}\right] = 0$, then the three term approximations are exact solutions. If not $N_1\left[\widehat{f}, \widehat{\theta}, \widehat{\phi}\right]$, $N_2\left[\widehat{f}, \widehat{\theta}, \widehat{\phi}\right]$ and $N_3\left[\widehat{f}, \widehat{\theta}, \widehat{\phi}\right]$ become residual error functions that can be evaluated at any point η in the domain of the problem. Taking square of the L^2-norm of error functions and setting converge control parameters to be $c_0 = c_2 = c_3$ define square residual error functions

$$E_\xi(Le, Nb, Pr, Nt, n, A, c_0, \delta) = \int_0^\infty \left(N_\xi\left[\widehat{f}(\eta), \widehat{\theta}(\eta), \widehat{\phi}(\eta)\right]\right)^2 d\eta, \tag{5.46}$$

for $\xi = 1, 2, 3$. Since we have three error functions we will take affine combination of them as

$$E(Le, Nb, Pr, Nt, n, A, c_0, \delta) = \sum_{\xi=1}^{3} E_\xi(Le, Nb, Pr, Nt, n, A, c_0, \delta). \tag{5.47}$$

74

But in practice the evaluation of $E_\xi(Le, Nb, Pr, Nt, n, A, c_0, \delta)$ is much time consuming so instead of exact residual error we use average residual error defined as

$$\widehat{E}_\xi(Le, Nb, Pr, Nt, n, A, c_0, \delta) = \frac{1}{M+1} \sum_{j=0}^{M} \left(N_\xi \left[\widehat{f}(j), \widehat{\theta}(j), \widehat{\phi}(j) \right] \right)^2. \qquad (5.48)$$

Now, we minimize error functions with respect to A, c_0, δ and obtained optimal values of A, c_0, δ. Substituting those values in to $\widehat{f}, \widehat{\theta}$ and $\widehat{\phi}$ we get three term approximation solution to the system (5.10)-(5.12) which satisfies the conditions (5.13)-(5.14).

We start with initial guesses $f_0(\eta), \theta_0(\eta)$ and $\phi_0(\eta)$ that satisfy the boundary conditions (5.13)-(5.14), respectively. We choose

$$f_0(\eta) = \frac{1}{\delta} - \frac{1}{\delta} e^{-\delta\eta}, \qquad (5.49)$$

$$\theta_0(\eta) = e^{-\delta\eta}, \qquad (5.50)$$

and

$$\phi_0(\eta) = e^{-\delta\eta}. \qquad (5.51)$$

Now, using the deformation equations (5.42)-(5.44) to find $f_1(\eta), \theta_1(\eta)$ and $\phi_1(\eta)$, they are

$$f_1(\eta) = -\frac{1}{2}\frac{c_0(n-1)}{(n+1)(4A+1)} + \frac{c_0(n-1)}{(n+1)(4A+1)} e^{-\delta\eta} - \frac{1}{2}\frac{c_0(n-1)}{(n+1)(4A+1)} e^{-2\delta\eta}, \qquad (5.52)$$

$$\theta_1(\eta) - \frac{1}{2}\frac{(1 + Nt \cdot \delta^2 + Nb \cdot \delta^2)c_0 \cdot \delta^2}{4A+1} e^{-\delta\eta} + \frac{1}{2}\frac{(1 + Nt \cdot \delta^2 + Nb \cdot \delta^2)c_0 \cdot \delta^2}{4A+1} e^{-2\delta\eta}, \qquad (5.53)$$

and

$$\phi_1(\eta) = -\frac{1}{4} \cdot \frac{Le \cdot c_0}{4A+1} e^{-\delta\eta} + \frac{1}{4} \cdot \frac{Le \cdot c_0}{4A+1} e^{-2\delta\eta}. \tag{5.54}$$

Using only three terms, let $\widehat{f}(\eta) = f_0(\eta) + f_1(\eta) + f_2(\eta)$, $\widehat{\theta}(\eta) = \theta_0(\eta) + \theta_1(\eta) + \theta_2(\eta)$ and $\widehat{\phi}(\eta) = \phi_0(\eta) + \phi_1(\eta) + \phi_2(\eta)$, the sum of the square residual error function is given by

$$E(A, c_0, \delta) = \frac{1}{500} \sum_{j=0}^{499} \left(\sum_{\xi=1}^{3} \left(N_\xi \left[\widehat{f}(j), \widehat{\theta}(j), \widehat{\phi}(j) \right] \right) \right)^2. \tag{5.55}$$

and it is a function of A, c_0 and δ with parameters Le, Nb, Pr, Nt and n in it.

Using three different sets of values for the parameters Le, Nb, Pr, Nt and n we found the sum of the square residual error $E(A, c_0, \delta)$ and are presented below.

Table 5.1: Minimum of the squared residual error $E(A, c_0, \delta)$ for three different sets of parameters.

Le	Nb	Pr	Nt	n	A	c_0	δ	$E(c_0, \delta, A)$
2	2	1	1	0.5	0.1314	-0.6195	0.673	9.71×10^{-5}
3	1	5	0	1	7.8902	-9.3020	1.0394	9.71×10^{-5}
2	2	7	0.5	0.8	0.2476	-0.6906	0.8463	8.28×10^{-5}

The plot of the error functions $E(A, c_0, \delta)$ is given in Figures 5.2-5.4 for three schemes at their optimum A values.

The plots of $\widehat{f}(\eta)$ and $\widehat{f}'(\eta)$ are presented in Figures 5.5-5.6, for parametric values in Table 5.1 for $E_1(A, c_0, \delta)$. In Figures 5.7-5.8 the plots of $\widehat{\theta}(\eta)$ and $\widehat{\phi}(\eta)$ are presented for parametric values in
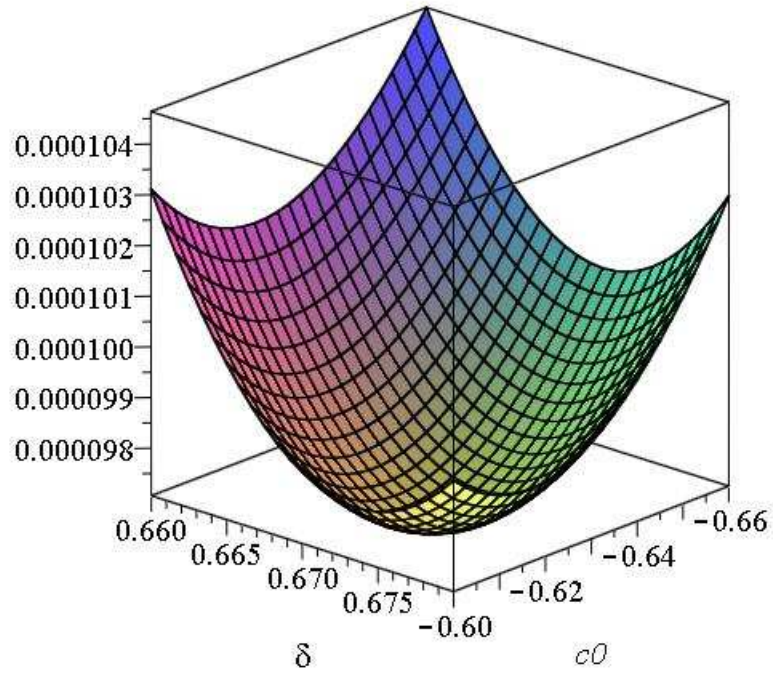
Figure 5.2: Plot of $E(c_0, \delta)$, the squared residual error over $\eta \in [0, 499]$ as a function of c_0 and δ using parameter values $Le = 2$, $Nb = 2$, $Pr = 1$, $Nt = 1$, $n = 0.5$, $A = 0.1314$. The error function has minimum $E(c_0, \delta, A) = 9.71 \times 10^{-5}$ where $c_0 = -0.6195$ and $\delta = 0.8462963$.

Table 5.1 for $E(A, c_0, \delta)$.

A very good validation of the present analytical results has been achieved with the numerical results as shown in Figure 5.9. Also, it is found that the squared residual error decreases as a function of the number of terms in the approximation series, as shown in Figure 5.10.

The skin friction at the surface $|-\widehat{f}''(0)|$ as a function of the stretching parameter n is presented in
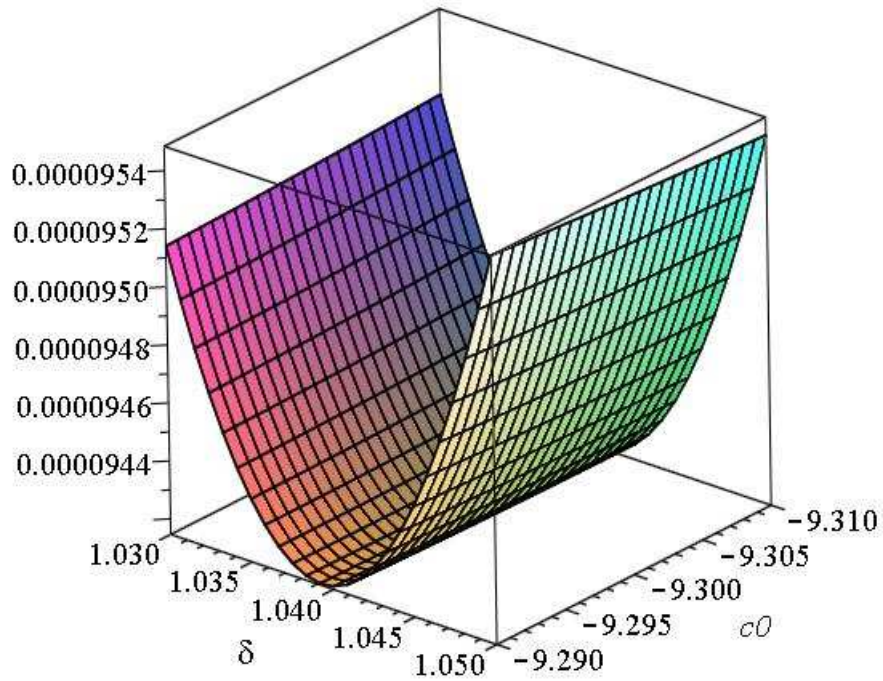
Figure 5.3: Plot of $E(c_0, \delta)$, the squared residual error over $\eta \in [0, 499]$ as a function of c_0 and δ using parameter values $Le = 3$, $Nb = 1$, $Pr = 5$, $Nt = 0$, $n = 1$, $A = 7.8902$. The error function has minimum $E(c_0, \delta, A) = 9.41 \times 10^{-5}$ where $c_0 = -9.30195$ and $\delta = 1.03944$.

Figure 5.11. It is found that skin friction decreases with an increase in stretching parameter. Figure 5.12 illustrated Nusselt number $|-\widehat{\theta}'(0)|$ as a function of Lewis number (Le) and Brownian motion parameter (Nb). It is found that Nusselt number decreases with increase Nt and Nb. Figure 5.13 illustrated Sherwood number $|-\widehat{\phi}'(0)|$ as a function of Nt, Nb and it is found that Sherwood number increases with increase Nt and but decreases with increasing Nb.
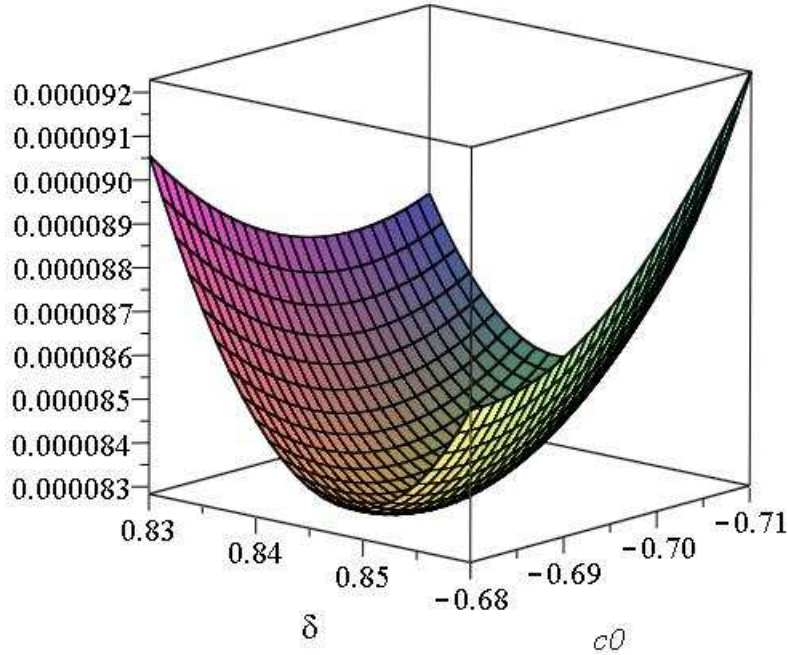
Figure 5.4: Plot of $E(c_0, \delta)$, the squared residual error over $\eta \in [0, 499]$ as a function of c_0 and δ using parameter values $Le = 2$, $Nb = 2$, $Pr = 7$, $Nt = 0.5$, $n = 0.8$, $A = 0.24764$. The error function has minimum $E(c_0, \delta, A) = 8.28 \times 10^{-5}$ where $c_0 = -0.690605$ and $\delta = 0.8462963$.

5.4 Discussion

Liao's Directly Defining inverse Mapping method is extended to a system of three nonlinear diferential equations. Approximate series solutions for $f(\eta), \theta(\eta)$, and $\phi(\eta)$ are obtained. Also, illustrated dimensionless velocity ($f(\eta)$), dimentionless temperature ($\theta(\eta)$) and dimensionless concentration ($\phi(\eta)$) profiles for three set of parameters (see Figures 5.5-5.8) are presented. Further, analytical results are compared with the numerical results (see Figure 5.9) and studied convergence of analytical results (see Figure 5.10).

Figure 5.5: Plot of $\widehat{f}(\eta)$, where Curve 1 has $Le = 2$, $Nb = 2$, $Pr = 1$, $Nt = 1$, $n = 0.5$, Curve 2 has $Le = 3$, $Nb = 1$, $Pr = 5$, $Nt = 0$, $n = 1$, and Curve 3 has $Le = 2$, $Nb = 2$, $Pr = 7$, $Nt = 0.5$, $n = 0.8$ using their respective error-minimizing convergence control parameter.

Since the inverse operator is directly defined, the series solutions are obtained with less CPU time. The freedom of choosing the inverse operator leads to obtaining less complicated terms for the approximation solution. Futher, the selected inverse linear operator leads to three term solution which is accurate up to five decimal places by optimizing square residual function with respect to A, δ, and c_0. Hence, we can conlude that MDDiM is not only easy to use, but also accurate. Theoretically, even if a smaller error was desired, it would just amount to computing more terms in the series by solving deformation equations.Furthermore, one can write an algorithm to iteration approach and truncate the approximate series solution at a given accuracy.

The idea is novel and is useful. This idea is not limited to a single nonlinear differential equation, but can be used for system of several equations. Also, it is important to note that finding an inverse operator that works well for the equation and it leads to an easily generated solution series. Hence,
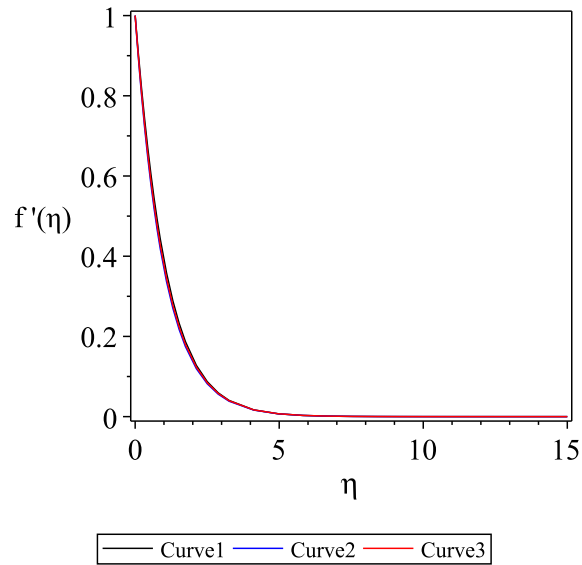
Figure 5.6: Plot of $\widehat{f}'(\eta)$, where Curve 1 has $Le = 2$, $Nb = 2$, $Pr = 1$, $Nt = 1$, $n = 0.5$, Curve 2 has $Le = 3$, $Nb = 1$, $Pr = 5$, $Nt = 0$, $n = 1$, and Curve 3 has $Le = 2$, $Nb = 2$, $Pr = 7$, $Nt = 0.5$, $n = 0.8$ using their respective error-minimizing convergence control parameter.

it is worth-while to investigate this inverse linear operator.
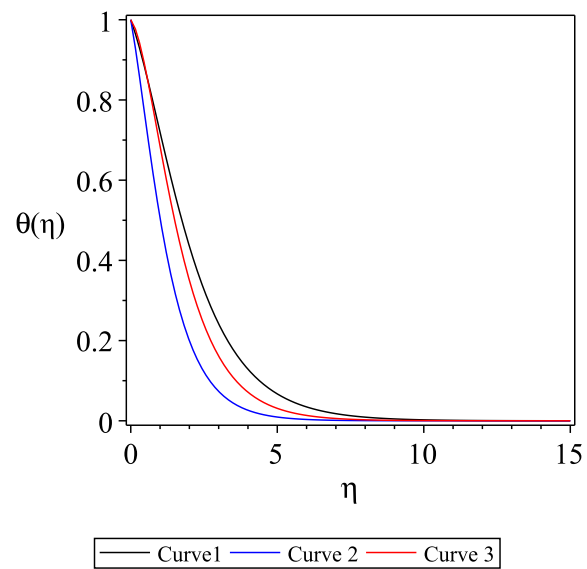
Figure 5.7: Plot of $\widehat{\theta}(\eta)$, where Curve 1 has $Le = 2$, $Nb = 2$, $Pr = 1$, $Nt = 1$, $n = 0.5$, Curve 2 has $Le = 3$, $Nb = 1$, $Pr = 5$, $Nt = 0$, $n = 1$, and Curve 3 has $Le = 2$, $Nb = 2$, $Pr = 7$, $Nt = 0.5$, $n = 0.8$ using their respective error-minimizing convergence control parameter.
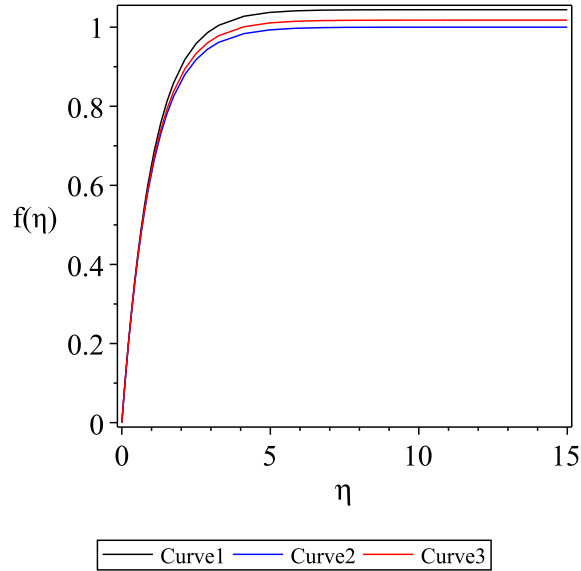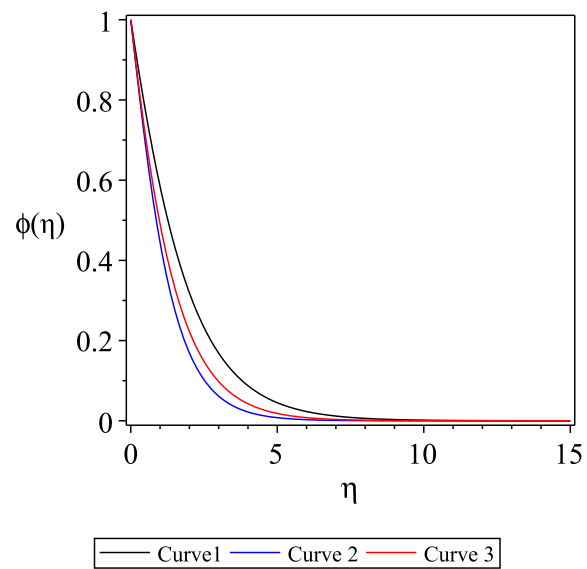
Figure 5.8: Plot of $\widehat{\phi}(\eta)$, where Curve 1 has $Le = 2$, $Nb = 2$, $Pr = 1$, $Nt = 1$, $n = 0.5$, Curve 2 has $Le = 3$, $Nb = 1$, $Pr = 5$, $Nt = 0$, $n = 1$, and Curve 3 has $Le = 2$, $Nb = 2$, $Pr = 7$, $Nt = 0.5$, $n = 0.8$ using their respective error-minimizing convergence control parameter.
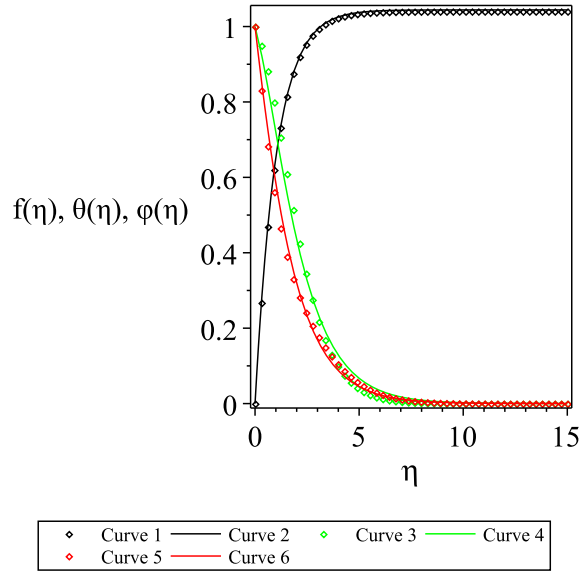
Figure 5.9: Comparison of $f(\eta), \theta(\eta)$ and $\phi(\eta)$ obtained by the MDDiM 3-term approximation and shooting method solutions with $Le = 2$, $Nb = 2$, $Pr = 1$, $Nt = 1$, $n = 0.5$, where Curve 1 is shooting method results of $f(\eta)$, Curve 2 is MDDiM results of $f(\eta)$, Curve 3 is shooting method results of $\theta(\eta)$, Curve 4 is MDDiM results of $\theta(\eta)$, Curve 5 is shooting method results of $\phi(\eta)$, Curve 6 is MDDiM results of $\phi(\eta)$.
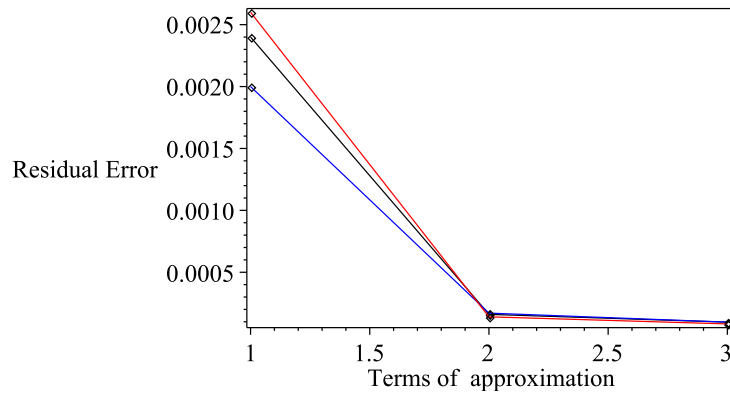
Figure 5.10: Plot of Residual Error function verses Terms of approximation , where Curve 1 has $Le = 2$, $Nb = 2$, $Pr = 1$, $Nt = 1$, $n = 0.5$, Curve 2 has $Le = 3$, $Nb = 1$, $Pr = 5$, $Nt = 0$, $n = 1$, and Curve 3 has $Le = 2$, $Nb = 2$, $Pr = 7$, $Nt = 0.5$, $n = 0.8$ using their respective error-minimizing convergence control parameter.

84
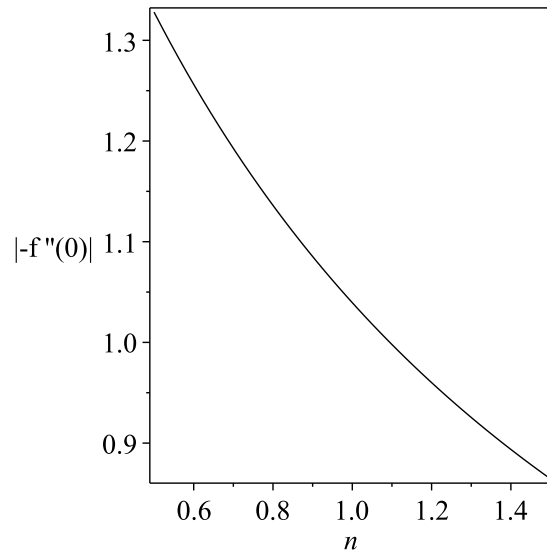
Figure 5.11: Plot of $|-\widehat{f}''(0)|$ versus n, using $Le = 3$, $Nb = 1$, $Pr = 5$ and $Nt = 0$.
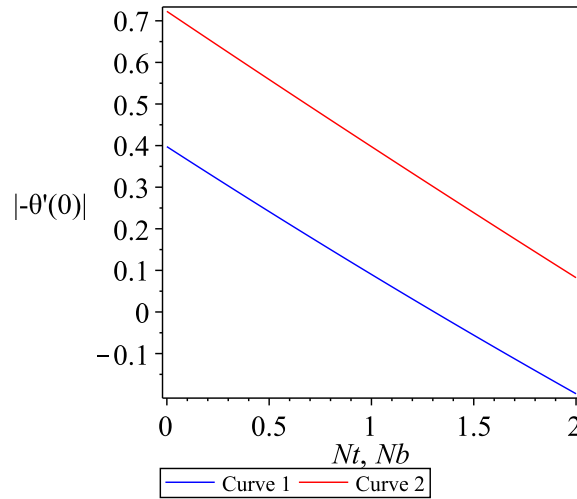
Figure 5.12: Plot of $|-\widehat{\theta}'(0)|$, where Curve 1 is $|-\widehat{\theta}'(0)|$ versus Nt using $Le = 3$, $Nb = 1$, $Pr = 5$, $n = 1$, Curve 2 is $|-\widehat{\theta}'(0)|$ versus Nb using $Le = 3$, $Pr = 5$, $Nt = 0$, $n = 1$.
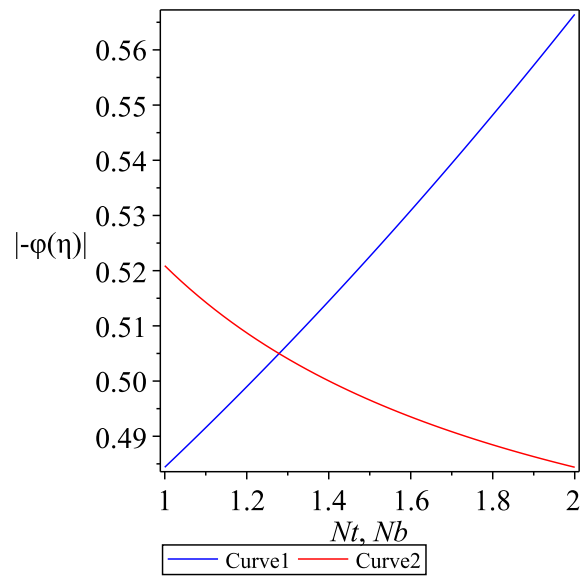
Figure 5.13: Plot of $|-\widehat{\phi}'(0)|$, where Curve 1 is $|-\widehat{\phi}'(0)|$ versus Nt using $Le = 2$, $Nb = 2$, $Pr = 1$, $n = 0.5$, Curve 2 is $|-\widehat{\phi}'(0)|$ versus Nb using $Le = 2$, $Pr = 1$, $Nt = 1$, $n = 0.5$.

CHAPTER 6: A METHOD OF DIRECTLY DEFINING THE INVERSE MAPPING (MDDIM) FOR SOLUTIONS OF NON-LINEAR COUPLED SYSTEMS ARISING IN SIR AND SIS EPIDEMIC MODELS

In this chapter, we extend Liao's newly invented MDDiM for a differential equation to a coupled system of nonlinear differential equations arising in SIR and SIS epidemic models. The method is novel, extended and is applied to the epidemiology models for the first time. This analytic approach is more general and can be used to analyze complicated models arising in mathematical biology, physics and engineering. These results were considered in Dewasurendra et al. [62]

6.1   Background

Epidemiology is the branch of biology that deals with the mathematical modeling of the spread of diseases. Since the time of Kermack and McKendrick [63], the study of mathematical epidemiology has grown repidly and multiple academic research papers discuss the SIR and SIS models (see [64]-[69]).

We consider the SIR model first, a model that is deterministic. The variables (S, I, and R) represent the number of people in each compartment at a particular time. The S stands for the susceptible, which can catch the disease. The I stands for the infective, which are infected and can transmit the disease to the susceptible. The R stands for the removed classes, who had the disease and recovered, died, developed immunity, or have been removed from contact with the other classes.

Some infectives, for example those from the common cold and influenza, do not result in long-lasting immunity for the previously affected. Here, the infectives can return to the susceptible class after being healed, and therefore we use the SIS model. The SIS modes are more effective for diseases caused by bacteria or helminthes agents, as well as for most sexually transmitted diseases.

Kermack and McKendrick [63] provided the mathematical models for SIR and SIS. We use the MDDiM to get approximate series solutions. This is a creative and effective technique, which has been proven to work for strongly nonlinear differential equations [3], [40]. In Sections 2 and 3 of this paper, we develop MDDiM solutions for SIR and SIS models, respectively. Our results are in very good agreement with Khan et al. [64], Singh [69], and also with the numerical results.

6.2 MDDIM for SIR Model

Consider the clasical SIR model [63] described by

$$s'(t) = -rs(t)i(t), \tag{6.1}$$

$$i'(t) = rs(t)i(t) - \alpha i(t), \tag{6.2}$$

with boundary conditions

$$s(0) = S_0, \quad i(0) = I_0, \quad i'(0) = I_0(rS_0 - \alpha), \quad s'(0) = -rS_0I_0, \quad s(\infty) = S_\infty, \quad i(\infty) = I_\infty, \tag{6.3}$$

where $s(t)$, $i(t)$, $r > 0$ and $\alpha > 0$ denote susceptibles, infectives, infectivity coefficient of the typical Lotka-Volterra interaction term, and recovery coefficient, respectively. Additional initial conditions $i'(0) = I_0(rS_0 - \alpha)$, $s'(0) = -rS_0I_0$ were obtained from (6.1) and (6.2). From previous studies, $i(t)$ decreases monotonically from I_0 to 0 when $\frac{rS_0}{\alpha} < 1$, but increases to a maximum value and then decreases to zero when $\frac{rS_0}{\alpha} > 1$. Hence, it always holds that $I_\infty = 0$. Further, it is known that

$$S_\infty + I_\infty - \frac{\alpha}{r} \ln S_\infty = S_0 + I_0 - \frac{\alpha}{r} \ln S_0 \tag{6.4}$$

and S_∞, I_∞ can be obtained for known values of S_0, I_0. Here, $I_0 > 0, S_0 > 0$ are given constants and I_∞, S_∞ defined to be as follows

$$I_\infty = i(\infty), \quad S_\infty = s(\infty). \tag{6.5}$$

6.2.1 MDDIM Deformation Equations

The MDDiM is an extension to Optimal Homotopy Analysis Method (OHAM) (see [1]-[2]) which is an analitical method that used to solve nonlinear differential equations. Here, we first discuss the space that the solution come from and obtain the deformation equations for the coupled system. Then, apply the MDDiM to solve the deformation equations by introducing a suitable inverse mapping $\mathscr{I}$.

Define two nonlinear operators

$$\mathcal{N}_1[s(t), i(t)] = s'(t) + rs(t)i(t), \tag{6.6}$$

$$\mathcal{N}_2[s(t), i(t)] = i'(t) - rs(t)i(t) + \alpha i(t) \tag{6.7}$$

so that $\mathcal{N}_1[s(t), i(t)] = 0$ and $\mathcal{N}_2[s(t), i(t)] = 0$ give the original coupled equations (6.1)-(6.2) respectively. After a thorough study of nonlinear sytem (6.1)-(6.2) with the boundary conditions (6.3), we define linearly independent set of functions

$$S_\infty = \{1, e^{-\beta t}, e^{-2\beta t}, ...\}, \tag{6.8}$$

with solution space for $s(t)$ and $i(t)$ as

$$V = \left\{ \sum_{k=0}^{\infty} a_k e^{-k\beta t} \,\middle|\, a_k \in \mathbb{R} \right\}. \tag{6.9}$$

Next, define the base set for the initial guess as $S^* = \left\{ 1, e^{-\beta t}, e^{-2\beta t} \right\}$ by taking the first three terms of the set S_∞, and define spaces for initial guesses for $s(t)$ and $i(t)$ as

$$V^* = \left\{ a_0 + a_1 e^{-\beta t} + a_2 e^{-2\beta t} \,\middle|\, a_0, a_1, a_2 \in \mathbb{R} \right\}. \tag{6.10}$$

Then the primary solutions, or the initial guesses, $\mu_1(t), \mu_2(t) \in V^*$, have the following forms

$$\mu_1(t) = \sum_{k=0}^{2} a_k e^{-k\beta t}, \quad \mu_2(t) = \sum_{k=0}^{2} a_k e^{-k\beta t}. \tag{6.11}$$

Next, define $\widehat{S}$ as

$$\widehat{S} = \left\{ e^{-3\beta t}, e^{-4\beta t}, ... \right\} \tag{6.12}$$

and then define $\widehat{V}$ so that $V = V^* \cup \widehat{V}$. Hence,

$$\widehat{V} = \left\{ \sum_{k=3}^{\infty} a_k e^{-k\beta t} \,\middle|\, a_k \in \mathbb{R} \right\}. \tag{6.13}$$

Now, define

$$S_R = \{\psi_1(t), \psi_2(t), ...\} \tag{6.14}$$

90

so that S_R is the basis for terms in the codomain of the nonlinear operators $\mathcal{N}_1$ and $\mathcal{N}_2$. Further, all the functions expressed by S_R form a set of functions, denoted by

$$U = \left\{ \sum_{k=1}^{\infty} c_k \psi_k(t) \big| c_k \in \mathbb{R} \right\}. \tag{6.15}$$

Assuming that $\mathcal{N}_1[s(t), i(t)]$, $\mathcal{N}_2[s(t), i(t)] \in U$, say, nonlinear differential operators where $\mathcal{N}_1, \mathcal{N}_2$ are mappings from V to U, i.e. $\mathcal{N}_1$, $\mathcal{N}_2 : V \to U$. Let us construct two homotopies of operators in order to apply OHAM as follows

$$0 \equiv \mathcal{H}_1(s, i, q) = (1-q)\mathcal{L}_1[s] - c_0 q \mathcal{N}_1[s, i], \tag{6.16}$$

$$0 \equiv \mathcal{H}_2(s, i, q) = (1-q)\mathcal{L}_2[i] - c_1 q \mathcal{N}_2[s, i]. \tag{6.17}$$

Here, $\mathcal{H}_1$ and $\mathcal{H}_2$ are the homotopies between linear operators $\mathcal{L}_1, \mathcal{L}_2$ and nonlinear operators $\mathcal{N}_1, \mathcal{N}_2$. Further, $q \in [0, 1]$ is the homotopy parameter and c_0, c_1 are non-zero auxiliary parameters, called the convergence control parameters. In the frame of MDDiM, let us assume series solutions for $s(t)$ and $i(t)$ in terms of the homotopy parameter as

$$s(t) = s_0(t) + \sum_{k=1}^{\infty} s_k(t) q^k \tag{6.18}$$

$$i(t) = i_0(t) + \sum_{k=1}^{\infty} i_k(t) q^k \tag{6.19}$$

where $s_0(t)$ and $i_0(t)$ are the initial guesses that satisfy the boundary conditions (6.3) and belong to V^*. It is straightforward to choose the initial guesses

$$s_0(t) = S_\infty + (2(S_0 - S_\infty) - \frac{rS_0I_0}{\beta})e^{-\beta t} + (-(S_0 - S_\infty) + \frac{rS_0I_0}{\beta})e^{-2\beta t}, \tag{6.20}$$

91

$$i_0(t) = (2I_0 + \frac{I_0(rS_0 - \alpha)}{\beta})e^{-\beta t} + (-I_0 - \frac{I_0(rS_0 - \alpha)}{\beta})e^{-2\beta t}. \qquad (6.21)$$

Obviously, when $q = 0$ the homotopies (6.16)-(6.17) become $\mathcal{L}[s] = 0$ and $\mathcal{L}_2[i] = 0$. Since, c_0 and c_1 are non-zero parameters, when $q = 1$, homotopies (6.16)-(6.17) are equivalent to the original nonlinear coupled system (6.1) and (6.2). Hence, when $q = 1$, the series solutions (6.18)-(6.19) are the solutions to the nonlinear coupled system (6.1)-(6.2). Substituting these series solutions (6.18)-(6.19) into (6.16), we obtain the so-called deformation equations for $k \geq 1$ as

$$\mathcal{L}_1[s_k(t)] = \chi_k \mathcal{L}_1[s_{k-1}(t)] + c_0 \delta^1_{k-1}(t), \qquad (6.22)$$

$$s_k(0) = 0, \quad s'_k(0) = 0, \quad s_k(\infty) = 0, \qquad (6.23)$$

where

$$\chi_k = \begin{cases} 0, & k \leq 1, \\ 1, & k > 1. \end{cases} \qquad (6.24)$$

Here δ^ξ_k, for $\xi = 1, 2$, are homotopy derivatives and are defined to be

$$\delta^\xi_{k-1}(t) = \frac{1}{(k-1)!} \left(\frac{\partial^{k-1}}{\partial q^{k-1}} \mathcal{N}_\xi \left[\sum_{j=0}^\infty s_j(t)q^j, \sum_{j=0}^\infty i_j(t)q^j \right] \right) \Bigg|_{q=0}. \qquad (6.25)$$

Similarly, substituting (6.18)-(6.19) into the homotopy defined in (6.17), the other set of deformation equations is obtained as

$$\mathcal{L}_2[i_k(t)] = \chi_k \mathcal{L}_2[i_{k-1}(t)] + c_1 \delta^2_{k-1}(t), \qquad (6.26)$$

92

$$i_k(0) = 0, \quad i'_k(0) = 0, \quad i_k(\infty) = 0, \tag{6.27}$$

for $k \geq 1$. In the frame of OHAM, equations (6.22)-(6.27) can be used to obtain approximate series solutions to the coupled nonlinear systems (see [2], [43] - [51]). The only drawback of OHAM is, it takes lot of CPU time. This happens because, first we choose auxiliary linear operators, and then solving the linear higher order deformation equation only to find out the inverse operator. However, in the frame of MDDiM we have freedom to define directly the inverse linear operator (see [3], [40]) leading to solve higher order deformation equations lot more faster than in OHAM. Now, following Liao's MDDiM, the deformation equations are

$$s_k(t) = \chi_k s_{k-1}(t) + c_0 \mathscr{J} \left[\delta^1_{k-1}(t) \right] + a_{k,2} e^{-2\beta t} + a_{k,1} e^{-\beta t} + a_{k,0}, \tag{6.28}$$

$$i_k(t) = \chi_k i_{k-1}(t) + c_1 \mathscr{J} \left[\delta^2_{k-1}(t) \right] + b_{k,2} e^{-2\beta t} + b_{k,1} e^{-2\beta t} + b_{k,0}, \tag{6.29}$$

with boundary conditions

$$s_k(0) = 0, \quad s'_k(0) = 0, \quad s_k(\infty) = 0, \quad i_k(0) = 0, \quad i'_k(0) = 0, \quad i_k(\infty) = 0. \tag{6.30}$$

Since we know initial guesses, can find rest of the terms of series solutions by solving deformation equations (6.28)-(6.30) In the present study we used the same inverse linear operator $\mathscr{J}$ for both equations. But some one could use different inverse linear operators to get different structures for solutions if required.

We defined $\mathscr{J} : U \to V$, by

$$\mathscr{J}[e^{-kt}] = \frac{e^{-k\beta t}}{Ak^3 + k}. \tag{6.31}$$

Figure 6.1: Plot of $E(h, A)$ over $t \in [1, 499]$ for parameter values $S_0 = 80$, $I_0 = 50$, $S_\infty = 29.19$, $I_\infty = 0$, $\alpha = 10$, $r = 0.1$, $\beta = 7.081$. Minimum of $E(h, A) = 3.42 \times 10^{-8}$ at $A = -0.0038$ and $h = 0.1282$.

where A, β are parameters which will be use to optimize the square residual error functions.

6.2.2   Results and Error Analysis

The approximate series solution for the coupled nonlinear system (6.1)-(6.2) with boundary conditions (6.3) are obtained using MDDiM. Further, error analysis is used to get a general idea about how accurate our approximate solutions are.

First, define a three term approximations for $\widehat{s}$ and $\widehat{i}$ which are sum of the first three solutions

94
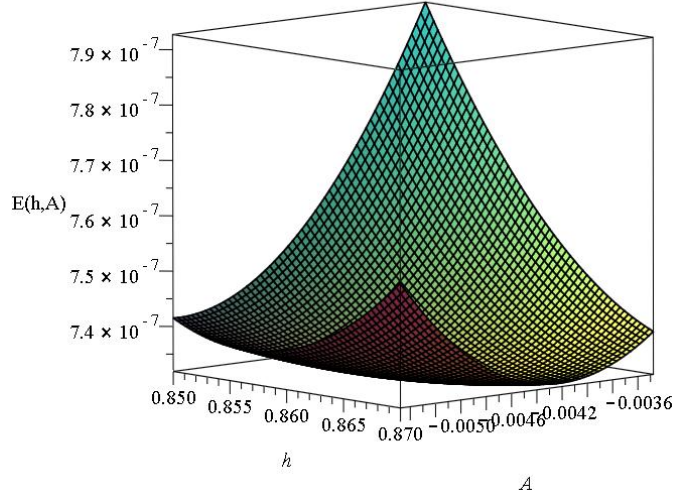
Figure 6.2: Plot of $E(h, A)$ over $t \in [1, 499]$ for parameter values $S_0 = 13$, $I_0 = 10$, $S_\infty = 3.556$, $I_\infty = 0$, $\alpha = 1.5$, $r = 0.1$, $\beta = 1.144$. Minimum of $E(h, A) = 7.32 \times 10^{-7}$ at $A = -0.0045$ and $h = 0.8659$.

to the MDDiM deformation equations. Then, define residual error functions $\mathcal{N}_1[\widehat{s}(t), \widehat{i}(t)]$ and $\mathcal{N}_2[\widehat{s}(t), \widehat{i}(t)]$ in order to obtain square residual error functions. Now, taking square of the L^2-norm of residual error functions and setting converge control parameters to be $c_0 = c_1 = h$ we define square residual error functions

$$E_\xi[h, A, \beta] = \int_0^\infty \left(\mathcal{N}_\xi \left[\widehat{s}(t), \widehat{i}(t) \right] \right)^2 dt \quad \text{for} \quad \xi = 1, 2. \tag{6.32}$$

But in practice the evaluation of $E_\xi[h, A, \beta]$ is much time consuming so instead of exact residual error we use average residual error defined as

$$E_\xi[h, A, \beta] = \frac{1}{M+1} \sum_{j=0}^M \left(N_\xi \left[\widehat{s}(t), \widehat{i}(t) \right] \right)^2 \quad \text{for} \quad \xi = 1, 2, \tag{6.33}$$
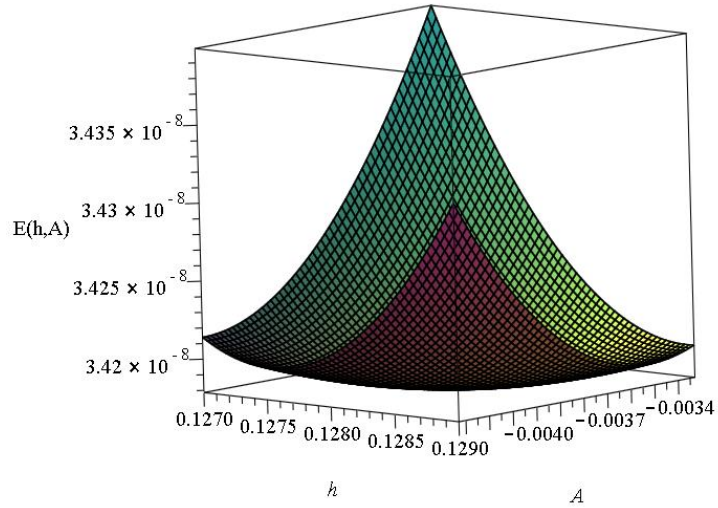
95
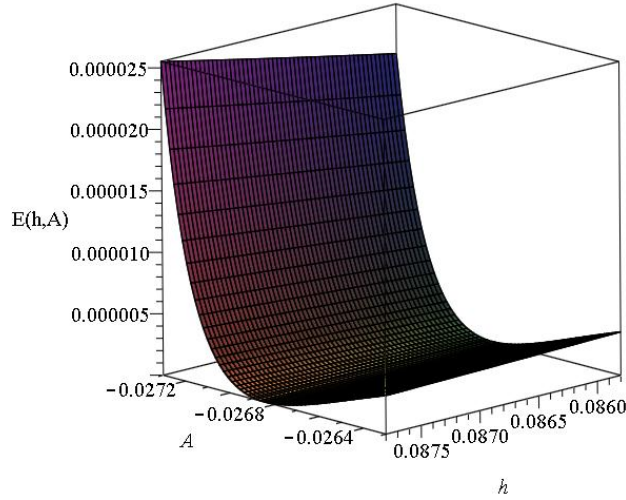
Figure 6.3: Plot of $E(h, A)$ over $t \in [1, 499]$ for parameter values $S_0 = 120$, $I_0 = 50$, $S_\infty = 29.421$, $I_\infty = 0$, $\alpha = 10$, $r = 0.1$, $\beta = 7.058$. Minimum of $E(h, A) = 1.01 \times 10^{-11}$ at $A = -0.0269$ and $h = 0.0868$.

and define a total error function by taking affine combination of two square residual functions

$$E[h, A, \beta] = \sum_{\xi=1}^{2} E_\xi[h, A, \beta]. \tag{6.34}$$

Next, we optimize the total error function with respect to h, A and β and obtain optimal values for h, A and β. Substituting optimal values of h, A and β we obtain three term approximation solution to the nonlinear coupled system (6.1)-(6.2) which satisfies the conditions (6.3).

Taking three sets of parametric values for S_0, I_0, α and r we obtained total error $E[h, A, \beta]$ and presented in the table below. The plots of the total error functions $E[h, A, \beta]$ for three sets of respective parametric values are presented in Figs. 6.1, 6.2 and 6.3. The plots of the approximate series solutions $\widehat{s}(t)$ and $\widehat{i}(t)$ were obtained for parametric values in the Table 5.1 and presened in

96

Figure 6.4: Comparison of $s(t)$ obtained by MDDiM 3-term approximation and Runge-Kutta method solutions with $S_0 = 80$, $I_0 = 50$, $S_\infty = 29.19, I_\infty = 0$, $\alpha = 10$, $r = 0.1$, where Curve 1 is Runge-Kutta method results of $s(t)$, Curve 2 is MDDiM results of $s(t)$, Curve 3 is Runge-Kutta method results of $i(t)$, Curve 4 is MDDiM results of $i(t)$.

Table 6.1: Minimum of the total error $E[h, A, \beta]$ for three different sets of parameters.

S_0	I_0	S_∞	I_∞	α	r	h	A	β	$E[h, A, \beta]$
80	50	29.19	0	10	0.1	0.1282	-0.0038	7.081	3.42×10^{-8}
13	10	3.556	0	1.5	0.1	0.8659	-0.0045	1.144	7.32×10^{-7}
120	50	29.421	0	10	0.1	0.0868	-0.0269	7.058	1.01×10^{-11}

Figs. 6.4-6.6 with numerical results. It is investigated that the present analytical results are in very good agreement with the numerical results (Runge-Kutta method). Also, we investigated that for $\frac{S_0 r}{\alpha} > 1$, I initially increases to some maximum number, but eventually decreases and aproches zero (see Fig. 6.6), and this indicates epidemic spreading behavior. But I tends to zero for $\frac{S_0 r}{\alpha} < 1$ (see Figs. 6.4 and 6.5) and this indicates no epidemic behaviour. Hence, our results agrees with
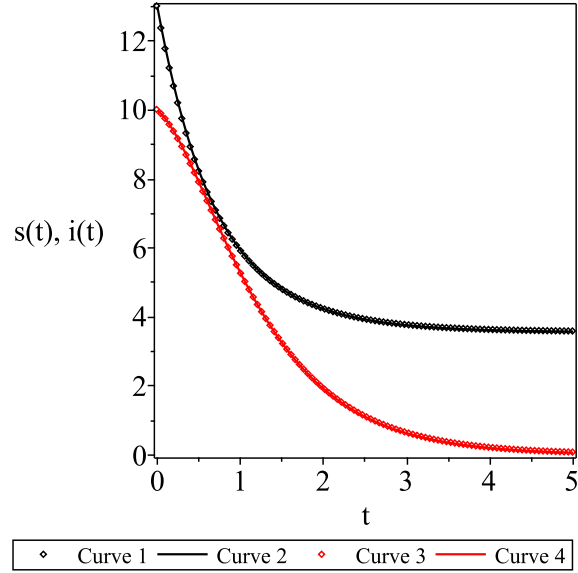
Figure 6.5: Comparison of $s(t)$ obtained by MDDiM 3-term approximation and Runge-Kutta method solutions with $S_0 = 13$, $I_0 = 10$, $S_\infty = 3.556$, $I_\infty = 0$, $\alpha = 1.5$, $r = 0.1$, where Curve 1 is Runge-Kutta method results of $s(t)$, Curve 2 is MDDiM results of $s(t)$, Curve 3 is Runge-Kutta method results of $i(t)$, Curve 4 is MDDiM results of $i(t)$.

qualitative analysis of Singh's [69]. Moreover, our analytical result agree well with the OHAM solution of Khan et al.[64].

6.3   MDDIM for SIS Model

Consider the basic SIS model [63] described by

$$s'(t) = -rs(t)i(t) + \gamma i(t), \tag{6.35}$$

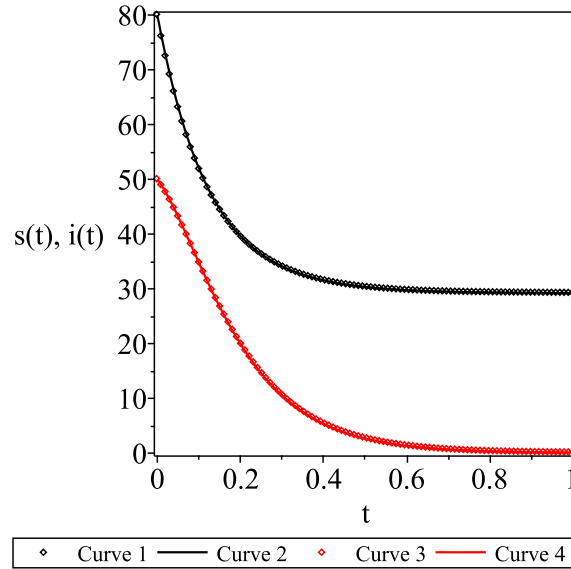$$i'(t) = rs(t)i(t) - \gamma i(t), \tag{6.36}$$
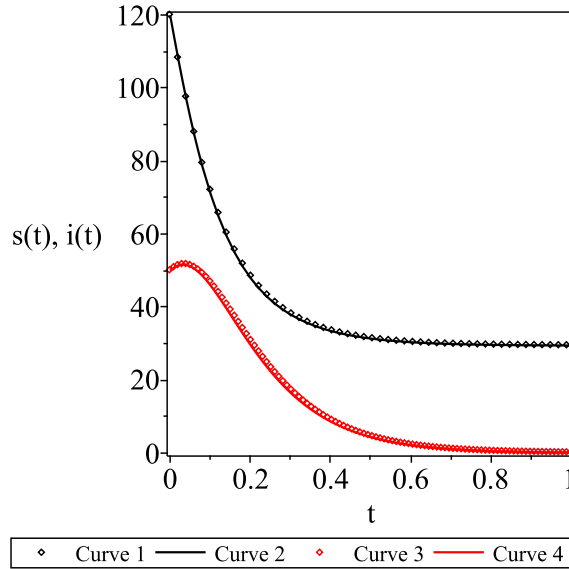
Figure 6.6: Comparison of $s(t)$ obtained by MDDiM 3-term approximation and Runge-Kutta method solutions with $S_0 = 120$, $I_0 = 50$, $S_\infty = 29.421$, $I_\infty = 0$, $\alpha = 10$, $r = 0.1$, where Curve 1 is Runge-Kutta method results of $s(t)$, Curve 2 is MDDiM results of $s(t)$, Curve 3 is Runge-Kutta method results of $i(t)$, Curve 4 is MDDiM results of $i(t)$.

with boundary conditions

$$s(0) = S_0, \quad i(0) = I_0, \quad s'(0) = -rS_0I_0 + \gamma I_0, \quad i'(0) = rS_0I_0 - \gamma I_0, \quad s(\infty) = S_\infty, \quad i(\infty) = S_\infty,$$

$$(6.37)$$

where $r > 0, I_0 > 0$ and $S_0 > 0$. From, (6.35) and (6.36) we obtained additional initial conditions

$s'(0) = -rS_0I_0 + \gamma I_0$, $i'(0) = rS_0I_0 - \gamma I_0$. Also, from (6.35) and (6.36), it is easy to see that,

$s + i = k$, where k is a constant. Further, there are two different cases for t approaching to ∞

(i) if $\frac{\gamma k}{r} \leq 1$ for any I_0, then

$$i(\infty) = 0, \quad s(\infty) = k; \tag{6.38}$$

99

(ii) if $\frac{\gamma k}{r} > 1$ for any I_0, then

$$i(\infty) = k - \frac{\gamma}{r}, \quad s(\infty) = \frac{\gamma}{r}. \tag{6.39}$$

In the SIS model, recovered members return to the class of susceptible at the rate of γi. Here, γ is the recovery coefficient.

6.3.1 MDDIM Deformation Equations

SIS model equations can be solved using a similar approach. From (6.35) and (6.36) we define

$$\mathcal{N}_1[s(t), i(t)] = s'(t) + rs(t)i(t) + \gamma i(t), \tag{6.40}$$

$$\mathcal{N}_2[s(t), i(t)] = i'(t) - rs(t)i(t) + \gamma i(t). \tag{6.41}$$

In the frame of MDDiM, we have the solution series for both $s(t)$ and $i(t)$

$$s(t) = s_0(t) + \sum_{k=0}^{\infty} f_k(t), \tag{6.42}$$

$$i(t) = i_0(t) + \sum_{k=0}^{\infty} i_k(t). \tag{6.43}$$

where $s_0(t)$ and $i_0(t)$ satisfies all the boundary conditions, and $s_k(t)$ and $i_k(t)$ is given by

$$s_k(t) = \chi_k s_{k-1}(t) + c_0 \mathscr{J}\left[\delta_{k-1}^1(t)\right] + a_{k,2}e^{-2\beta t} + a_{k,1}e^{-\beta t} + a_{k,0}, \tag{6.44}$$

$$i_k(t) = \chi_k i_{k-1}(t) + c_1 \mathscr{J}\left[\delta_{k-1}^2(t)\right] + b_{k,2}e^{-2\beta t} + b_{k,1}e^{-2\beta t} + b_{k,0}. \tag{6.45}$$

100

with boundary conditions

$$s_k(0) = 0, \quad s'_k(0) = 0, \quad s_k(\infty) = 0, \quad i_k(0) = 0, \quad i'_k(0) = 0, \quad i_k(\infty) = 0, \qquad (6.46)$$

where c_0 and c_1 are convergence-control parameters, $\mathscr{I}$ is directly defined inverse mapping, and

$$\delta^{\xi}_{k-1}(t) = \frac{1}{(k-1)!} \left(\frac{\partial^{k-1}}{\partial q^{k-1}} \mathcal{N}_\xi \left[\sum_{j=0}^{\infty} s_j(t)q^j, \sum_{j=0}^{\infty} 1_j(t)q^j \right] \right) \Bigg|_{q=0} \qquad \text{for} \quad \xi = 1, 2. \qquad (6.47)$$

According to (6.46), $s'_k(t)$ and $i'_k(t)$ tends to infinity. So, we define the spaces

$$V = \left\{ \sum_{k=0}^{\infty} a_k e^{-k\beta t} \big| a_k \in \mathbb{R} \right\} = U. \qquad (6.48)$$

$$V^* = \left\{ a_0 + a_1 e^{-\beta t} + a_2 e^{-2\beta t} \big| a_0, a_1, a_2 \in \mathbb{R} \right\}. \qquad (6.49)$$

$$\widehat{V} = \left\{ \sum_{k=3}^{\infty} a_k e^{-k\beta t} \big| a_k \in \mathbb{R} \right\}. \qquad (6.50)$$

such that $V = \widehat{V} \cup V^*$. It is obvious that $s(t), i(t) \in V$ and $\delta_k(t) \in \widehat{V}$. Then, the initial guesses s_0 and i_0 satisfying conditions (6.37) are

$$s_0(t) = S_\infty + (2(S_0 - S_\infty) + \frac{I_0(\gamma - rS_0)}{\beta})e^{-\beta t} + (S_\infty - S_0 + \frac{I_0(rS_0 - \gamma)}{\beta})e^{-2\beta t} \qquad (6.51)$$

$$i_0(t) = I_\infty + (2(I_0 - I_\infty) + \frac{I_0(rS_0 - \gamma)}{\beta})e^{-\beta t} + (I_\infty - I_0 + \frac{I_0(\gamma - rS_0)}{\beta})e^{-2\beta t} \qquad (6.52)$$

from the space V^*. Now we can obtain other terms of the series solutions using deformation equations (6.44), (6.45) and conditions (6.46). Further, we use the same inverse linear mapping
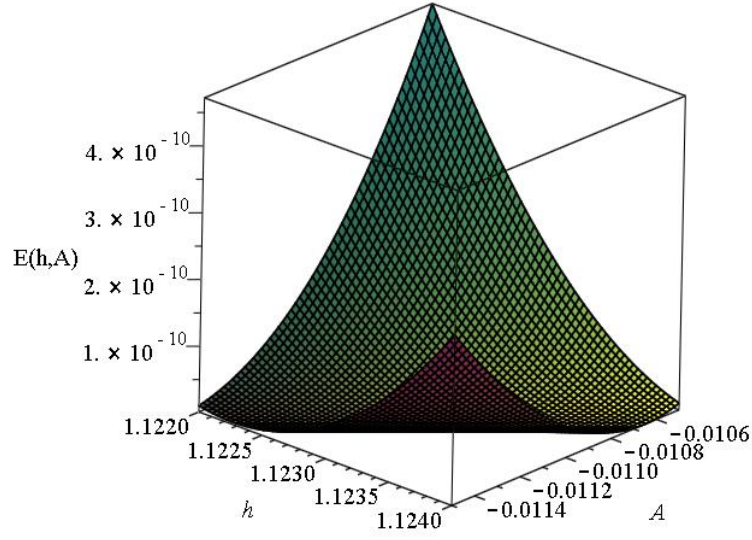
Figure 6.7: Plot of $E(h, A)$ over $t \in [1, 499]$ for parameter values $S_0 = 25$, $I_0 = 10$, $S_\infty = 15$, $I_\infty = 20$, $\gamma = 1.5$, $r = 0.1$, $\beta = 2$. Minimum of $E(h, A) = 2.61 \times 10^{-12}$ at $A = -0.0110$ and $h = 1.1233$.

$\mathscr{J}$ defined in (6.31) to obtain series solutions.

6.3.2 Results and Error Analysis

As in SIS model we defined total error

$$E[h, A, \beta] = \sum_{\xi=1}^{2} E_\xi[h, A, \beta], \tag{6.53}$$

where

$$E_\xi[h, A, \beta] = \frac{1}{M+1} \sum_{j=0}^{M} \left(N_\xi \left[\widehat{s}(j), \widehat{i}(j) \right] \right)^2 \quad \text{for} \quad \xi = 1, 2. \tag{6.54}$$
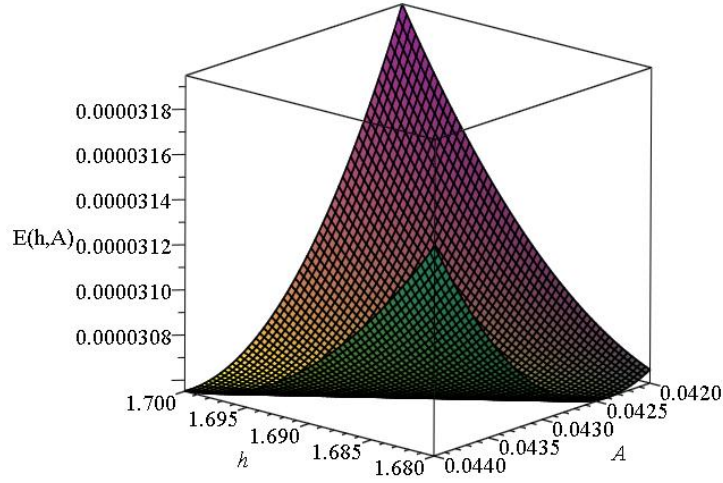
Figure 6.8: Plot of $E(h, A)$ over $t \in [1, 499]$ for parameter values $S_0 = 10$, $I_0 = 25$, $S_\infty = 1.5$, $I_\infty = 33.5$, $\gamma = 0.1$, $r = \frac{1}{15}$, $\beta = 1$. Minimum of $E(h, A) = 3.06 \times 10^{-5}$ at $A = 0.0432$ and $h = 1.6906$.

Here, $\widehat{s}$ and $\widehat{i}$ are the three-term MDDiM solutions and set $c_0 = c_1 = h$. Next, we optimize total

error function with respect to h, A and β. Then, obtained three term approximation solution to

the nonlinear coupled system (6.35)-(6.36) which satisfies the conditions (6.37) by substituting

optimal values of h, A and β. Taking three schemes of parametric values for parameters S_0, I_0, α

Table 6.2: Minimum of total error $E[h, A, \beta]$ for three different sets of parameters.

S_0	I_0	S_∞	I_∞	γ	r	h	A	β	$E(h, A, \beta)$
25	10	15	20	1.5	0.1	1.1233	-0.0110	2	2.61×10^{-12}
10	25	1.5	33.5	0.1	$\frac{1}{15}$	1.6906	0.0432	1	3.06×10^{-5}
15	5	20	0	2	0.05	0.6054	-0.0313	1	2.89×10^{-17}

and r we obtained a total error $E[h, A, \beta]$ and presented in the Table 5.2. The plots of total error

functions $E[h, A, \beta]$ for the three schemes were presented in Figs. 6.7, 6.8 and 6.9.

103
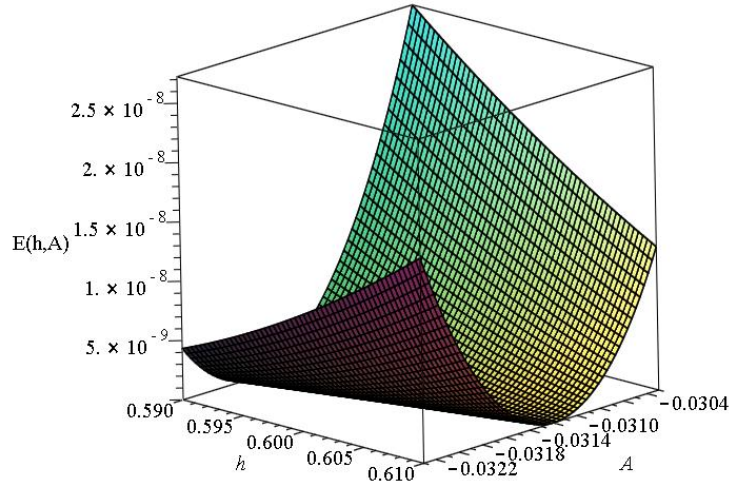
Figure 6.9: Plot of $E(h, A)$ over $t \in [1, 499]$ for parameter values $S_0 = 15$, $I_0 = 5$, $S_\infty = 20$, $I_\infty = 0$, $\gamma = 2$, $r = 0.05$, $\beta = 1$. Minimum of $E(h, A) = 2.89 \times 10^{-17} \times 10^{-5}$ at $A = -0.0313$ and $h = 0.6054$.

The plots of approximate series solutions $\widehat{s}(t)$ and $\widehat{i}(t)$ were obtained for parametric values in the Table 5.2 and presented with numerical results in Figs. 6.10-6.12. Our results, agree very well with the numerical results. Further, we investigated that for $\frac{rk}{\gamma} > 1$, the infection continues, this indicates the epidemic case. For $\frac{rk}{\gamma} < 1$, indicating the infection vanish. Hence, our results agree with Singh's [69] qualitative analysis. Moreover, our analytical results agree well with the OHAM solution of Khan et al. [64].

Figure 6.10: Comparison of $s(t)$ obtained by MDDiM 3-term approximation and Runge-Kutta method solutions with $S_0 = 25$, $I_0 = 10$, $S_\infty = 15$, $I_\infty = 20$, $\gamma = 1.5$, $r = 0.1$, where Curve 1 is Runge-Kutta method results of $s(t)$, Curve 2 is MDDiM results of $s(t)$, Curve 3 is Runge-Kutta method results of $i(t)$, Curve 4 is MDDiM results of $i(t)$.

6.4   Discussion

In the present study, MDDiM has been developed and used to solve the SIR and the SIS models in biology. Approximate analytical solutions for the susceptibles and the infectives were found. Further, our analytical solutions are in good agreement with Khan et al. [64] and Singh [69], and also with the numerical results.

The freedom of directly defining the inverse linear mapping leads to three term solutions with less complicated terms for the approximate series solutions and thus reduce the CPU time. Further, selected inverse linear mapping leads to three term solution with total error between 10^{-5} to 10^{-17} (see Table 5.1 and Table 5.2). Hence, we can conclude that MDDiM is not only efficient, but also

105

Figure 6.11: Comparison of $s(t)$ obtained by MDDiM 3-term approximation and Runge-Kutta method solutions with $S_0 = 10$, $I_0 = 25$, $S_\infty = 1.5$, $I_\infty = 33.5$, $\gamma = 0.1$, $r = \frac{1}{15}$, where Curve 1 is Runge-Kutta method results of $s(t)$, Curve 2 is MDDiM results of $s(t)$, Curve 3 is Runge-Kutta method results of $i(t)$, Curve 4 is MDDiM results of $i(t)$.

accurate. Further, it is worth investigating how to find an inverse linear operator which gives high accuracy, or leads to easily generated solution terms, or both.

To our best knowledge, this is the first time MDDiM is used to solve mathematical models related to epidemiology. Further, this novel method is more general and can be used to analyze more complicated mathematical biology and other models in science and engineering.
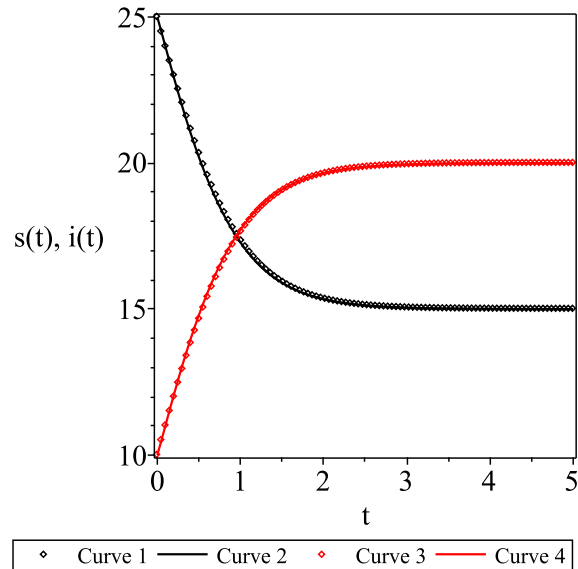
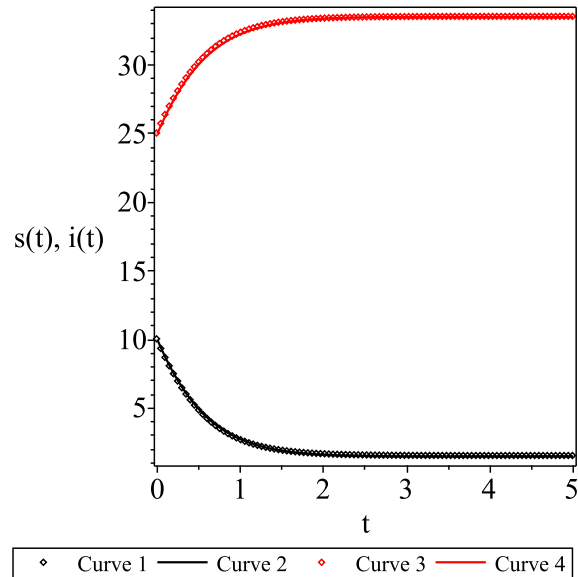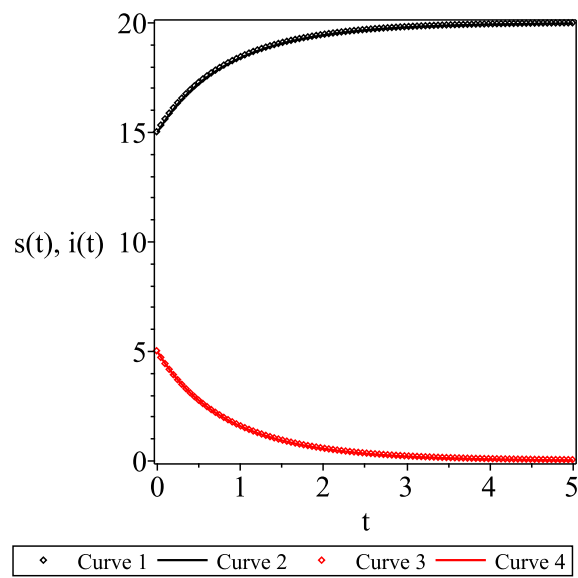Figure 6.12: Comparison of $s(t)$ obtained by MDDiM 3-term approximation and Runge-Kutta method solutions with $S_0 = 15$, $I_0 = 5$, $S_\infty = 20$, $I_\infty = 0$, $\gamma = 2$, $r = 0.05$, where Curve 1 is Runge-Kutta method results of $s(t)$, Curve 2 is MDDiM results of $s(t)$, Curve 3 is Runge-Kutta method results of $i(t)$, Curve 4 is MDDiM results of $i(t)$.

CHAPTER 7: CONCLUSION AND FUTURE WORK

Method of Directly Defining the inverse mapping was extended and successfully used to solve systems of coupled nonlinear differential equations. Approximate solutions were compared with numerical solutions and OHAM solutions, and found a great match.

It is found that MDDiM solutions can be obtained with less CPU time compare to OHAM solutions. In our study, a single inverse linear map was used to solve deformation equations, and this was lead to a solution with less complicated terms. Further, it was found that the rate of change of the series solutions depend on inverse linear map. So, it is worth investigating further how the inverse map effects the convergence of the series solution.

MDDiM has been extended to solve systems of ordinary differential equations. However, it is still an open problem to apply this novel method to solve partial differential equations. Hence, I am focusing my attention to solve partial differential equations arising in science and engineering applications with MDDiM.

APPENDIX : PAPERS PUBLISHED

1. M. Dewasurendra, M. Baxter, K. Vajravelu, "A Method of Directly Defining the Inverse Mapping for Fourth Order Non-Linear Systems Arising in Combined Free and Forced Convection in a Second Grade Fluid," Applied Mathematics and Computation **339** (2018) 758-767.

2. M. Dewasurendra, K. Vajravelu, On the Method of Inverse Mapping for Solutions of Coupled Systems of Nonlinear Differential Equations Arising in Nanofluid Flow, Heat and Mass Transfer, Applied Mathematics and Nonlinear Sciences **3** (2018) 1-14.

3. M. Baxter, M. Dewasurendra, K. Vajravelu, "A Method of Directly Defining the inverse Mapping for Solutions of Coupled Systems of Nonlinear Differential Equations," Numerical Algorithm **77** (2017) 1199-1211.

4. K. Vajravelu, R. Li, M. Dewasurendra, K.V. Prasad, "Mixed Convective Boundary Layer MHD Flow Along a Vertical Elastic Sheet," International Journal of Applied and Computational Mathematics **3** (2016), 2501-2518.

Accepted Paper

1. M. Dewasurendra, Y. Zhang, K. Vajravelu, A Method of Directly Defining the inverse Mapping (MDDiM) for solutions of non-linear coupled systems arising in SIR and SIS epidemic models, Communications in Numerical Analysis, Accepted.

LIST OF REFERENCES

[1] S. J. Liao, Beyond Perturbation: Introduction to the Homotopy Analysis Method, Chapman & Hall/CRC Press, Boca Raton, 2003.

[2] S. J. Liao, Homotopy Analysis Method in Nonlinear Differential Equations. Springer & Higher Education Press, Heidelberg, 2012.

[3] S. Liao, Y. Zhao, On the method of directly defining inverse mapping for nonlinear differential equations, Numerical Algorithms 72 (2015) 989 - 1020.

[4] K. Vajravelu, R. Li, M. Dewasurendra, K.V. Prasad, Mixed Convective Boundary Layer MHD Flow Along a Vertical Elastic Sheet, International Journal of Applied and Computational Mathematics 3 (2016)1-18.

[5] H. Blasius, Grenzschichten in Flüssigkeiten mit kleiner Reibung. Z. Math. Phys. 56 (1908) 1 – 37.

[6] E. Pohlhausen, E.: Der Wärmeaustausch zwischen festen Körpern und Flüssigkeiten mit kleinerReibung und kleiner Wärmeleitung. Z. Angew. Math. Mech. 1 (1921) 121–151.

[7] L. Howarth, On the solution of the laminar boundary layer equations. Proc. Roy. Soc. Lond. A. 164 (1938) 547–579.

[8] A. M. M. Abu-Sitta, A note on a certain boundary-layer equation. Appl. Math. Comp. 64 (1994) 73–77.

[9] L. Wang, A new algorithm for solving classical Blasius equation. Appl. Math. Comput. 157 (2004) 1–9.

[10] R. Cortell, Numerical solutions of the classical Blasius flat-plate problem. Appl. Math. Comput. 170 (2005) 706 – 710.

[11] B. C. Sakiadis, Boundary-layer behaviour on continuous solid surfaces: boundary-layer equations for two dimensional and axisymmetric flow. AIChE J. 7 (1961) 26–28.

[12] L. J. Crane, Flow past a stretching plate. ZAMP 21 (1970) 645–647.

[13] C. K. Chen, Char, M.I.: Heat transfer of a continuously stretching surface with suction and blowing. J. Math. Anal. Appl. 135 (1988) 568–580.

[14] M. E. Ali, On thermal boundary layer on a power-law stretched surface with suction or injection. Int. J. Heat Fluid Flow 16 (1995) 280–290.

[15] F. Aman, A. Ishak, I. Pop, Mixed convection boundary layer flow near stagnation-point flow on vertical surface with slip. Appl. Math. Mech. Engl. Ed. 32 (2011) 1599–1606.

[16] Z. Abbas, S. Rasool, M. M. Rashidi, Heat transfer analysis due to an unsteady stretching/shrinking cylinder with partial slip condition and suction. Ain Shams Eng. J. 6 (2015) 939–945.

[17] M. M. Rashidi, M. Ali, N. Freidoonimehr, B. Rostami, M. Anwar Hossain, Mixed convective heat transfer forMHD viscoelastic fluid flow over a porous wedge with thermal radiation. Adv. in Mech. Eng. 6, (2014) 735-939.

[18] M. M. Rashidi, N. Rahimzadeh, M. Ferdows, M. J. Uddin, O. A. Bég, Group theory and differential transform analysis of mixed convective heat and mass transfer from a horizontal surface with chemical reaction effects. Chem. Eng. Commun. 199(8) (2012) 1012–1043.

[19] F. Garoosi, G. Bagheri, M. M. Rashidi, Two-phase mixture modeling of mixed convection of nanofluids in a square cavity with internal and external heating. Powder Technol. 275 (2015) 304–321.

[20] O. A. Bég, M. J. Uddin, M. M. Rashidi, N. Kavyani, Double-diffusive radiative magnetic mixed convective slip flow with Biot and Richardson number effects. J. Eng. Thermophys. 23(2) (2014) 79–97.

[21] A. Chakrabarti, A. S. Gupta, Hydro magnetic flow and heat transfer over a stretching sheet. Quart. Appl. Math. 37 (1979) 73–78.

[22] K. Vajravelu, L.C. Andrews, R. N. Mohapatra, Exact solutions of the unsteady hydrodynamic and hydromagnetic flows past an infinite plate. Acta Mech. 74 (1988)185–193.

[23] H. I. Andersson, K. H. Bech, B. S. Dandapat, Magnetohydrodynamic flow of a power law fluid over a stretching sheet. Int. J. Non-Linear Mech. 27 (1922) 929–936.

[24] Y. I. Seini, O. D. Makinde, MHD boundary layer due to exponentially stretching surface with radiation and chemical reaction. Math. Probl. Eng. 2013, 7 (2013).

[25] M. M. Rashidi, S. Bagheri, E. Momoniat, N. Freidoonimehr, Entropy analysis of convective MHD flow of third grade non-Newtonian fluid over a stretching sheet. Ain Shams Eng. J. in press (2015).

[26] T. Fang, J. Zhang, Y. Zhong, Boundary layer flow over a stretching sheet with variable thickness. Appl. Math. Comput. 218 (2012) 7241–7252.

[27] L. L. Lee, Boundary layer over a thin needle. Phys. Fluids 10 (1967) 822–828.

[28] A. Ishak, R. Nazar, I. Pop, Boundary layer flow over a continuously moving thin needle in a parallel free stream. Chin. Phys. Lett. 24 (2007) 2895–2897.

[29] S. Ahmad, N. M. Arifin, R. Nazar, I. Pop, Mixed convection boundary layer flow along vertical moving thin needles with variable heat flux. Heat Mass Transf. 44 (2008) 473–479.

[30] M. M. Khader, A. M. Megahed, Boundary layer flow due to a stretching sheet with a variable thickness and slip velocity. J. Appl. Mech. Tech. Phys. 6 (2015) 241–247.

[31] K. Vajravelu, K. V. Prasad, Vaidya, Hanumesh: Influence of hall current on MHD flow and heat transfer over a slender stretching sheet in the presence of variable fluid properties. Commun. Num. Anal. 1 (2016) 17–36.

[32] K. V. Prasad, K. Vajravelu, Vaidya, Hanumesh, MHDcasson nanofluid flow and heat transfer at a stretching sheet with variable thickness. J. Nanofluids. 5 (2016) 1–13.

[33] S. Liao, A new branch of solutions of boundary-layer flows over a stretching at plate. Int. J. Heat Mass Transf. 48 (2005) 2529–2539.

[34] S. Liao, A new branch of solutions of boundary-layer flows over a permeable stretching plate. Int. J. Non-Linear Mech. 42 (2007) 819–830.

[35] R. A. Van Gorder, K. Vajravelu, Analytic and numerical solutions to the Lane–Emden equation. Phys. Lett. A. 372 (2008) 6060–6065.

[36] K. Mallory, R. A. Van Gorder, Control of error in the homotopy analysis of solutions to the Zakharov system with dissipation. Num. Algorithms 64 (2013) 633–657.

[37] K. Mallory, R. A. Van Gorder, Optimal homotopy analysis and control of error for solutions to the non-local with Ham equation. Num. Algorithms 66 (2014) 843–863.

[38] R. Li, R. A. Van Gorder, K. Mallory, K. Vajravelu, Solution method for the transformed time-dependent michaelismenten enzymatic reaction model. J. Math. Chem. 52 (2014) 2494–2506.

[39] R. A. Van Gorder, E. Sweet, K. Vajravelu, Nano boundary layers over stretching surfaces. Commun. Nonlinear Sci. Num. Simul. 15 (2010) 1494–1500.

[40] M. Baxter, M. Dewasurendra, K. Vajravelu, A method of directly defining the inverse mapping for solutions of coupled systems of nonlinear differential equations, Numerical Algorithms 77 (2017) 1199-1211.

[41] K. Vajravelu, J.R. Cannon, J. Leto, R. Semmoum, S Nathan, M. Draper, and D. Hammock, Nonlinear convection at a porous flat plate with application to heat transfer from a dike, Journal of Mathematical Analysis and Applications 277 (2003) 609-623.

[42] P. Cheng, The influence of lateral mass flux on free convection boundary layers in saturated porous medium, International Journal of Heat Mass Transfer 20 (1977) 201-206.

[43] R.A. Van Gorder and K. Vajravelu, On the selection of auxiliary functions, operators, and convergence control parameters in the application of the Homotopy Analysis Method to nonlinear differential equations: A general approach, Communications in Nonlinear Science and Numerical Simulation 14 (2009) 4078-4089.

[44] K. Vajravelu and R. A. Van Gorder, Nonlinear Flow Phenomena and Homotopy Analysis: Fluid Flow and Heat Transfer. Springer, Heidelberg 2013.

[45] R. A. Van Gorder, Gaussian waves in the Fitzhugh-Nagumo equation demonstrate one role of the auxiliary function $H(x)$ in the homotopy analysis method, Communications in Nonlinear Science and Numerical Simulation 17 (2012) 1233-1240.

[46] M. Baxter, R. A. Van Gorder and K. Vajravelu, On the choice of auxiliary linear operator in the optimal homotopy analysis of the Cahn-Hilliard initial value problem, Numerical Algorithms 66 (2014) 269-298.

[47] M. Baxter and R. A. Van Gorder, Exact and analytical solutions for a nonlinear sigma model, Mathematical Methods in the Applied Sciences 37 (2014) 1642-1651.

[48] Y. Tan and S. Abbasbandy, Homotopy analysis method for quadratic Riccati differential equation, Communications in Nonlinear Science and Numerical Simulation 13 (2008) 539-546.

[49] S. Liao, An optimal homotopy-analysis approach for strongly nonlinear differential equations, Communications in Nonlinear Science and Numerical Simulation 15 (2010) 2315-2332.

[50] M. Baxter, R. A. Van Gorder and K. Vajravelu, Optimal analytic method for the nonlinear Hasegawa-Mima equation, The European Physical Journal Plus 129 (2014) 98.

[51] R. A. Van Gorder, Stability of the Auxiliary Linear Operator and the Convergence Control Parameter in the Homotopy Analysis Method. Advances in the Homotopy Analysis Method. Ed. S.-J. Liao. World Scientific, 2014. pp. 123-180.

[52] R. A. Van Gorder, Analytical method for the construction of solutions to the Föppl-von Kármán equations governing deflections of a thin flat plate, International Journal of Non-linear Mechanics 47 (2012) 1-6.

[53] M. Dewasurendra, M. Baxter, K. Vajravelu, "A Method of Directly Defining the InverseMapping for Fourth Order Non-Linear Systems Arising in Combined Free and ForcedConvection in a Second Grade Fluid," Applied Mathematics and Computation 339 (2018)758-767.

[54] B.D. Coleman, H. Markovitz, Normal Stress Effect in Second-Order Fluids, Journal of Applied Physics 35 (1964) 1-9.

[55] B. D. Coleman, W. Noll, An approximation theorem for functions with applications in continuum mechanics, Arch. Rational Mech. Anal. 6 (1960) 355-370.

[56] K. Vajravelu, E. Soewono. Fourth order non-linear systems arising in combined free and forced convection flow of a second order fluid, International journal of non-linear mechanics 29 (1994) 861-869.

[57] W.C. Troy, E.A. Overman II, G.B. Ermentrout, Uniqueness of flow of a second-order fluid past a stretching sheet, Quarterly of Applied Mathematics 4 (1987) 753-755.

[58] K. Vajravelu, D. Rollins,Heat Transfer in a Viscoelastic Fluid over a Stretching Sheet, Journal of Mathematical Analysis and Applications 158 (1991) 241-255.

[59] K. Hsiao, Heat and mass mixed convection for MHD visco-elastic fluid past a stretching sheet with ohmic dissipation, Commun Nonlinear Sci Numer Simulat 15 (2010) 1803-1812.

[60] M. Dewasurendra, K. Vajravelu, On the Method of Inverse Mapping for Solutions of Coupled Systems of Nonlinear Differential Equations Arising in Nanofluid Flow, Heat and Mass Transfer, Applied Mathematics and Nonlinear Sciences 3 (2018) 1-4.

[61] P. Rana, R. Bhargava, 1. (2012),Flow and heat transfer of a nanofluid over a nonlinear stretching sheet: A numerical study, Communication in Nonlinear Science and Numerical Simulation 17, 212-226.

[62] M. Dewasurendra, Y. Zhang, K. Vajravelu, "A Method of Directly Defining the inverse Mapping (MDDiM) for solutions of non-linear coupled systems arising in SIR and SIS epidemic models," Communications in Numerical Analysis (2018).

[63] W.O. Kermack, A.G. MCKendrick, Contribution to the mathematical theory of epidemics, Procc. Soc. A115 (1927) 700-721.

[64] H. Khan, R.N. Mohapattra, K. Vajravelu, S.J. Liao,The explicit series solution of SIR and SIS epidemic models, Applied Mathematics and Computation, 215 (2009): 653-669.

[65] O. Diekmann, J.A.P. Heesterbeek, J.A.J. Metz, On the definition and computation of the basic reproductive ratio in models for infectious diseases in heterogeneous population, J. Math. Biol. 28 (1990) 365-382.

[66] H.W. Hethcote, The mathematics of infectious diseases, SIAM Rev. 42 (2000) 599-653.

[67] R.W. West, J.R. Thompson, Models for the simple epidemic, Math. Biosci. 141 (1997) 29-39.

[68] G.C. Pietro, How mathematical models have helped to improve understanding the epidemiology of infection, Early Hum. Dev. 83 (2007) 141-148.

[69] N. Singh, Epidemiological models for mutating pathogen with temporary immunity, Ph.D. Dissertation (in English), University of Central Florida,Orlando, FL, 2006.